INVESTIGATION OF TRANSITION METAL DOPED CERIUM ALUMINIUM GARNET AND GADOLINIUM ALUMINIUM GARNET FOR SOLID-STATE LIGHT SOURCES

Thesis Submitted for the Award of the Degree of

DOCTOR OF PHILOSOPHY

in

Physics

By

Anu Bala

Registration Number: 42000153

Supervised By

Suman Rani (11795)

Department of Physics (Associate Professor)

School of Chemical Engineering and Physical Sciences

LOVELY PROFESSIONAL UNIVERSITY, PUNJAB

2024

DECLARATION

I, hereby declared that the presented work in the thesis entitled "Investigation of Transition Metal doped Cerium Aluminum Garnet and Gadolinium Aluminum Garnet For solid-state light sources." in fulfillment of degree of Doctor of Philosophy (Ph.D.) is outcome of research work carried out by me under the supervision of Suman Rani, working as Associate Professor, in the Dept. of Physics, School of chemical Engineering and Physical sciences of Lovely Professional University, Punjab, India. In keeping with general practice of reporting scientific observations, due acknowledgements have been made whenever work described here has been based on findings of other investigator. This work has not been submitted in part or full to any other University or Institute for the award of any degree.

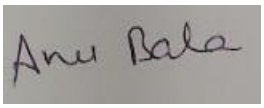

(Signature of Scholar)

Name of the scholar: Anu Bala

Registration No.: 42000153

Department/school: Dept. of Physics, School of chemical Engineering and Physical sciences.

Lovely Professional University,

Punjab, India

CERTIFICATE

This is to certify that the work reported in the Ph.D. thesis entitled "Investigation of Transition Metal doped Cerium Aluminum Garnet and Gadolinium Aluminum Garnet For solid-state light sources" submitted in fulfillment of the requirement for the award of degree of **Doctor of Philosophy (Ph.D.)** in the Dept. of Physics, School of Chemical Engineering and Physical sciences, is a research work carried out by Anu Bala (42000153), is bonafide record of his/her original work carried out under my supervision and that no part of thesis has been submitted for any other degree, diploma or equivalent course.

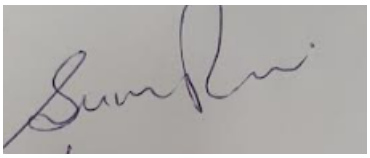

(Signature of Supervisor)

Name of supervisor: Suman Rani

Designation: Associate Professor

Department/school: Dept. of Physics, School of chemical Engineering and Physical sciences

University: Lovely Professional University

Abstract

Solid-state light sources, particularly light-emitting diodes (LEDs), have expanded prominence in lighting applications due to their industrial, technical, and environmental advantages. Garnet materials have emerged as pivotal candidates in this domain, offering key benefits for LEDs. Garnets exhibit excellent thermal stability, high light transmittance, and compatibility with different wavelengths. Their crystal structure allows for efficient light emission and enhances the performance of LED devices. Moreover, garnets contribute to the development of eco-friendly lighting solutions, aligning with the growing emphasis on sustainability in various industries. This makes garnets integral to the advancement of solid-state lighting technologies, shaping the future of energy-efficient illumination. To develop efficient and promising material in the field of SSLSs investigation on Gadolinium Aluminum Garnet (GAG) and Cerium Aluminum Garnet (CAG) attempted and visible emission properties of both the material with transition metal doping carried out.

The material and method Chapter describes the synthesis methods used to prepare material, instrumentation, and the characterization techniques that are employed in the current work. All the samples of host, doped, and co-doped GAG and CAG were synthesized via Sol-gel. The prepared powder samples were sintered at 1100^{o}C for GAG and 1200^{o0}C. Further, all the sintered samples were characterized by using techniques of X-ray diffraction (XRD), Fourier Transform Infrared Spectroscopy (FTIR), Field Emission Scanning Electron Microscopy (FE-SEM), UV-visible Spectroscopy and Fluorescence Spectroscopy. The observed results from FTIR and UV-visible studies reveal the functional groups and absorption. Under the Fluorescence spectroscopy, the emission and excitation of GAG were studied along with its transition lines. The effect of doping of Cobalt and chromium also studied on the GAG. The CIE, CCT, Color Purity and CRI all the parameters evaluated for GAG and CAG host and with doping and results show the practical application of garnet in solid –State lighting.

The results of XRD and FTIR revealed that in both cases GAG and CAG host material has the pure phase of garnet and doping or co-doping of transition metal into it did not affect the crystal structure of host material. The change in crystalline size and lattice constant was found due to the introduction of a dopant in the host of GAG and CAG and strain in the lattice was also observed as diffraction peaks get shifted. This shift may be caused due to strain or due to defects in the crystal lattice. The crystalline structure and morphology were also investigated by FESEM and results were verified to XRD results. The optical analysis of both materials is done with UV-Vis spectroscopy (used to analyze the absorption spectrum and optical band gap of the material) and Fluorescence spectroscopy (emission spectrum analysis with some optical parameters). Both the materials were shown the broad visible spectrum and wide optical band gap. GAG had an optical band gap near 4.17 eV and CAG host material had around 3 eV. The broad visible emission spectrum was observed in both GAG and CAG and multiple peaks in the spectrum induced the transition lines and states. The peaks in the blue, green, and red regions of the spectra indicate the applicability of the material for the production of white light. Apart from this, the color coordinates values for the GAG are (0.333,0.334) and for CAG are (0.331,0.332) which are close to ideal CIR coordinates values for white light i.e.(0.333,0.333). thus, the present work discussed in the thesis may be beneficial for white light in solid-state light sources.

ACKNOWLEDGMENT

I want to express my sincere gratitude to all those who have supported and guided me throughout the journey of completing this research work.

First and foremost, I am deeply thankful to my research supervisor, Dr. Suman Rani, for their precious guidance, encouragement, unwavering support, and insightful feedback throughout this research work. Their expertise and encouragement have been instrumental in shaping the direction of this research. I'm extremely grateful to him for his assistance and direction during this process. Their unwavering support and motivation for my work will always be acknowledged.

I extend my heartfelt thanks to Dr. Kailash Juglan for their constructive criticism and valuable suggestions that significantly enhanced the quality of this work.

I am indebted to the faculty members of the physics department for providing a stimulating academic environment and resources essential for the successful completion of this research.

Special thanks are due to my family for their unconditional love and support throughout this endeavor. I pay my humble respect to my father and mother Mr. Hemraj and Mrs. Suman Bala for their blessings are always with me and raising me the way I am with unlimited affection & care. I further deeply respect my husband Mr. Rahul Kreer for his support and trust. His encouragement and understanding have been my pillars of strength. I remember & thank my mother and father-in-law Mr. Binder Pal and Mrs. Sunita for their tremendous love and moral support. I pay my hearty admiration to my brother and sister Mr. Sahil Kumar and Miss Neha who always understand & support me. I am also grateful to my friends and colleagues who have inspired and motivated me. Their camaraderie has made this academic journey more enjoyable.

The author is grateful to the Council of Scientific & Industrial Research (CSIR), Government of India for providing financial support to carry out the research program.

Last but not least, I want to express my appreciation to all the participants who generously shared their time and insights, contributing crucial data to this study.

This thesis would not have been possible without the collective support and encouragement of these individuals, and for that, I am truly grateful.

November, 2023 ***Anu Bala***

Contents

Abbreviations and symbols

Å – Angstrom

α – Absorbance

a- Lattice Constant

β – Full Width Half Maxima

D – Crystalline Size

δ – Dislocation Density

d – Interplanar Spacing

ε – Lattice Strain

eV – Electron Volt

E_g – Energy Band Gap

θ- Bragg's Diffraction angle

K – Kelvin

λ – Wavelength

n- Refractive Index

υ – Frequency

V- Volt

CAG- Cerium Aluminum Garnet

CRI- Color Rendering Index

CIE- Commission Internationale de l'Eclairage

CCT- Corelated Color Temperature

CP- Color Purity

EDX- Energy Dispersive X-ray Spectroscopy

FE-SEM – Field Emission Scanning Electron Spectroscopy

FTIR – Fourier Transform Infrared Spectroscopy

GAG- Gadolinium Aluminum Garnet

JCPDS- Joint Committee on Powder Diffraction Standards

nm – Nanometer

QY- Quantum Yield

RE- Rare Earth

SEM- Scanning Electron Microscopy

TEM- Transmission Electron Microscopy

UV-Vis- Ultraviolet Visible Spectroscopy

XRD – X-Ray Diffraction

List of Figures

List of Tables

Chapter 1

Introduction

1. Introduction

In the history of lighting, there have been several noteworthy turning points occurred from the discovery of fire to the extensive use of fluorescent tubes and incandescent lamps in the 19^{th} and 20^{th} centuries. Certainly, these technologies were beneficial for humanity but there are issues with lifespan, efficiency, and environmental effects. Thus, solid-state lighting came into being as an improved, extra-efficient, and environment-friendly lighting option. These light sources clutch the domination of lightning by beating all other ancient sources because of great versatility, long lifespan, etc and these are most demanding in this era of physics luminescence research due to the vast field of applications. The solid-state electroluminescence phenomenon was first coined by Henry Joseph Round in 1907 by using solid-state silicon carbide. Light-emitting diodes (LEDs), polymer light-emitting diodes (PLEDs), or organic light-emitting diodes (OLEDs) are light sources originating from solid-state lighting (SSLS). [1,2] The Performance and characteristics of solid-state light sources (SSLS) entirely rely on the various optical materials used to produce these light sources. The emission, transmission, and control of light are significantly influenced by optical materials. SSLS can emit light in a wide range of wavelengths; it covers the complete visible spectrum range (400-700 nm) and within this range of spectrum red, green, and blue primary colors are included. White LED is typically created by combining these multicolor lights of the visible spectrum. Apart from the visible spectrum the Ultraviolet (UV) (100-400 nm) as well as the region of Near Infrared (NIR) (700-2500nm) spectrum is also incorporated by the emission wavelength range of SSLS. [3, 4]

1.1. Optical materials

Optical materials are those materials that play a pivotal role in exploring, modifying, and controlling light and electromagnetic spectrum in the visible, UV, and NIR regions. Optical materials are typical materials that interact with visible light and other EM radiation of the optical spectrum and allow them to perform certain functions such as refraction, dispersion, absorption, and emission of visible light. Due to these functions, the material applies to wide ranges across numerous fields including optoelectronic devices, optical healthcare, telecommunication, industries, etc. Optical materials have a wide range of phosphors, quantum dots, organic, inorganic, and semiconductor materials can produce the electromagnetic spectrum. One of the key categories of optical materials that are mainly applicable in the context of solid-state lighting is phosphors. Phosphors are optoelectronic materials that have gained prominence due to their ability to produce emissions in the visible region of the electromagnetic spectrum. They are particularly valuable in developing effective and adaptable solid-state light sources, such as light-emitting diodes (LEDs). To accomplish the demand for solid-state light sources optical material should have excellent properties in favor of these sources. [5]

1.1.1. Properties of optical material

Some key properties of optical materials those are important for white light sources or solid-state light sources.

The optical material has transparency in the visible spectrum and exhibits high capacity to transmit visible light with minimal distortion or absorption of incident light which can emit light of good efficiency with less energy loss. For instance, optical materials like garnets or phosphors used in the display or lighting devices need to be transparent within the visible spectrum such as, yttrium aluminum garnet (YAG) is transparent and has low absorption in the near-infrared range, making it suitable for laser and lighting applications [6].

The optical material has a high refractive index that is impactful to enhance the light extraction to improve the light output [7]. The choice of materials with appropriate

refractive indices is a significant consideration in optical materials to maximize the performance of various optical systems.

Optical materials are thermally stable and have color consistency, longevity, and good efficiency while they go through high-temperature conditions. High thermal conductivity materials like diamonds, gems, or aluminate nitrides are deal as substrates to dissipate heat and ensure stability of optical device (LED) operation.

The development of energy-efficient, long-lasting, and color-accurate LED lighting solutions relies on the optical material properties and the terminology used in solid-state lighting. The researchers and engineers continue to advance the field of SSL with the research or optimization of materials such as semiconductors, phosphors, and encapsulates for providing us SSLS with brighter, more efficient, and environmentally friendly lighting options. As the SSL industry continues to grow, it is important to examine and exploit the optical characteristics of materials for enhanced lighting solutions and to resolve emerging challenges in the field.

1.2. Phosphor

Among the wide range of optical materials, phosphor is one of the most demanding candidates due to its unique use for LEDs to produce white light. Over the last few decades, the development of solid-state lighting (SSLS) has seen a notable influence from white light-emitting diodes (WLEDs) and other sources of white light, contributing significantly to advancements in the display and lighting sectors. WLEDs and other white light sources has compactness, good material stability, high efficiency, eco-friendliness, long lifetime or durability, and color tenability, thus WLEDs have become the preferred research choice for a variety of application in lighting and display devices. [8]

Research proved that phosphor is the key material for the production of white light. “Phosphor” is the Greek word which means light bearer. The phosphor material used to produce white light/solid-state light is also named “luminescent materials”. The phosphor material has unique properties like the ability to emit maximum visible light by absorbing

UV light, long and short band gap to emit short as well as long wavelength, crucial efficiency, good stability, and narrow spectrum to produce light of definite color. These are the materials that supply the requisite red, yellow, and green light along with initial blue light to produce white light. [9-11] The phosphors are made up of rare-earth or transition metals and there is the numeral of phosphors prepared by researchers with a variety of techniques. The garnets are the category of phosphor that stands with outstanding optical or luminescence outputs. Thus, the present time's most challenging task for to prepare material with excellent properties. As proven by research the material should have great emission efficiency to produce white light.

1.3 Garnets

Garnets are also named rare-earth garnets which play a crucial role in modern optical device technology because of their unique physical and optical characteristics. Nowadays cubic crystallographic structure of synthetic garnets has been prolonged into the advanced type from the prototype. Garnet possesses a crystal structure that is body-centered cubic and is classified within the space group la3d.The general chemical formula for the garnets is $A_3B_5O_{12}$. According to this formula, site A is a dodecahedral site engaged via rare earth elements for instance Lu^{3+},Y^{3+}, Ce^{3+}, Sc^{3+}, Gd^{3+}, Tb^{3+}, and La^{3+} ions surrounded by eight oxygen (O -) ions and B site is tetrahedral or octahedral occupied by Al^{3+}(in case of aluminate garnet).[12,13] Rare-earth (RE) elements are part of the lanthanide series in the periodic table and the electronic arrangement is represented as [Xe] 4f 5d 6s. The RE metals are widely used in metallothermic reactions because of their extraordinary reduction character. The trivalent series of rear earths like Ce^{3+}, Y^{3+}, Gd^{3+}, Eu^{3+}, Tb^{3+}, etc. proved great elements for garnets. A huge range of garnets exist, but rare-earth aluminate garnets have a wide range of applications due to favorable luminescence properties. Yttrium aluminum was the first reported garnet used for various applications with different doping elements. YAG: Ce was the very first yellow emission phosphor used due to its beneficial characteristics, including strong blue absorption, broad emission in region 500-700 nm, quick decay time around 100 ns, and nearly 75% of luminescence efficiency. [14] The

prominent and extensively investigated garnets are YAG, terbium aluminum garnet (TAG), lutetium aluminum garnet (LuAG), and recently gadolinium aluminum garnets (GAG). These have been focus of researched to applications in the realization of solid-state light devices or photonic devices. The preparation of garnet with the appropriate synthesis method is a crucial task since the synthesis technique is also advantageous for the enhancement of the properties of any material. Some common synthesis techniques are a solid-state process, auto-combustion technique, and sol-gel technique. Thus, studied the structure, optical, and electric properties of garnet with the doping or co-doping of rare-earth metals. However, two rare-earth garnets GAG and cerium aluminum garnet (CAG) have been investigated in present work with the doping or co-doping of transition metals. Due to the paucity of research Cerium Aluminum garnet has been introduced as a new member of the garnet family.

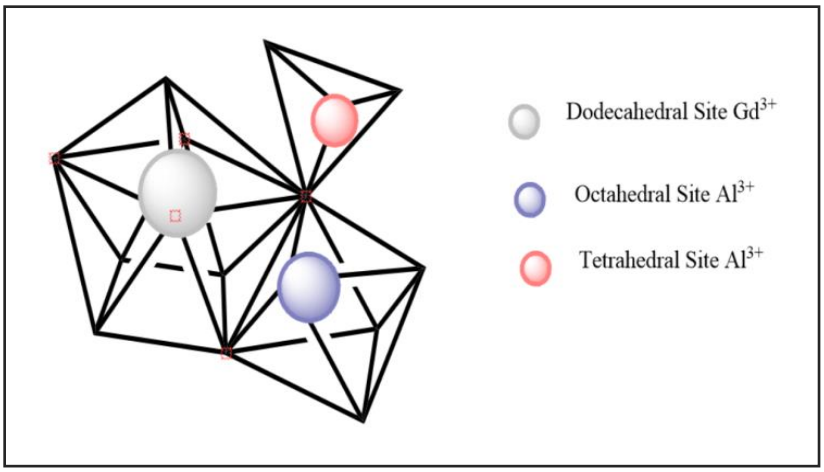

Fig 1.1. Crystallographic three-dimensional representation of Gd3Al5O12 garnet unit cell.

1.3.1 Gadolinium Aluminum Garnet (GAG)

Gadolinium Aluminum Garnet (Gd3Al5O12) is an already known material for its optical properties doped with rare–earth elements. While the utilization of Gadolinium as a host material can be costly, its adoption has increased significantly because of its uniform cubic structure, good reactivity, high melting point, and chemical and emission stability making it a promising host. The atomic number of Gadolinium is 64 having partially filled 4f

electrons in configuration. Its intricate energy level configuration arises from the organization of electrons. The material based on gadolinium has good luminescent properties. Consequently, GAG was elected for the present work and significant research efforts have been made to synthesize a material by the sol-gel method with controlled morphology to enhance luminescence properties. The phase obtained at 1100°C with excellent crystalline and structural properties along with favorable optical properties. GAG has an absorption spectrum of 200-400 nm range and an emission spectrum ranging from 200 to 800 nm with maximum visible emission. The color properties are excellent with CRI around 95, color purity near 0-0.5%, and CIE coordinates are very near to the ideal one i.e. (0.333,0.333). Further, the GAG hosts undergo doping and co-doping with transition metals to explore their impact on the optical and structural characteristics of the GAG host.

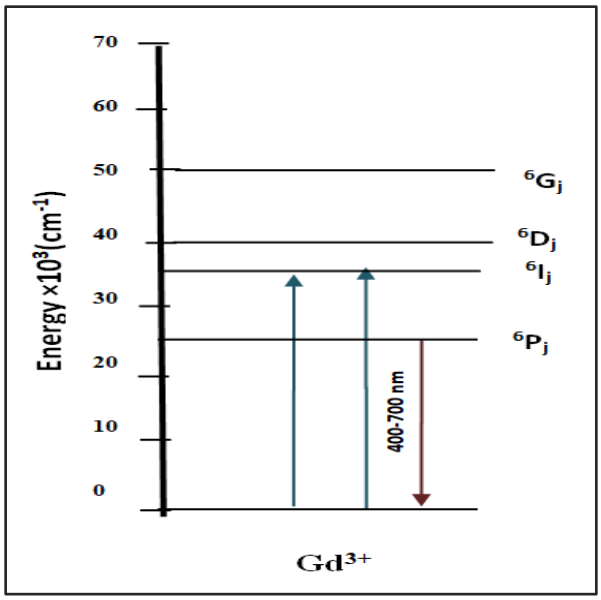

Fig 1.2. Typical energy level diagram of Gd^{3+} (transition lines).

1.3.2. Cerium Aluminum Garnet (CAG)

Cerium Aluminum Garnet ($Ce_3Al_5O_{12}$) is a new material in the family of rare-earth aluminate garnets. Cerium is the cheapest element of the rare-earth family and the trivalent state i.e. Ce^{3+} has excellent optical proprieties due to its transition energy levels. Hence,

Cerium Aluminate Garnet can be proved as a good host garnet. Cerium Phosphor has good luminescent properties and is used to produce color-tunable light in various applications. In this work, the challenging task of preparing Cerium Aluminum Garnet was prepared successfully. Cerium was used as a host to prepare. The examination of CAG revealed impressive structural and optical characteristics. The material exhibits absorption in both the UV and IR regions, along with a wide-ranging emission in the visible region spanning from 400 to 700 nm.

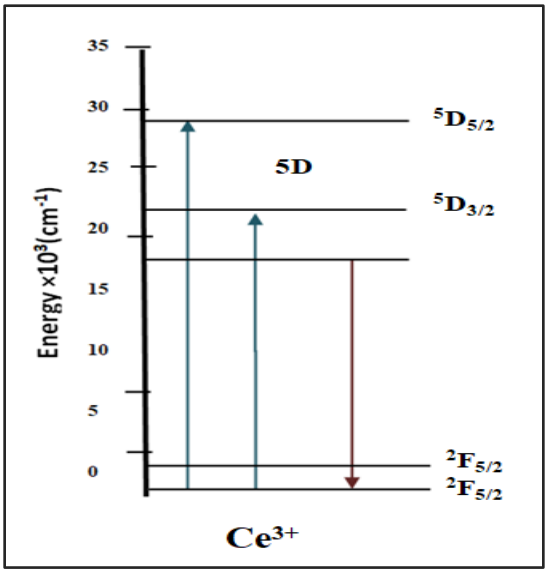

Fig 1.3. Transition lines/Energy level diagram of Ce^{3+}.

1.3.1. Properties of garnets

In terms of physical appearance, the garnets are a hard multicolor compound because of the strong bonding in the atoms and the range of hardness is 6 to 7.5 Mohs scale the garnets are insoluble in water. Garnet has excellent optical properties which they consider a great luminescence material. The density of the garnet is 3.5 to 4.3 gm/cm^{-3} and they have sintering temperatures between 900-1700ºC. The refractive index of garnets ranges from 1.7-2.2 but it can vary with doping or change in its composition. Along with these properties, garnets have some important optical properties like absorption, optical band

gap, optical spectrum, quantum yield, and fluorescence lifetime that make them applicable for light sources, lasers, scintillators, LEDs, etc.

Optical Band-gap

In the context of crystalline material, the optical band gap is considered as the energy gap in the highest energy level in the valance band (VB) and the conduction band's (CB) minimum energy level, while the photon is absorbed. There are two kinds of optical band gaps: one is a direct band gap in which the magnitude and the direction of a photon (i.e. k vector) are the same for both the valance band and conduction band and another one is an indirect band gap, where the value of k vector for valance band the and conduction band differ as shown in figure 1.4.

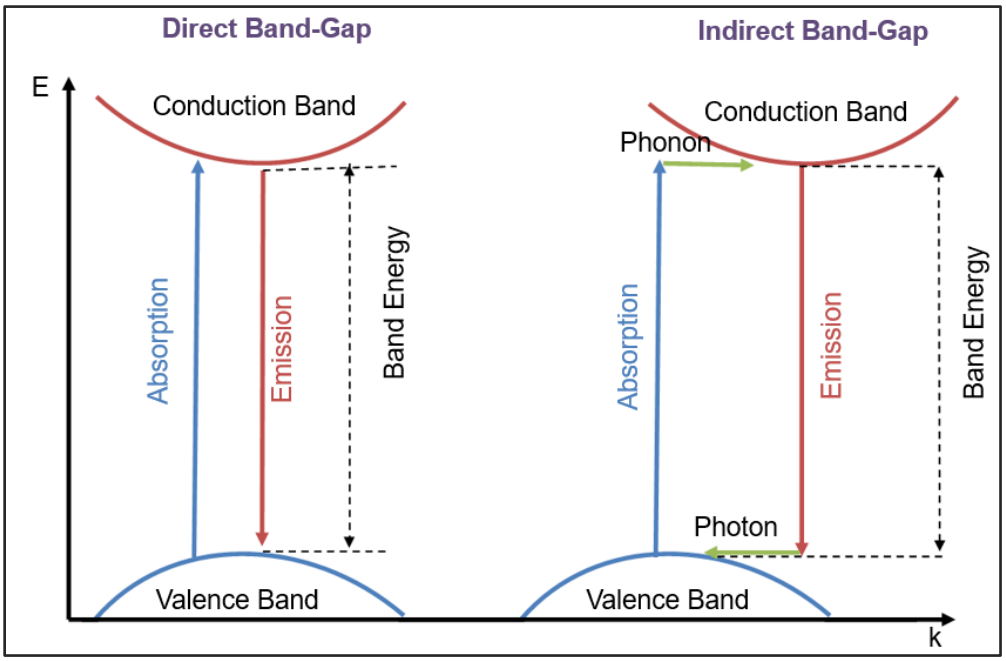

Fig 1.4. Graphical view of the direct and indirect band gap.

The optical band gap denoted as Eg, signifies the energy difference in VB and CB and it depends upon the ability of a material to absorb or emit photons. Thus, the optical band gap is the critical parameter used to explain the ability of a material to interact with photons and its emission or absorption properties. [15,16] The garnets have a wide optical band gap

typically ranging from 3 to 6 eV depending on the precise composition of material and doping. These wide band gaps of garnets make them transparent to the wide range of visible and infrared light. Moreover, garnets are useful for lasers, and versatile for various optical and photonic devices due to effective band gap [17].

Luminescence

Luminescence processes play a significant role in various applications. Its mechanism and properties depend on the material. Luminescence is related to the emission of light at low temperatures either by chemical or physiological process and it involves the process of excitation in which the atom moves from the ground state to the excited state, after staying in the excited state it gets de-excited due to the lack of stability in the excited level. The atom gets back to the ground state either directly or by jumping to the transition levels, during the process of emission the atom emits energy in the form of light or photons. Phosphorescence and fluorescence are the two important parts by which material used in white light sources can achieve luminescence. [18,19]. Based on the excitation mechanism the luminescence distributed in various parts of it is shown in the figure below.

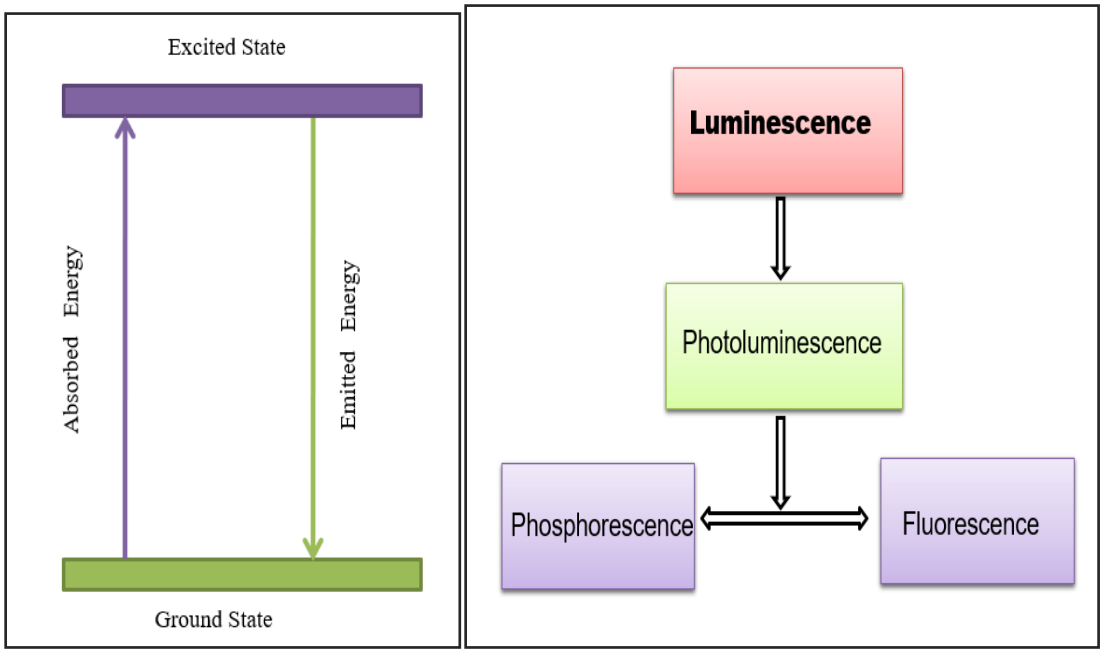

Fig 1.5. Energy diagram for Luminescence and flow diagram of types of luminescence.

Fluorescence Lifetime

Fluorescence lifetime is characterized as the period or average duration during which a fluorophore remains in the excited state before returning to the ground state. After the excitation fluorophore gets unstable at the excited state and returns to the ground state this transition takes time to reach a ground state time is known as decay time. The fluorescence lifetime is also defined as the amount of time fluorophore takes to exponentially decline to 1/e or 37% of the initial population because of loss in energy by the Radiative or non-Radiative process. [20]

The Fluorescence lifetime of Garnets fall in the range of microseconds to millisecond. The variation depends on various factors like dopant, the energy level of fluorescence spectroscopy, temperature, quality of crystal, and energy transition of dopant. The decay and fluorescence lifetime for single exponential decay is expressed by the equation:

$$I(t) = I_o e^{-t/\tau} \ldots\ldots\ldots\ldots\ldots (1.1)$$

Where I_o is considered as the intensity at time zero and τ stands for the lifetime. 0

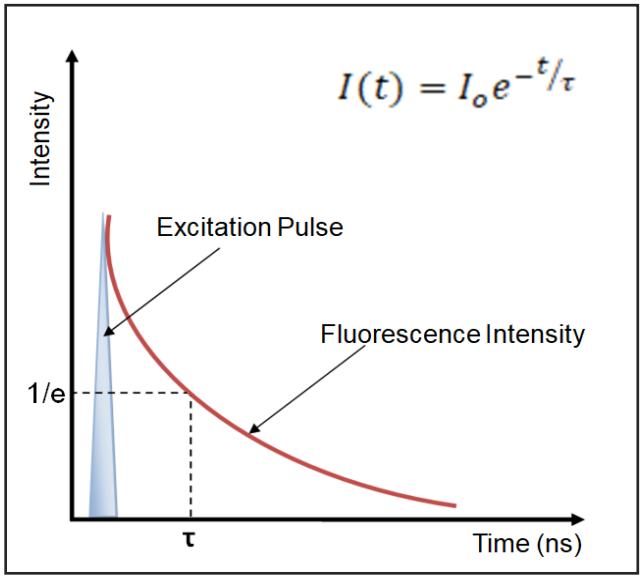

Fig 1.6. Fluorescence lifetime imaging.

Fluorescence Quantum Yield

The fluorescence quantum yield used to determine the efficiency of the material by which it emits the fluorescent light. It is ascertained by contrasting the material's emission with a standard reference of known quantum yield. Additionally, it is computed by the ratio of photons absorbed during the process to the number of photons emitted. The quantum yield is dimensionless and its value typically ranges from 0 to 1. The 0 means 0% quantum efficiency and no absorbance of photon and if the value is 1 then quantum efficiency is 100% and it signifies that all the photons get absorbed and converted into fluorescence. [21, 22]

The quantum yield depends upon several factors including electronic transitions and energy levels of the fluorescence process, dopant, temperature, and presence of quenchers. The quantum material of garnet (like YAG) depends on the crystal structure, composition, and dopant used in the material. Quantum yield can be determined using both the absolute method and the relative method. According to the absolute method, quantum yield (denoted by the symbol ϕ) is calculated by comparing the fraction of emitted photons to the number of absorbed photons during the process of fluorescence in a particular period.

$$\phi = \frac{photons\ emitted}{photons\ absorbed} = \frac{N_E}{N_A}$$

Besides, according to the relative method, the fluorescence quantum yield is quantified by comparing the intensity and absorbance of the unknown sample to the slandered reference known sample. The formula for the relative method:

$$\phi = \phi_r \frac{I_s}{I_r}\frac{A_r}{A_s}\frac{n_s^2}{n_r^2} \ldots\ldots\ldots\ldots\ldots\ldots (1.2)$$

Where ϕ_r represents the quantum yield of the standard reference, I_s and I_r signify the integrated intensity of the sample and standard reference, while n_s and n_r correspond to the refractive index of the sample and standard reference, respectively. [23]

Transmission/ Absorption

When electromagnetic radiations fall on the surface of the material the radiations go through the absorption and transmission process shown in the figure. Under the absorption, some of the rays get absorbed by the material and it occurs when the frequency of the light matches with frequency of the electron in the atom of the material. Transmission is the other side of the same coin, in this process, the radiation gets passed through the material without being reflected or absorbed by the material and fundamental properties of the material affect the efficiency of transmission.

Colorimetry

Colorimetry, a vital scientific field, quantifies color for diverse applications in commerce, industry, and laboratories. Key concepts like CRI, CCT, and CIE are pivotal in color science and lighting. Human vision relies on cones—specialized cells sensitive to different light wavelengths—following the trichromatic theory. This theory posits that three types of color receptors in the eye collaborate to perceive the full color spectrum. CRI evaluates how well a light source can faithfully reproduce the colors of objects in comparison to a reference source.

CIE (Commission Internationale De l'Eclairage or International Commission on Illumination) is a system used to define the relationship between the physiologically experienced color vision and the Electromagnetic visible spectrum wavelength distribution. The system is used to measure the colors by using luminescence parameters Y and (x, y) points on the chromaticity diagram. [24] The CIE 1931 was proved as an effective system for color specification.

CRI (Color Rendering Index) term measures the capacity or the accuracy of produced light by any light source. Hence, it examines how much pure light a source can produce to show the original or natural color of the object in its light as compared to the natural sunlight. The CRI values lie between the numbers 1-100. The CRI of sunlight is 100, therefore if the

light source has a CRI near the value of 100, it can show the original color of the object. The International Commission on Illumination defines the term CRI.

$$Ra = 100 - 4.6\Delta E \ldots\ldots\ldots\ldots\ldots\ldots \quad (1.3)$$

where $\triangle E$ = color difference.

CCT (Correlated Color temperature) is used to quantify the color of emitted light by the light source and is used to quantify in Kelvin (K). color temperature of light gave the idea of cool and warm light, if light has a color temperature of 5500 K or near, it will be considered as cool light (i.e. blue) but if the color temperature is around 3000 K then it will be warm light (yellow). The natural white light has a color temperature of around 4000 K. [25] The CCT can be calculated by using the formula:

$$CCT = -449m3 + 3525m2 - 6823.3m + 5520.33 \ldots\ldots\ldots\ldots \quad (1.4)$$

Here $m = \frac{x - x_e}{y - y_e}$ (inverse slope of the line)

CP (Color Purity) is defined as the color resemblance between the light emitted by a light source and the natural light. The values of color purity fall between 0-100% for white light lower values of color purity were considered. The color purity can be quantified by using the formula:

$$CP = \frac{\sqrt{(x_s - x_i)^2 + (y_s - y_i)^2}}{\sqrt{(x_d - x_i)^2 + (y_d - y_i)^2}} x\ 100\% \ldots\ldots\ldots\ldots (1.5)$$

By equation x_i and y_i are the CIE coordinates of standard illumination of white light, x_s and y_s are the coordinates of the entire spectrum and x_d and y_d are the CIE coordinates of the dominant wavelength.

Table 1.1. Comparison of a few popular garnets based on their key properties.

Parameter	YAG	TAG	LuAG	GAG
Chemical formula	$Y_3Al_5O_{12}$	$Tb_3Al_5O_{12}$	$Lu_3Al_5O_{12}$	Gd3Al5O12
Density (g/cm^3)	4.56	7.15	6.71	7.08
Crystal structure	Cubic	Cubic	Cubic	Cubic
Melting Point (^{o}C)	1970	1700	1980	1300
Sintering Temperature (^{o}C)	1300	1100	900	1100^{o}C
Optical Band Gap (eV)	6-8.5	6.5-7.5	0.2-0.3	4-4.5
Emission (color)	Yellow- Green	Green	Green –Yellow	Red, yellow-green
Hardness (moh)	8-8.5	8.5	8.5	8.5
Refractive Index	1.82 (at 1064 nm)	1.8-2.1	1.83 (1003.98 nm)	1.8
Reference	[26,27]	[28]	[29,26]	[30,31]

1.4. Transition Metal

Transition metals are the elements that belong to the d-block of the periodic table and serve as the bridge between both sides of the periodic table. Their distinctive electronic configuration (i.e. [Ar] $4s^2$ $3d^{1-10}$) and distinctive properties make them unique. Their partially filled d-orbital leads to multiple oxidation states and a huge range of reactivity. Nowadays Transition metals play a crucial role as excellent dopants for phosphor materials because of their unique electronic configuration, and physical and optical properties. The most commonly used transition metal as a dopant is Cr^{3+}, Fe^{3+}, Co^{3+}, Ni^{3+}, and, Cu^{3+}. The doping of transition metals can enhance the absorption as well as conductivity of the host as it initiates impurity levels. Hence transition metals can change optical (absorption, luminescence, band-gap), electrical, and magnetic properties of material as dopant. Luminescence in the transition metals leads to the emission of electromagnetic radiations or light by the transition metal ions or complexes, while they return to the ground state after being excited to a higher energy level. Apart from this, transition metals have several general properties:

1. Transition metals are reactive metals due to various oxidation states and formed colored ions.
2. Transition metals are hard usually and have high density.
3. Transition metals possess high melting and boiling points.
4. The coordination numbers of transition metals are in the wide range of 1-12. Thus, they have partially filled d-orbital due to which their stability and reactivity can form compounds with different coordination geometries.
5. Transition metal compounds are paramagnetic.
6. The transition metal complexes are colorful, due to electronic transitions occurring inside the d-orbital of the metal ions; certain colors are produced by the absorption and emission of particular light wavelengths.
7. Transition metals form strong metallic bonds within the crystal structure.

In the present work, Chromium and Cobalt are used as dopants in Gadolinium Aluminum garnet and Cerium Aluminum Garnet for single and double doping. This results in the electronic transition among the d-orbital of the transition metal ions. Fluorescence and phosphorescence are the process that occurs due to the transition. The transition lines of Cr^{3+} and Co^{3+} have been illustrated in the figure 1.7.

When the chromium ions go through the transition between the energy levels according to electronic configuration transition lines are observed which results the absorption and emission. While Cr ion doped on host material, then transition depends upon the chemical properties of that material. The common transitions of Cr^{3+} are shown in Figure 8, thus in the octahedral coordination absorption was observed around 400 (blue-green) and 600 nm (red) due to the $^4A_2 \rightarrow ^4T_1$ and $^4A_2 \rightarrow ^4T_2$ transition correspondingly. After excitation gets relaxed and moves back to a lower energy level emission takes place around 695 nm (red line) due to the $^4T_2 \rightarrow ^4A_2$ transition. The typical transition of Cr^{3+} may vary according to the host and its crystal structure. [32]

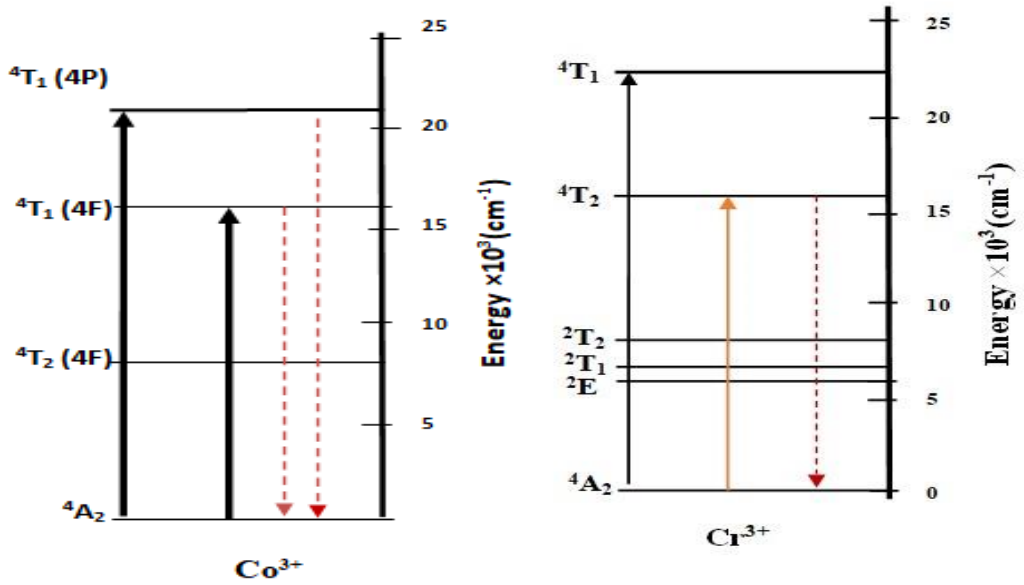

Fig 1.7. Transition lines of chromium (Cr^{3+}) and Cobalt (Co^{3+}).

In the case of Cobalt (Co^{3+}) d^6 and d^5 configurations are responsible for the exhibition of transition that results in the absorption and emission in the UV- Vis spectrum. The absorption near the blue and green regions of the visible region is due to the d^6 configuration or low spin Co^{3+} ions and absorption in the IR and red region is due to the d^5 configuration or high-spin of Co^{3+} ions. Along with this emission takes place after ions get excited and relaxed, and typical emission of Co^{3+} ions takes place in visible and IR regions owed to the $^4T_1(4P) \rightarrow {}^4A_2$ and $^4T_1(4F) \rightarrow {}^4A_1$.The corresponding wavelengths of these transitions vary and depend on the host or cobalt complex. [33]

1.5 Research Motivation

The Garnets have excellent properties due to which they have vast application areas. Based on these properties' the Garnet was chosen for the current study and investigated their optical properties for application in solid-state light sources. Garnets are of great interest for their applications in applications such as WLEDs, sensors, display devices, scintillators,

lasers, and lighting devices. In recent decades, garnets have emerged as highly promising materials in the field of lighting due to their exceptional physical and chemical characteristics. Several well-known garnets such as YAG, TAG, and LuAG with cubic structures have been studied for their optical properties. However, there were only limited reports available on the Gadolinium aluminum garnet nanoparticles and no report was able to demonstrate a systematic study of the structural and optical properties of cerium Aluminum Garnet. To provide a detailed study on the structural and magnetic properties of transition metals doped Garnets (GAG and CAG) we proposed to synthesize garnets with various dopant concentrations through the Sol-gel method. This research aims to enhance the properties of GAG and CAG garnet materials, focusing on their crystallinity, emission, and excitation qualities. By intentionally doping these garnets with transition metals, we seek to improve key parameters such as color rendering index (CRI), correlated color temperature (CCT), luminous efficacy (CP), and color coordinates (CIE). Through a thorough exploration of their luminescence behavior, this study not only contributes to fundamental understanding but also holds promise for advancing solid-state light sources with enhanced performance and versatility in various applications.

This work reported the synthesis and characterization of nano-sized polycrystalline powder material namely gadolinium aluminum garnet and cerium aluminum garnet. The choice of these materials for application in SSLS has been because of their incongruent melting properties, optical properties, and stability. The sol-gel method was utilized for the synthesis of both materials with or without dopant. The prepared precursors are followed by sintering and several characterization methods including X-ray Diffraction (XRD), Fourier Transform Infrared Spectroscopy (FTIR), Field Emission Scanning Electron Spectroscopy (FE-SEM), and Fluorescence spectroscopy are employed to evaluate both the material's structural and optical properties.

1.5. Research Objectives

GAG (Gadolinium aluminum garnet, $Gd_3Al_5O_{12}$) and CAG (Cerium aluminum garnet, $Ce_3Al_5O_{12}$) investigated to study luminescence properties by doping/co-doping with transition metals.

1. To Synthesis of the un-doped and doped GAG and CAG by sol-gel.
2. To study the effect of singly and doubly doping of transition metal in CAG and GAG on excitation and emission spectra.
3. Qualitative analysis of emission response for solid-state light sources.

References:

1. D. Zhu and C. J. Humphreys, "Solid-state lighting based on light emitting diode technology," Optics in Our Time, pp. 87-118, 2016.
2. E. F. Schubert and J. K. Kim, "Solid-state light sources getting smart," Science, vol. 308, no. 5726, pp. 1274-1278, 2005.
3. Bergh, G. Craford, A. Duggal, and R. Haitz, "The promise and challenge of solid-state lighting," Phys. Today, vol. 54, no. 12, pp. 42-47, 2001.
4. J. Y. Tsao, M. E. Coltrin, M. H. Crawford, and J. A. Simmons, "Solid-state lighting: an integrated human factors, technology, and economic perspective," Proc IEEE, vol. 98, no. 7, pp. 1162-1179, 2010.
5. V. Sudarsan, "Optical materials: fundamentals and applications," in Functional Materials: Preparation, Processing and Applications, pp. 285-322, 2012.
6. S. Kostić, Z. Ž. Lazarević, V. Radojević, A. Milutinović, M. Romčević, N. Ž. Romčević, and A. Valčić, "Study of structural and optical properties of YAG and Nd: YAG single crystals," Mater. Res. Bull., vol. 63, pp. 80-87, 2015.:
7. A. I. Zhmakin, "Enhancement of light extraction from light-emitting diodes," Phys. Rep., vol. 498, no. 4-5, pp. 189-241, 2011.
8. K. N. Shinde, S. J. Dhoble, H. C. Swart, and K. Park, "Phosphate phosphors for solid-state lighting," Springer Science & Business Media, 2012.
9. D. R. Vij, Ed., Luminescence of Solids. Springer Science & Business Media, 2012.
10. R. J. Xie, N. Hirosaki, K. Sakuma, and N. Kimura, "White light-emitting diodes (LEDs) using (oxy) nitride phosphors,"J. Phys. D: Appl. Phys., vol. 41, no. 14, p. 144013, 2008.
11. H. Zhang, H. Zhang, A. Pan, B. Yang, L. He, and Y. Wu, "Rare earth-free luminescent materials for WLEDs: recent progress and perspectives," Adv. Mater. Technol., vol. 6, no. 1, p. 2000648, 2021.
12. M. A. Musa, N. H. Osman, J. Hassan, and T. Zangina, "Structural and magnetic properties of yttrium iron garnet (YIG) and yttrium aluminum iron garnet (YAlG) nanoferrite via sol-gel synthesis," Results Phys., vol. 7, pp. 1135-1142, 2017.

13. X. Wang and Y. Wang, "Synthesis, structure, and photoluminescence properties of Ce3+-doped Ca2YZr2Al3O12: a novel garnet phosphor for white LEDs," J. Phys. Chem. C, vol. 119, no. 28, pp. 16208–16214, 2015.
14. C. R. Varney, S. M. Reda, D. T. Mackay, M. C. Rowe, and F. A. Selim, "Strong visible and near infrared luminescence in pure host YAG single crystals," AIP Adv., vol. 1, no. 4, 2011.
15. P. Makuła, M. Pacia, and W. Macyk, "How to correctly determine the band gap energy of modified semiconductor photocatalysts based on UV–Vis spectra," J. Phys. Chem. Lett., vol. 9, no. 23, pp. 6814-6817, 2018,
16. A. Dolgonos, T. O. Mason, and K. R. Poeppelmeier, "Direct optical band gap measurement in polycrystalline semiconductors: A critical look at the Tauc method," J.Solid State Chem., vol. 240, pp. 43-48, 2016.
17. A. Kumar et al., "Effect of the band gap and the defect states present within band gap on the non-linear optical absorption behavior of yttrium aluminium iron garnets," Opt. Mater., vol. 108, p. 110163, 2020.
18. K. V. R. Murthy and H. S. Virk, "Luminescence phenomena: an introduction," Defect Diffus. Forum., vol. 347, pp. 1-34, 2014.
19. B. Valeur and M. N. Berberan-Santos, "A brief history of fluorescence and phosphorescence before the emergence of quantum theory," J. Chem. Educ., vol. 88, no. 6, pp. 731-738, 2011.
20. A. Rossetta, "The bright future of fluorescence lifetime analysis," in Reporters, Markers, Dyes, Nanoparticles, and Molecular Probes for Biomedical Applications XIV, vol. 12398, pp. 19-22, SPIE, March 2023.
21. J. Zheng et al., "An efficient synthesis and photoelectric properties of green carbon quantum dots with high fluorescent quantum yield," J. Nanomater., vol. 10, no. 1, p. 82, 2020.

22. C. Würth, M. Grabolle, J. Pauli, M. Spieles, and U. Resch-Genger, "Relative and absolute determination of fluorescence quantum yields of transparent samples," Nat. Protoc., vol. 8, pp. 1535–1550, 2013.
23. J. Hu and C. Y. Zhang, "Simple and accurate quantification of quantum yield at the single-molecule/particle level," Anal. Chem., vol. 85, no. 4, pp. 2000-2004, 2013.
24. S. Westland, "Review of the CIE system of colorimetry and its use in dentistry," J. Esthet. Restor. Dent., vol. 15, pp. S5-S12, 2003.
25. D. Durmus, "Correlated color temperature: Use and limitations," Light. Res. Technol., vol. 54, no. 4, pp. 363-375, 2022.
26. J. Hrabovský, M. Kučera, L. Paloušová, L. Bi, and M. Veis, "Optical characterization of Y3Al5O12 and Lu3Al5O12 single crystals," Opt. Mater. Express., vol. 11, no. 4, pp. 1218-1223, 2021.
27. Z. Fang, Y. Li, F. Zhang, Z. Ma, G. Dong, and J. Qiu, "Enhanced Sunlight Excited 1-μm Emission in Cr3+–Yb3+ Codoped Transparent Glass-Ceramics Containing Y3Al5O12 Nanocrystals," J. Am. Ceram. Soc., vol. 98, no. 4, pp. 1105-1110, 2015.
28. Z. Y. Gorbenko, V. T. Voznyak, T. Zorenko, B. Kuklinski, R. Turos-Matysyak, and M. Grinberg, "Luminescence Properties of Phosphors Based on Tb3Al5O12 (TbAG) Terbium-Aluminum Garnet," Opt. Spectrosc., vol. 106, pp. 365-374, 2009.
29. Y. Kuwano, K. Suda, N. Ishizawa, and T. Yamada, "Crystal growth and properties of (Lu, Y) 3Al5O12," J. Cryst. Growth, vol. 260, no. 1-2, pp. 159-165, 2004.
30. M. Letz, A. Gottwald, M. Richter, V. Liberman, and L. Parthier, "Temperature-dependent Urbach tail measurements of lutetium aluminum garnet single crystals," Phys. Rev. B., vol. 81, no. 15, p. 155109, 2010.
31. S. V. Nizhankovsky et al., "Growth and the luminescence properties of a lutetium gadolinium garnet doped with Ce3+ and Pr3+ ions," Phys. Solid State, vol. 53, pp. 127-130, 2011.
32. J. G. Li and Y. Sakka, "Recent progress in advanced optical materials based on gadolinium aluminate garnet (Gd3Al5O12)," Sci. Technol. Adv. Mate., 2015.

33. F. F. Zhang, J. Yuan, Y. Liu, W. C. Wang, D. C. Yu, M. Y. Peng, and Q. Y. Zhang, "Efficient 2.0 μm fluorescence in Ho3+-doped fluorogermanate glass sensitized by Cr3+," Opt. Mater. Express., vol. 4, no. 7, pp. 1404-1410, 2014.
34. B. Suresh, M. S. Reddy, J. Ashok, A. S. S. Reddy, P. V. Rao, V. R. Kumar, and N. Veeraiah, "Enhancement of orange emission of Co2+ ions with Bi3+ ions in lead silicate glasses," J. Lumin. , vol. 172, pp. 47-52, 2016.

Chapter 2

Review of Literature

1. **Bulyga et al. (2023)** synthesized the YAG: Ce nanophosphor by using the polymer salt method and studied the structural as well as optical properties. The XRD reveals the average size of nanoparticles around 25-30 nm and phase of the YAG: Ce. The photoluminescence study results with the substitution of Gd in the YAG: Ce spectrum shifted to the red region and long wave excitation band. The lifetime and quantum yield of the material decreases with the rise in the concentration of Gd and concluded that 30-40% substitution of Gd in YAG: Ce on the place of Y is favorable for WLEDs fabrication.

2. **Dubovet al.(2023)** investigated the photoluminescence characteristics of GYAGG:Ce ($(Gd,Y)_3Al_2Ga_3O_{12}$:Ce) using scanning confocal microscopy and fluorescence lifetime imaging microscopy (FLIM). The material was prepared via the co-precipitation method. The study revealed that the increase in concentration of Ce in GYAGG leads to a decrease in luminescence properties. Transparent ceramic samples were prepared by pressure less sintering in an oxygen atmosphere. Notably, the research reveals that as the Ce concentration increases, the photoluminescence intensity at grain boundaries decreases compared to the inner volume. Conversely, photoluminescence kinetics exhibit the opposite behavior, with slower decay at grain boundaries and faster decay within the grain volume, particularly pronounced at a high Ce content of 0.060 f.u. These effects are attributed to the increased heterogeneity in activator distribution at high Ce concentrations, setting a limit on the Ce concentration for achieving high-performing luminescence in GYAGG:Ce ceramics. These findings have practical implications for optimizing the technology of GYAGG:Ce ceramic luminescent materials, specifically in determining the activator concentration.

3. **Jiang et al.(2023)** studied the luminescence properties and WLED application of (Gd, Lu)3Al5O12: Dy garnet. the material was prepared with vacuum sintering at transmittance near 60%. XRD analysis resulted the cubic garnet phase of the material and the effect of doping amount on the structural properties and the emission spectra revealed that doping of Dy enhanced the thermal stability and luminescence behavior of the material. the CIE coordinates and CRI value were calculated around (0.300,0.258) and 60.82 respectively. The (Gd, Lu)3Al5O12: Dy garnet shows a good application in lighting and display devices.

4. **Cao et al. (2023)** investigate the effect of non-stoichiometric compositions of Yttrium Aluminum Garnet (YAG)/ Y3+xAl5-xO12, on its optical properties. The researchers successfully synthesized highly non-stoichiometric YAG ceramics with varying degrees of excess Y3+ ions, allowing for up to 20% substitution of the AlO6 sublattice via Y3+ ions using advanced melt-quenching methods. This substantial alteration in the crystal structure influences the up-conversion luminescence of Yb3+/Er3+-doped systems, resulting in a shift from red-orange to yellow-green emission compared to their stoichiometric counterparts. Notably, the study highlights that YAG: Ce3+ is less affected by host non-stoichiometry since Ce3+ ions predominantly occupy the YO8 sublattice. Overall, this study presents a novel approach to modulating the optical characteristics of garnet-type materials through non-stoichiometric variations, with potential implications for various technological applications.

5. **Laurikenas et al. (2020)** studied the impact of replacing lanthanum with yttrium in Yttrium Aluminum Garnets (YAG), specifically focusing on Y3-xLaxAl5O12 (YLuAG). These YLuAG materials were prepared through the sol-gel method and subjected to characterization using X-ray diffraction (XRD), solid-state nuclear magnetic resonance (NMR), and electron paramagnetic resonance (EPR) techniques. According to XRD the parity of YLuAG depends upon the quantity of lanthanum and as the content of lanthanum increased in YLuAG perovskite crystalline phase was

found and EPR revealed the presence of Ce^{3+} impurity. The emission spectra for YLuAG excitation at 450 nm obtained about 560 nm The study emphasizes the vital role of solid-state NMR and EPR methods in investigating the processes and properties of recently synthesized Y3-xLaxAl5O12 compounds.

6. **Jasmeen et al. (2020)** studied the Gadolinium Aluminum Garnet (GAG) doped with Eu prepared by using the sol-gel method and annealed at 1100^0C. XRD for GAG-Eu observed there was no supplementary phase same as pure host GAG and FT-IR observed various peaks in the 400 to 700cm^{-1} range. The study resulted in the particle size around 70nm with immense emission spectra so, GAG-Eu will be useful for the emission of visible light.

7. **Bolek (2020) et al.** has compared the luminescent properties of nanopowder (NP), thin film, and single crystalline films (SCFs) of terbium aluminum garnets (TAG) by using cathodoluminescence (CL) and photoluminescence (PL). The preparation of NPs, 300 nm NP thin films, and SCFs done by combustion synthesis, spin coating process, and liquid phase epitaxial respectively. CL spectra show the applicability of TAG NP films in CL and micro imaging as it has a peak near 550-580 nm and PL spectra for TAG noticed a peak about 307-350 nm which reveals its thermodynamic uncertainty. Besides this in SCFs of TAG UV bands were completely missing. so, these can be favorable to study the luminescence of TAG.

8. **L.V. Taralaet al.(2022)** prepared a $Y_{3-x}Ce_xAl_5O_{12}$ sample to check the effect of doping concentration and sintering temperatures on the luminescent. Observed the phase and structure of YAG remains unaltered, but the transmittance and conductivity increased. The luminescence intensity was found altered by the doping concentration (0.01-0.025) and sintering temperature of 1675-1725^{o}C as well. Additionally, the study detected a cerium concentration-dependent shift of the luminescent band peak from 535 to 545 nm, along with a decrease in the bandwidth as the vacuum sintering temperature

increased from 1675 to 1725 °C. These findings deliver insights into the ability to fine-tune the transparency and luminescent spectrum of YAG:Ce ceramics through the careful selection of vacuum sintering parameters and activator concentration, which has practical implications for the development of efficient luminescent materials in applications like high-power LEDs.

9. **Popoviciet al.(2022)** investigated the properties of prepared samples by sol-gel method and various characterizations done. The band gap of yttrium aluminate was found near 4.77 eV and for lanthanum aluminate, it was 5.47 eV and found that YAO has broad UV absorption as compared to the LnAO. The emission spectra revealed higher and wider emission intensity in the visible region of LnAO rather than YAO. The study concluded due to the presence of the YAG phase in Yttrium aluminate they possess more applicability in dyes by wastewater.

10. **Zhanturinaet al.(2023)** prepared the YAG: Eu by solid-state method. The prepared material was excited by 298 nm and observed a number of peaks in the 500-800 nm region due to the transitions of Eu. The intensity of peaks totally depends upon the doping concentration of Eu not on the host. Observed that the band gap of the material decreases with the rise of doping concentrations of Eu in YAG.

11. **Skruodieneet al.(2022)**prepare the YAG: Eu by adding yttrium vanadate by using the sol-gel method and mixing manually to both. The study observed that the impurity phase was obtained in XRDC due to YVO and PL spectra observed under the excitation 395 nm. The spectra found multiple dominant peaks due to YVO and two peaks at 589 nm and 709 nm in the YAG: Eu which are due to Eu3+. The decay time also gets increased because of the addition of YVO in YAG: Eu.

12. **Varela et al.(2021)** synthesized using solid-state reaction sintered at 1200ºC , to analyze its optical and structural properties. Absorption band observed at 450 nm due to 4f ($^2F_{5/2}$) → ^2E_g ($5d_1$) Ce3+ transition and emission spectra observed under the 436 nm (blue) excitation 450 nm, thus observed the broad emission band in 450-600 nm. the broadening of the band mentioned due to the Strong phonon coupling. Due to the doping of Fe3+, the band gap of the material falls strongly, and green to orange emission is observed by Ce3+. The CIE coordinates and color purity for the highest concentration of Ce3+ are (0.4817, 0.510) and 95.2% respectively. The color purity of the material increased with the rise of doping concentration.

13. **Zhao et al. (2021)** synthesized the $Tb_{2.93}Al_5O_{12}$: $0.07Ce^{3+}$ phosphor using soldi-state method and sintering at 1500ºC temperature. Pure and better phase formed at 1500ºC. A photoluminescence spectrum consists of a broad emission peak near 553 nm which exhibits yellow light by the excitation of blue light at 450 nm. The observed CIE coordinates (0.4709, 0.51175) were reported as favorable for WLED in blue light.

14. **Dai et al. (2021)**Y3(Al,Ga)5O12 (YAGG) materials doped with Ce3+, Cr3+, and Pr3+ were synthesized via the Pechini method, and the impact of varying annealing temperatures on their properties was investigated. The results indicated that as the annealing temperature increased, the crystalline size exhibited a simultaneous increase and broadening. This observation was substantiated by both X-ray diffraction (XRD) and transmission electron microscopy (TEM) analyses. The FTIR revealed that with increasing temperature O-H group vanished which can enhance the luminescence. The PL spectra were taken at the 405 nm blue excitation and observed the peaks at 520 nm due to Ce3+, 690 nm due to Cr3+, and 606 nm due to Pr3+ transition, thus found the energy gets transferred from Ce3+ to the Cr3+/Pr3+.

15. **Lee et al.(2021)** prepared the [(Gd0.6Lu0.4)0.99Ce0.01]3Al5O12 with sintering at 1300ºC and XRD confirmed the phase of garnet with a cubic and high crystalline

structure. The optical analysis by PL spectra revealed that at the excitation 571 nm,an emission peak at 275 nm was observed due to the f-f transition of Gd3+ and other peaks at 342, 453 and 506 nm are due to the transition of Ce3+. The study concluded that with the rise in annealing temperature, the crystallinity and the PL properties were found to be increased.

16. **Sun et al.(2020)** synthesized the (Gd,Lu)3Al5O12:Ce by co-precipitation method sintered at high temperature 1715ºC. the PL spectra for prepared material show the strong emission in the region 490-750 nm under the excitation wavelength 457 nm and two emission peaks at 568 and 630nm are due to the Ce3+ electronic transition. Quantum yield was found to improve with the enhancement in PL intensity and the lifetime of the material was found 1.7 ns for powder phosphor. The material found applicable for scintillation and luminescence.

17. **Meng et al.(2020)** fabricated the (Gd,Lu)3Al5O12:Ce garnet material by using the gel combustion method sintering at 1100ºC and investigating the effect of substituting Mg or Si on the optical behavior and preparation of material. The XRD results reveal that average crystalline size increases with increasing concentration of Mg/Si in GAG garnet and also found that activation energy lowers with the substitution corresponding to sintering temperature. The PL spectra observed under the excitation 460 nm and material showed the broad emission in region 450-750 nm. CIE coordinated shifted towards the red region on the chromaticity diagram.

18. **Carvalohet al.(2019)** synthesized the (Y2.99- xGdx)Al5O12 doped with Eu3+ via the sol-gel methodand XRD analysis showed that the cubic structural phase of garnet remains attained by material while Y replaced the Gd. The crystalline size lies between 26 to 32 nm. The UV spectra showed broad and strong bands around 206 nm, 267 nm, and 220 nm and a band gap between 5.6 eV to 6.5 eV. The PL spectra observed by excitation 220 nm had strong emission peaks at 590nmand 707 nm due to $^{5}D_{0} \rightarrow {}^{7}F_{1}$

and $^{5}D_0 \rightarrow {}^{7}F_4$ transition of Eu3+ and also reveals that Gd substitution caused the change in peak positions. The Gd concentration rises and the band gap of the material is found to decrease along it.

19. **Hakeem et.al(2019)** prepared Y2-xLaCaGa3ZrO12:xLn3+ phosphor using solid-state reaction method. Structure and photoluminescence properties observed by X-ray diffraction, Rietveld refinement, and photoluminescence. Observed that garnet is a cubic crystal structured in la3d space group, Y/La/Ca, Y/Ga, and Ga/Zr cations had the dodecahedron, octahedron, and tetrahedron sites, respectively. The doping Eu and Tb showed the deep red and green color light emission for garnet respectively. This study revealed the application of Y2-xLaCaGa3ZrO12:xLn3+ phosphors in optoelectronic devices as like LEDs.

20. **Ding (2018) et al.** studied the electrical, optical, and luminescence properties of terbium aluminum garnets (TAG) and terbium scandium aluminum (TSAG) theoretically and experimentally, which have gained substantial attention due to their versatile applications. Compared optical band gap calculated by using the DFT theoretical approach and experimentally. Both TAG and TSAG have a direct band gap of 4.46 and 4.05eVrespectively. Experimental data, including band gaps, refractive indices, and reflectivity, were found to be in excellent agreement with the theoretical predictions. The luminescence properties of TSAG were discovered, with a specific focus on its potential as a visible phosphor and laser matrix. Judd-Ofelt theory provided insights into the radiative transitions of Tb-4f configurations, yielding three Judd–Ofelt intensity parameters of 4.47, 1.37, and 4.23×10-20 cm^2, respectively. These findings contribute to a fundamental understanding of TAG and TSAG garnet materials, facilitating their further exploration in various applications

Table 2.1. Summary of work done on luminescent material for Solid-State White Light.

Sr .No.	Investigator (year)	Material Used	Experimental synthesis technique	Crystalline size/ Phase	Luminescence analysis findings			Application	Reference
					Excitation wavelength	Emission Wavelength	CIE/CCT/ CRI		
1	Kumar P et al (2023)	$Gd_{3-x}Al_5O_{12}:x\ Dy^{3+}$	Sol-Gel combustion method	20-80 nm/ single cubic phase	274 nm	Found blue emission at 4820nm, emission at 666, and due to $^4F_{9/2}\rightarrow{}^6H_J$ transition of Dy peak of yellow emission at 576 nm.		Applicable for WLEDs	[21]
2	Lin et al.(2023)	Ce/Mn/Cr : (Re,Y)3Al5O12	Solid-state reaction method		450 nm	Emission peaks by Ce3+ at 542-561 nm and 595 nm.	CIE-(0.483,0.511) CRI- 83.97 CCT- 3922	LED chips	[22]
3	C Ji et al. (2023)	GdAG:Ce	Solid –state method	20-60nm	528 nm	Peaks around 340 nm and Blue line emission peaks around 460 nm	CRI- 62.3 CCT- 3208	WLEDs	[23]

4	Zhang et al.(2023)	$Y_{2.96}Sm_{0.04}Ga_5O_{12}$ (YGG: Sm^{3+})	Optical Floating Zone method	1.201 nm lattice constant	613 nm and 407nm	For 613 nm -407 nm and 468 nm. For 407 nm- 572 nm,611 nm, and 654 nm.	CIE- (0.590,0.407) Color Purity- 85%	WLEDs and Orange red solid-state lasers.	[24]
5	Rathi et al. (2023)	YAG: Dy3+	Electrospinning technique	Cubic phase with Ia-3d space group. 130-160 nm average diameter.	483 nm	350nm and 365 nm .	CIE- (0.1308,0.1012) Color Purity- 91.7	Flexible devices, smart displays and light emitting applications.	[25]
6	Kumar et al.(2022)	Gd3-xAl5O12: xEr^{3+}	Sol-gel combustion technique	Cubic phase with la-3d space group and 18-30 nm.	278 nm	407 nm , 526 nm and strong peak at 548 nm.	CIE- (0.314,0.5790 CCT- 5836.16 Color Purity- 91.23%	Luminescent applications	[26]
7	Meng et al (2022)	$Gd_2LuAl_5O_{12}$:Ce	Sol-gel technique		450 nm	Emission peaks at 528 nm and 565 nm because of the $4f\text{-}5d^1$ transition line of Ce3+	CCT- 3625 k CRI- 95.2	w-WLED	[27]

8	Park et al. (2023)	Lu3Al5O 12: Ce3+	Sol-gel method	Cubic crystal structure With lattice volume near 1701 Å	521 nm	345 nm due to ^{2}f5/2- ^{2}d5/2 transition and 445 nm due to ^{5}f5/2-^{2}d3/2 transition of Ce3+.	CIE- (0.352,0.578) CCT- 5174 CP- 92.4	White LEDs	[28]
9	Park et al. (2022)C	Lu2.94Al 5O12:0.0 6Ce3+	Sol-gel method	Crystalline size increase with temperature from 45.7-115 nm.	515nm	350 and 444 nm due to transition lines of Ce3+	CIE- (0.345,0.627) (1600ºC) CCT-		[29]
10	Yang Qu et a. (2022)	Lu3GaxA l5− xO12: Ce3+	Solid-state reaction method	Crystalline size changes from 20-30 µm with rise in temperature.	450 nm	Broad Emission peak near 500 nm	CIE- (0.361,0.367) CCT- 4531K CRI- 89.5	WLEDs	[30]

11	Singh et al (2021)	Y3Al5O12: Dy3+	Solution combustion method with the use of Urea	Crystalline size varies between 40-50 nm with an increase of sintering temperature from 600-1050ºC.	352 nm	With 352 nm excitation strong emission was found at 480nmowing to 4 F9/2→6 F15/2 and 577 nm caused by 4 F9/2→6 F13/2 (577 nm) transition of Dy3+.	At 1050ºC CIE: (0.357,0.336) CCT: 4470 K CP:		[31]
12	Hu et al.(2021)	Gd3 (ScAl) 2Al3O12: Ce3+	Sol- gel technique	The lattice constant rises with the increase due to the increase in substitution of Sc/Al.	565 nm	The peak at 315-370 nm is due to 4f-5d_1 and 370-400 nm due 4f-5d_2 transition of Sc3+.	CIE: (0.379,0.370) CCT: 3981 CRI: 82.1	White-light illumination.	[32]
13	DU et al.(2021)	YAG: Ce	Solid-state method	Grain size decreases with the increase in doping concentration and falls between 21-5 µm.	450 nm and 525 nm	With 525 nm emission peaks found at 340 nm and 460 nm. At 450 nm broad emission peak was found at 530 nm.	At 0.0005 doping CIE: (0.331,0.382) CCT:5528 CRI: 62.8	LEDs	[33]

14	Ali et al.(2021)	Sm doped YAG	Co-precipitation method	Crystalline size is 30-40 nm shown from HRTEM and XRD.	360 nm	Peak at 567 nm (yellow) , 618 nm (orange),652 nm (red) and 712 nm.	CIE:(0.404,0.423) CCT: 3763 CRI: 86	Lighting Application	[34]
15	Yu.S et al.(2021)	(Gd,Y)AG:Mn2+, Ce3+	Solid state Reaction method	Particle diameter falls between 20-100 nm with respect to doping	585 nm and 461 nm	At 585 nm excitation peaks were found near 461 nm and 330 nm due to Mn3+ and Ce3+. At 461 excitation strong peak was obtained at 585 nm.	CIE: (0.49,0.50) CCT:2919	Use in the field of lighting	[35]
16	Tomalaet al.(2021)	$Gd_{2.97}Tb_{0.03}Ga_{5-x}Al_xO_{12}$	Pechini Method	At x=1 crystalline size is 124 nm and decreases with increase in doping concentration.	542.6 nm	Peak near 280nm and 330 nm due to forbidden transition of Tb3+.	At x=1 CIE: (0.341,0.489)		[36]

17	Ma.Y et al.(2021)	$Gd_3Sc_2Al_3O_{12}:Ce^{3+}$	Vacuum Sintering Technique	Crystalline size and lattice volume increase with doping concentration	460 nm and 578 nm	For 460 nm: peaks at 552 nm (strong) due to Ce3+. For 578 nm: peaks at 275nm,312 nm due to Gd3+.	CIE:(0.320,0.227) CCT:7766 CRI: 69.5	High power white LEDs	[37]
18	Zaman stal.(2019)	Gd-based doped with Dy3+	Melt quenching technique	Crystal glass thickness 0.44 cm.	575nm	Seven peaks at 324nm, 350nm, 365nm, 425nm, 452nm, and 472 nm due to Dy3+	At lowest conc. CIE:(0.36,0.40) CCT:4488	WLEDs	[38]
19	Baklanova et al.(2019)	Li6SrLa2-xEuxTa2O12	Solid-State reaction method	Large irregular particle-sized 1-20 μm	298 nm	Intense peaks at 609 nm owing to Eu3+ and peaks around 590 nm, 655 nm, and 708 nm.	CIE:(0.637,0.346) CCT: 2212 CP: 94.5%.	White LEDs	[39]
20	Wang et al.(2018)	[(Gd0.9Y0.1)0.9-xTb0.1Cex]AG	Co-precipitation method	Particle size near 40nm	546 nm	Major peaks at 223nm, 275 nm, and 327 nm due to transition pf Tb3+.	CIE: (0.43,0.53) CCT: 3853	Lighting and display devices	[40]

21	Chen et al.(2018)	(Gd0.97–xEuxTb0.03)AlO3	Co-precipitation method		617 nm	The broad peak at 263 nm due to Eu3+ and minor peaks at 320 nm, 367 nm, 377 nm and 395 nm .	CIE: (0.65,0.35) CCT: 2558	Lighting and display devices	[41]
22	Liu S. et al.(2018)	GAGG:Ce3+	Solid-state reaction method	Grain size 5-12μm	570 nm	Peaks around 340 nm and 455 nm due to Ce3+ and the narrow band near 275 nm due to Gd3+.	At 0.75 % of Ce3+ doping CIE:(0.289,0.202) CCT:3485 CRI:63.1	WLEDs or LEDs/ LD lighting.	[42]

Research Gap

While extensive research has been conducted on singly rare earth-doped garnets, there is a notable scarcity of investigations focused on transition metal co-doped garnets. To the best of our knowledge, no studies have been identified regarding the characterization of cubic aluminum garnet (CAG) both in its pure host state and when subjected to doping. This research gap highlights the potential for novel insights and advancements in the field of garnet-based materials, particularly in exploring the effects of transition metal co-doping on the properties of CAG.

Research Objectives

GAG (Gadolinium aluminum garnet, Gd3Al5O12) and CAG (Cerium aluminum garnet, $Ce_3Al_5O_{12}$) were investigated to study luminescence properties by doping/co-doping with transition metals.

1. To Synthesis of the un-doped and doped GAG and CAG by sol-gel.
2. To study the effect of singly and doubly doping of transition metal in CAG and GAG on excitation and emission spectra.
3. Qualitative analysis of emission response for solid-state light sources.

References

1. D. V. Bulyga, D. A. Gavrilova, S. K. Evstropiev, I. A. Arefina, M. K. Myagkih, and A. A. Shelemanov, "YAG: Ce Nanophosphors Synthesized by the Polymer–Salt Method for White LEDs with Isomorphic Substitution of Yttrium by Gadolinium," Cryst., vol. 13, no. 8, p. 1156, 2023.
2. V. Dubov, M. Gogoleva, R. Saifutyarov, O. Kucherov, M. Korzhik, D. Kuznetsova, I. Komendo, and P. Sokolov, "Micro-Nonuniformity of the Luminescence Parameters in Compositionally Disordered GYAGG: Ce Ceramics," Photonics, vol. 10, no. 1, p. 54, Jan. 2023.
3. L. Jiang, H. Qian, Z. Sun, T. Liang, M. Wang, H. Chen, and X. Wang, "Transparent (Gd, Lu)$_3$Al$_5$O$_{12}$: Dy Garnet Ceramics for Luminescence and White Led Applications," SSRN 4514294, 2023.
4. W. Cao, A. I. Becerro, V. Castaing, X. Fang, P. Florian, F. Fayon, D. Zanghi, E. Veron, A. Zandonà, C. Genevois, and M. J. Pitcher, "Highly Nonstoichiometric YAG Ceramics with Modified Luminescence Properties," Adv. Funct. Mater., vol. 33, no. 14, p. 2213418, 2023.
5. A. Laurikenas, D. Sakalauskas, A. Marsalka, R. Raudonis, A. Antuzevics, V. Balevicius, A. Zarkov, and A. Kareiva, "Investigation of lanthanum substitution effects in yttrium aluminium garnet: importance of solid-state NMR and EPR methods," J. Sol-Gel Sci. Technol., vol. 97, pp. 479-487, 2021.
6. J. Kaur, S. Rani, and B. Lal, "Luminescence properties of Eu^{3+} doped gadolinium aluminum garnet phosphors," Optik, vol. 212, p. 164745, 2020.
7. P. Bolek, J. Zeler, V. Gorbenko, T. Zorenko, P. Popielarski, K. Bartosiewicz, A. Osvet, M. Batentschuk, E. Zych, and Y. Zorenko, "Luminescent properties of nanopowder and single-crystalline films of TbAG: Ce garnet," phys. status solidi (b), vol. 257, no. 8, p. 1900495, 2020.

8. L. V. Tarala, A. A. Kravtsov, O. M. Chapura, V. A. Tarala, D. S. Vakalov, F. F. Malyavin, S. V. Kuznetsov, V. A. Lapin, L. V. Kozhitov, and A. V. Popkova, "Effect of vacuum sintering conditions on the properties of $Y_3Al_5O_{12}$: Ce luminescent ceramics," Mod. Electron. Mater., vol. 8, no. 3, pp. 123-130, 2022.
9. I. C. Popovicia, A. Diaconb, F. Moscaluc, and A. Dumbravaa, "A comparative study of the properties of yttrium and lanthanum aluminates obtained by Pechini sol–gel process," J. Ovonic Res., vol. 18, p. 259, 2022.
10. N. Zhanturina, D. Sergeyev, Z. Aimaganbetova, A. Zhubaev, and K. Bizhanova, "Features of the Spectroscopic Characteristics of Yttrium–Aluminum Garnets Doped with Europium at Different Concentrations," Cryst., vol. 13, no. 4, p. 702, 2023.
11. M. Skruodiene, R. Juodvalkyte, M. Kemere, R. Ramanauskas, A. Sarakovskis, and R. Skaudzius, "Enhanced optical properties of yttrium aluminum garnet with the yttrium vanadate impurity phase," Heliyon, vol. 8, no. 11, 2022.
12. C. F. Varela, Y. D. Molina, S. S. Gutiérrez, L. C. Moreno-Aldana, and C. P. Vargas, "Optical and structural properties of the Fe^{3+}-doped $Lu_3Al_5O_{12}$: Ce^{3+} garnet phosphor," RSC adv., vol. 11, no. 20, pp. 11804-11812, 2021.
13. L. Zhao, W. Kunyao, W. Yanan, C. Jing, W. Yongfeng, and L. Yuanyuan, "Synthesis and luminescence properties of yellow-emitting phosphor $Tb_{2.93}Al_5O_{12}$: 0.07 Ce^{3+} under blue light excitation," Ferroelectrics, vol. 582, no. 1, pp. 63-69, 2021.
14. Z. Dai, V. Boiko, K. Grzeszkiewicz, M. Markowska, F. Ursi, J. Hölsä, M. L. Saladino, and D. Hreniak, "Effect of annealing temperature on persistent luminescence of $Y_3Al_2Ga_3O_{12}$: Cr^{3+} co-doped with Ce^{3+} and Pr^{3+}," Opt. Mater., vol. 111, p. 110522, 2021.
15. J. H. Lee, J. G. Li, B. N. Kim, Q. Meng, X. Sun, and B. K. Jang, "Effect of annealing on microstructure and luminescence characteristics in spark plasma sintered Ce^{3+}-activated $(Gd, Lu)_3Al_5O_{12}$ garnet ceramics," J. Eur. Ceram. Soc., vol. 41, no. 2, pp. 1586-1592, 2021.

16. Z. Sun, Z. Chen, M. Wang, and B. Lu, "Production and optical properties of Ce^{3+}-activated and Lu^{3+}-stabilized transparent gadolinium aluminate garnet ceramics," J. Am. Ceram. Soc., vol. 103, no. 2, pp. 809-818, 2020.
17. Q. Meng, X. Wang, Q. Zhu, and J. G. Li, "The effects of Mg^{2+}/Si^{4+} co-substitution for Al^{3+} on sintering and photoluminescence of $(Gd, Lu)_3Al_5O_{12}$: Ce garnet ceramics," J. Eur. Ceram. Soc., vol. 40, no. 8, pp. 3262-3269, 2020.
18. I. D. S. Carvalho, A. I. D. S. Barbosa, A. J. Silva, P. A. Nascimento, A. B. Andrade, D. V. Sampaio, D. O. Junot, T. R. da Cunha, L. M. Jesus, R. S. Silva, and M. V. D. S. Rezende, "Structural and photoluminescence properties of Eu^{3+}-doped $(Y_{2.99}-xGd_x)Al_5O_{12}$ phosphors under vacuum ultraviolet and ultraviolet excitation," Mater. Chem. Phys., vol. 228, pp. 9-14, 2019.
19. D. A. Hakeem, D. H. Kim, S. W. Kim, and K. Park, "Crystal structure and photoluminescence properties of novel garnet Y_2-$xLaCaGa_3ZrO_{12}$: xLn^{3+} (Ln= Eu and Tb) phosphors," Dyes Pigm., vol. 163, pp. 715-724, 2019.
20. S. Ding, H. Zhang, R. Dou, W. Liu, D. Sun, and Q. Zhang, "Theoretical and experimental studies of electronic, optical and luminescent properties for Tb-based garnet materials," J. Solid State Chem., vol. 263, pp. 123-130, 2018.
21. P. Kumar, S. Singh, I. Gupta, K. Nehra, V. Kumar, and D. Singh, "Structural and luminescent behaviour of Dy (III) activated $Gd_3Al_5O_{12}$ nanophosphors for white-LEDs applications," Mater. Chem. Phys., vol. 295, p. 127035, 2023.
22. H. Lin, H. Teng, S. Hanson, Z. Liu, C. Pang, and J. Jiang, "Ce/Mn/Cr:$(Re, Y)_3Al_5O_{12}$ Phosphor Ceramics (Re= Gd, Tb and Lu) for White Led Lighting with Significant Spectral Redshift and Improved Color Rendering Index."
23. C. Ji, H. Su, Z. Huang, X. Tian, T. Zeng, H. He, J. Xu, J. Wen, and Y. Peng, "GdAG: Ce fluorescent ceramic formed by aqueous tape casting and isostatic pressing process for WLED applications," Appl. Phys. A, vol. 129, no. 5, p. 375, 2023.
24. H. Zhang, Z. Zhu, S. Ta, N. Zeng, L. Wu, W. Wu, P. Zhang, S. Xu, B. A. Goodman, and W. Deng, "Highly Efficient Orange-Red Emission in Sm^{3+}-Doped Yttrium Gallium Garnet Single Crystal," Cryst., vol. 13, no. 8, p. 1273, 2023.

25. K. A. Rathi, T. A. Rathi, S. S. Kondawar, S. R. Dhakate, and S. B. Kondawar, "Influence of La^{3+} co-doping on the photoluminescence properties of YAG: Dy^{3+} electrospun light emitting nanofibers," Results Opt., vol. 12, p. 100492, 2023.
26. P. Kumar, S. Singh, I. Gupta, K. Nehra, V. Kumar, and D. Singh, "Structural refinement and optical characteristics of single-phase $Gd_3Al_5O_{12}$: Er^{3+} nanophosphors for luminescent applications," J. Lumi., vol. 252, p. 119338, 2022.
27. Q. Meng, G. Zhao, Q. Zhu, X. Sun, and J. G. Li, "Remarkable structure and luminescence regulation of a $Gd_2LuAl_5O_{12}$: Ce garnet phosphor with a Ca^{2+}/Si^{4+} pair for high-quality w-WLED lighting," Dalton Trans., vol. 51, no. 8, pp. 3159-3169, 2022.
28. K. Park, H. Kim, D. H. Kim, and S. Y. Gwon, "Influence of lattice distortions on the emission wavelengths of Y^{3+}– and Gd^{3+}–substituted $Lu_3Al_5O_{12}$: Ce^{3+} phosphors," Ceram. Int., vol. 49, no. 10, pp. 15176-15182, 2023.
29. K. Park, H. Kim, S. Y. Gwon, G. W. Jung, and S. W. Kim, "Photoluminescence improvement of $Lu_3Al_5O_{12}$: Ce^{3+} phosphors by controlling synthesizing temperature and adding fluoride fluxes," Ceram. Int., vol. 48, no. 22, pp. 33848-33860, 2022.
30. M. Y. Qu, T. Q. Li, and Q. L. Liu, "Photoluminescence Properties of Cyan-Emitting $Lu_3GaxAl_{5-x}O_{12}$: Ce^{3+} Garnet Phosphors Synthesized in Nonreducing Atmosphere and at Different Temperature for High Quality w-LEDs," Materials, vol. 15, no. 19, p. 6817, 2022.
31. S. Singh, A. P. Simantilleke, and D. Singh, "Crystal structure and photoluminescence investigations of $Y_3Al_5O_{12}$: Dy^{3+} nanocrystalline phosphors for WLEDs," Chem. Phys. Lett., vol. 765, p. 138300, 2021.
32. C. Hu, G. Liu, M. Wang, S. Ma, J. Zhang, J. Wu, G. Jing, S. Wang, and Z. Ye, "Preparation and characterization of $Gd_3(ScAl)_2Al_3O_{12}$: Ce^{3+} garnet phosphors towards high-color-rendering white-light illumination," J. Lumin., vol. 235, p. 118062, 2021.

33. A. Du, Q. Du, X. Liu, Y. Yang, C. Xia, J. Zou, and J. Li, "Ce: YAG transparent ceramics enabling high luminous efficacy for high-power LEDs/LDs," J. Inorg. Mater., vol. 36, no. 8, 2021.
34. H. Ali, P. Masschelein, S. Bruyere, P. Pigeat, A. Dauscher, H. Rinnert, D. Horwat, M. A. Khedr, and A. E. Giba, "White light emission from Sm-doped YAG ceramic controlled by the excitation wavelengths," Opt. Laser Technol., vol. 142, p. 107223, 2021.
35. S. Yu, Q. Chen, Y. Lu, B. Cao, J. Li, and Z. Liu, "Synthesis, luminescent properties and crystal stabilization of GdAG: Mn^{2+}/Ce^{3+} via Y^{3+} doping for warm w-LED application," Opt. Mater., vol. 111, p. 110566, 2021.
36. R. Tomala, K. Korkus, V. Boiko, D. Hreniak, and P. Głuchowski, "Electronic structure engineering of $Gd_{2.97}Tb_{0.03}Ga_{5-x}Al_xO_{12}$ persistent luminescence phosphors," J. Alloys Compd., vol. 889, p. 161745, 2021.
37. Y. Ma, L. Zhang, J. Huang, R. Wang, T. Li, T. Zhou, Z. Shi, J. Li, Y. Li, G. Huang, and Z. Wang, "Broadband emission $Gd_3Sc_2Al_3O_{12}$: Ce^{3+} transparent ceramics with a high color rendering index for high-power white LEDs/LDs," Opt. Express, vol. 29, no. 6, pp. 9474-9493, 2021.
38. F. Zaman, G. Rooh, N. Srisittipokakun, T. Ahmad, I. Khan, M. Shoaib, J. Rajagukguk, and J. Kaewkhao, "Comparative investigations of gadolinium based borate glasses doped with Dy^{3+} for white light generations," Solid State Sci., vol. 89, pp. 50-56, 2019.
39. Y. V. Baklanova, L. G. Maksimova, O. A. Lipina, A. P. Tyutyunnik, A. Y. Chufarov, and V. G. Zubkov, "A red-emitting phosphor based on Eu^{3+}-doped $Li_6SrLa_2Ta_2O_{12}$ garnets for solid state lighting applications," Mater. Res. Express., vol. 6, no. 6, p. 066201, 2019.
40. W. Wang, J. Li, X. Teng, and Q. Chen, "Luminescence properties of Y^{3+} stabilized $Gd_3Al_5O_{12}$: Tb^{3+}/Ce^{3+} phosphors with yellow light-emitting for warm white LEDs," J. Lumin., vol. 202, pp. 176-185, 2018.

41. Q. Chen, J. Li, and W. Wang, "Synthesis and luminescence properties of Tb^{3+}/Eu^{3+} co-doped $GdAlO_3$ phosphors with enhanced red emission," J. Rare Earths., vol. 36, no. 9, pp. 924-930, 2018.
42. S. Liu, P. Sun, Y. Liu, T. Zhou, S. Li, R. J. Xie, X. Xu, R. Dong, J. Jiang, and H. Jiang, "Warm white light with a high color-rendering index from a single $Gd_3Al_4GaO_{12}$: Ce^{3+} transparent ceramic for high-power LEDs and LDs," ACS Appl. Mater. Interfaces., vol. 11, no. 2, pp. 2130-2139, 2018.

Chapter 3

Research Methodology

3.1 Introduction

The garnets are now produced synthetically for a variety of applications in various areas like industry, scientific field, and technical. These are expanding ahead of their original function as gemstone replicas. The encroachment in synthesis techniques has performed a fundamental job in matching the demands of modern applications such as magnetic material, solid-state lighting, laser systems, and many more. From past research found that various methods used to prepare garnets for instance solid-state reaction method, sol-gel auto combustion methods, forced hydrolysis method, homogeneous precipitation method, and hydrothermal method, etc. The Solid-State method known for its simplicity and used for bulk materials and hydrothermal synthesis is suitable for controlling crystal growth and solubility but at high temperatures. After that Sol-gel auto combustion is the single step synthesis method utilized for production of voluminous, fine powder particularly in the realm of materials science and chemistry. Moreover, forced hydrolysis method also used to prepare nanoparticles concluded controlled hydrolysis of mrtal precursor under precise conditions and it require intensive energy and complex conditions to prepare pure material. However, among all these sol-gel method is the more advantageous and demanding method due to its versatility and capability to form homogeneous material at low temperatures. Therefore, the current research employs the sol-gel method to fabricate the material. The focus of the current work is on the Gadolinium Aluminum garnet (GAG) and Cerium Aluminum Garnet (CAG) and their single and double doping with transition metals alike: Cobalt (Co) and Chromium (Cr). The Co and Cr have been added in tandem to both the garnets. This work examines the structural and optical properties of GAG and CAG host and transition metal-doped GAG and CAG are investigated. The purity and homogeneity of material are prerequisites for the exploration of these properties of material via the sol-gel technique of both the GAG and CAG host as well as for Cobalt and Chromium doped

GAG and CAG materials and the synthesis method affects the structural as well as optical properties of material. The synthesized material was examined via XRD, FTIR, UV-Vis Spectroscopy, and Fluorescence Spectroscopy.

3.2. Sol-Gel Method

The sol-gel method also known as the wet chemical process is used to create a variety of metal oxides and nanostructures. There are undoubtedly many other techniques that might be used to create nanoparticles, but the sol-gel approach has a high demand in both academic and commercial settings due to its extremely distinctive characteristics. This technique seems effective for producing fibers and powder. The materials produced by the sol-gel process are of good purity and composition, and share many of the same chemical and physical characteristics as experimental materials. The technique might be used to simultaneously produce two or more various types of nanoparticles. Consequently, alloy compounds may be created by combining the various metal oxide precursors in the right proportion. Several processes or several chemically irreversible actions are performed to create the end product in this approach, which creates nanoparticles from a precursor. Sol-gel method involves the following steps:

In the first step the metal salts are individually dissolved in water to produce a clear solution, and then combined while being continually stirred and heated. This process is known as hydrolysis and poly-condensation. Then, the next step of Chelation and gel formation involves the addition of a chelating agent, such as citric acid, to the prepared mixture, and continuing to heat and agitate it at a sufficient temperature will result in the creation of a sol. After that Gelation is the most significant phase in the sol-gel process, in which generated sol after some time converts into a network of condensed colloidal clusters with micrometer holes. Moreover, Aerogel is created in the drying step where all pore liquids have been evacuated. The final step of the sol-gel method i.e. crystallization proceeds to the transformation of a substance into pure nanoscale powder, fibers, or films by heating. All these steps of the sol-gel method are shown in the figure below.

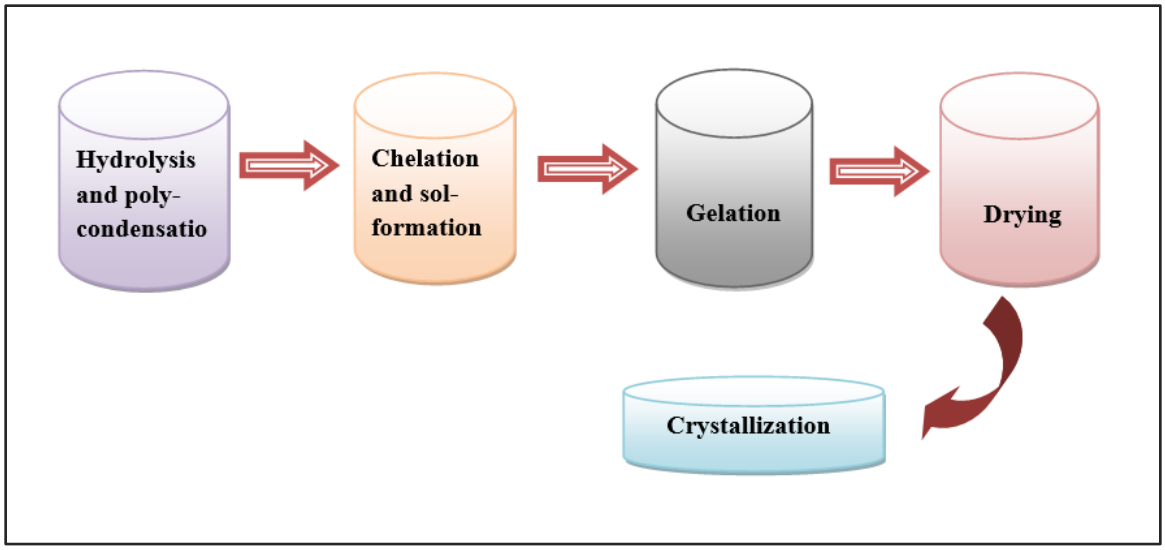

Fig 3.1. Flow diagram of steps implicated in the Sol-Gel method.

3.3. Materials and synthesis:

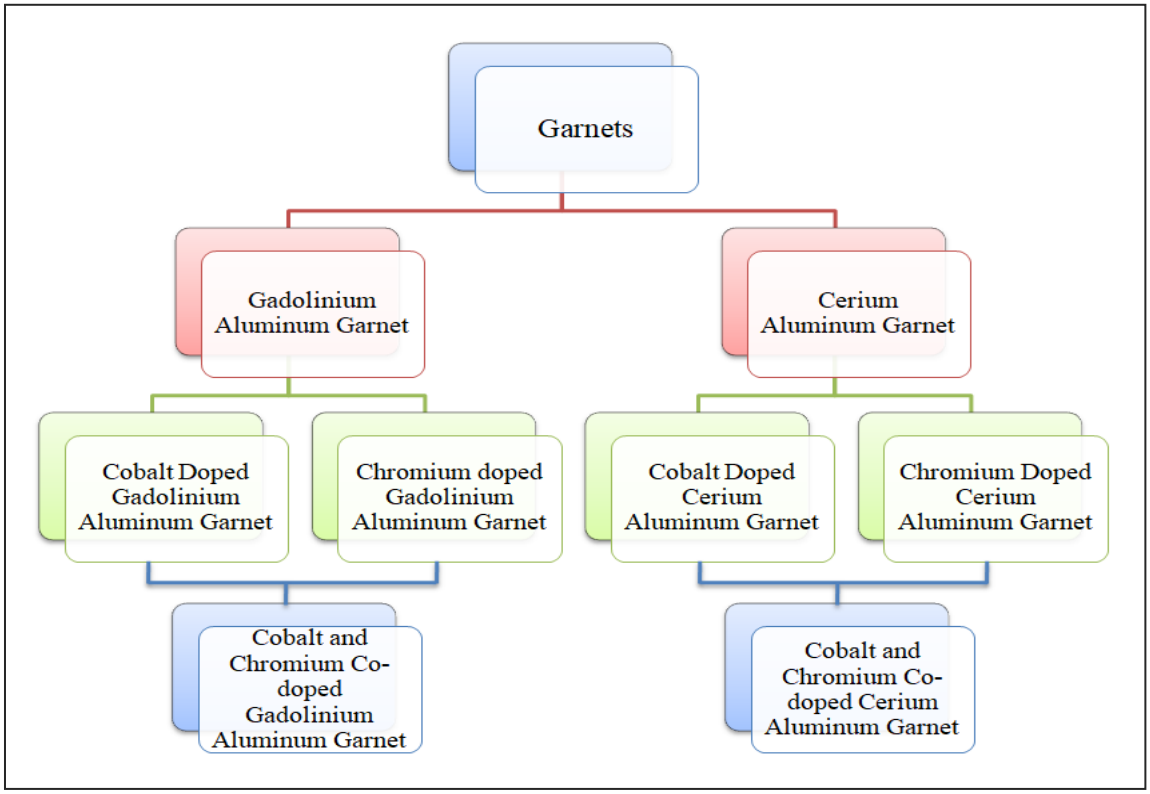

Fig 3.2. Hierarchy tree diagram of sample materials synthesized and prepared.

Table 3.1. List of chemicals used to prepare GAG and CAG pure host and doped samples.

Sr.No	Chemical name	Chemical Formula	Molecular Weight (g/mol)	Chemical Purity
1	Gadolinium Nitrate	$Gd(NO_3)_3.6H_2O$	343.26	99.9%
2	Cerium Nitrate	$Ce\ (NO_3)_3.6H_2O$	434.23	99.9%
3	Aluminum Nitrate	$Al(NO_3)_3.9H_2O$	375.13	98.0%
4	Citric Acid	$C_6H_8O_7.H_2O$	210.14	99.5%
5	Cobalt Nitrate	$Co(NO_3)_2.6H_2O$	291.03	98.0%
6	Chromium Nitrate	$Cr(NO_3)_3.9H_2O$	400.15	98.0%

3.4. Synthesis of pure host and doped Gadolinium Aluminum Garnet (GAG) and Cerium Aluminum Garnet (CAG)

3.4.1 Synthesis of Gadolinium Aluminum Garnet (GAG)

Using the sol-gel technique, the gadolinium aluminum garnet host and doped GAG with Co and Cr were produced. Gadolinium nitrate and aluminum nitrate were each dissolved separately in 100 ml of distilled water, maintaining the proper stoichiometric ratio (3:5). The corresponding solutions were continually and independently stirred until a clear solution was seen at room temperature. Both solutions were combined, and the temperature was raised to between 60 and 70ºC while being constantly stirred by a magnetic field. A chelating agent, citric acid, in the quantity of 0.04 gm, was added to the solution after 3 hours of constant stirring and heating, and the resulting mixture was then heated and continuously stirred to evaporate water. After 8–10 hours, a gel that is a linked, stiff network with sub-micrometer-sized holes was produced. To dry the obtained gel, it was placed on a hot plate. The dried material was then placed in a motor pestle and ground into a fine powder. The sample that was prepared was subjected to drying in an oven set at 150°C for 4-5 hours. Subsequently, the sample was divided into four portions and sintered at temperatures of 500°C, 700°C, 900°C, and 1100°C.

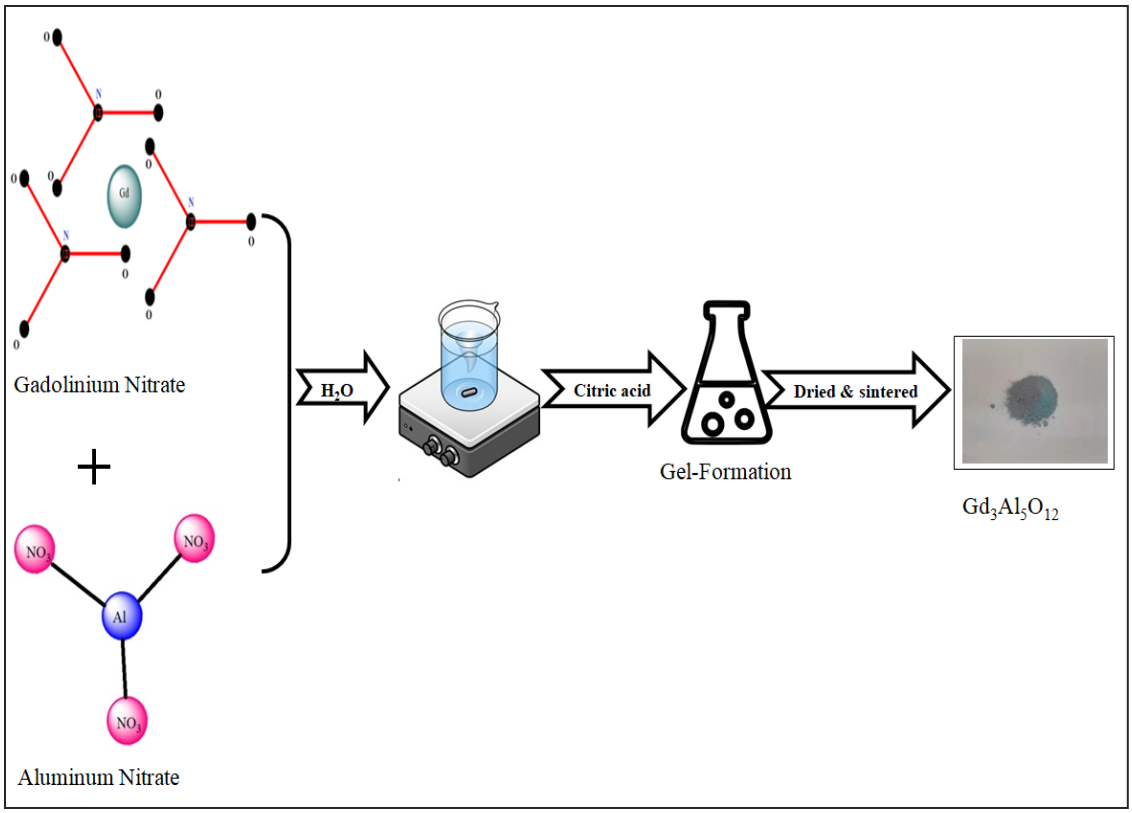

Fig 3.3. Pictorial representation for the synthesis of Gadolinium Aluminum Garnet via sol-gel method.

Table 3.2. List of GAG samples synthesized with different concentrations of Cobalt and Chromium.

Sr. No	Concentration of Chromium /Cobalt (wt %)	Sample composition(GAG:Cr)	Sample composition(GAG: Co)	Sintering Temperature (ºC)
1	0.2	$Gd_{2.8}Cr_{0.2}Al_5O_{12}$	$Gd_{2.8}Co_{0.2}Al_5O_{12}$	1100
2	0.4	$Gd_{2.6}Cr_{0.4}Al_5O_{12}$	$Gd_{2.6}Co_{0.4}Al_5O_{12}$	1100
3	0.6	$Gd_{2.4}Cr_{0.6}Al_5O_{12}$	$Gd_{2.4}Co_{0.6}Al_5O_{12}$	1100
4	0.8	$Gd_{2.2}Cr_{0.8}Al_5O_{12}$	$Gd_{2.2}Co_{0.8}Al_5O_{12}$	1100
5	1.0	$Gd_{2.0}Cr_{1.0}Al_5O_{12}$	$Gd_{2.0}Co_{1.0}Al_5O_{12}$	1100

3.4.2 Synthesis of Cobalt and Chromium doped Gadolinium Aluminum Garnet

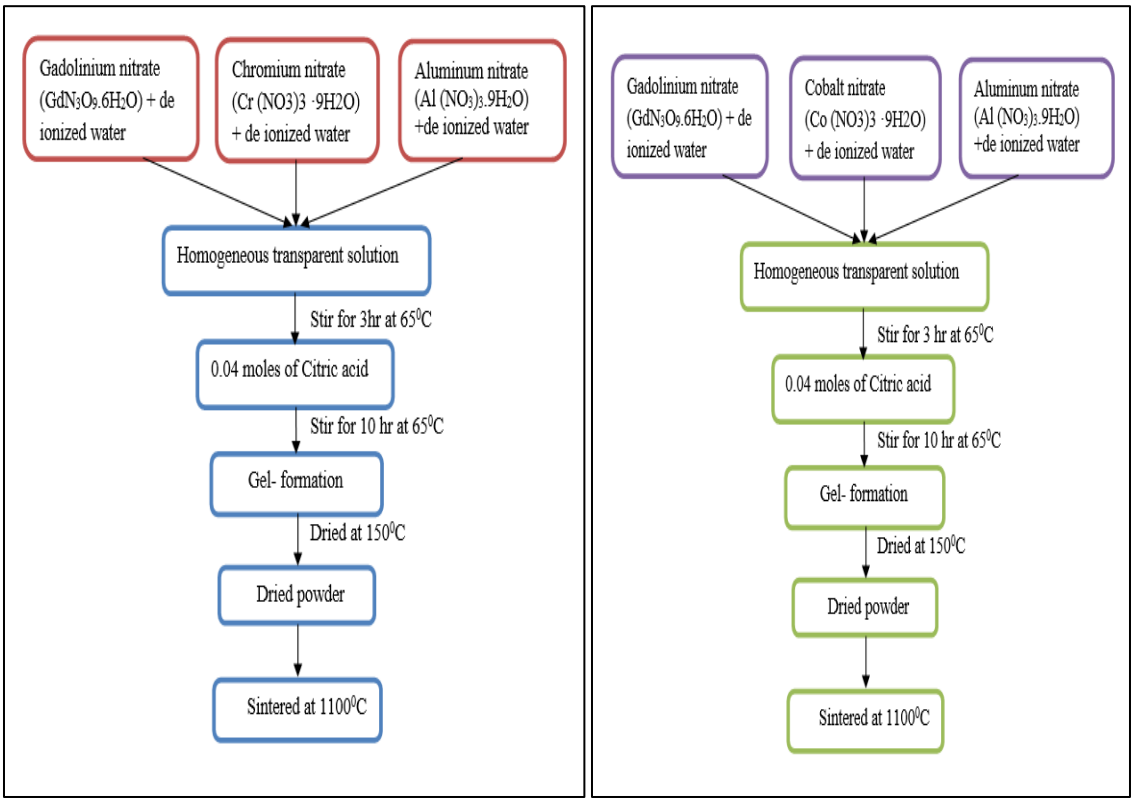

Fig 3.4. Typical flowchart for synthesis steps of GAG: Co and GAG: Cr by sol-gel method.

3.4.3 Synthesis of Cerium Aluminum Garnet (CAG)

To synthesize the CAG, Cerium Nitrate, and Aluminum Nitrate were first taken in distilled water at a stoichiometric ratio of 3:5 and mixed to create a transparent solution. Both solutions were combined to create a homogenous mixture, which was then heated and agitated for three hours. Then, citric acid was added, and the mixture was agitated at a temperature between 60 and 70°C until gel formation occurred. The prepared gel was placed on a hot plate and cooked until it turned into a powder. To get the ideal temperature for the garnet phase, the finished powder product was sintered at various temperatures.

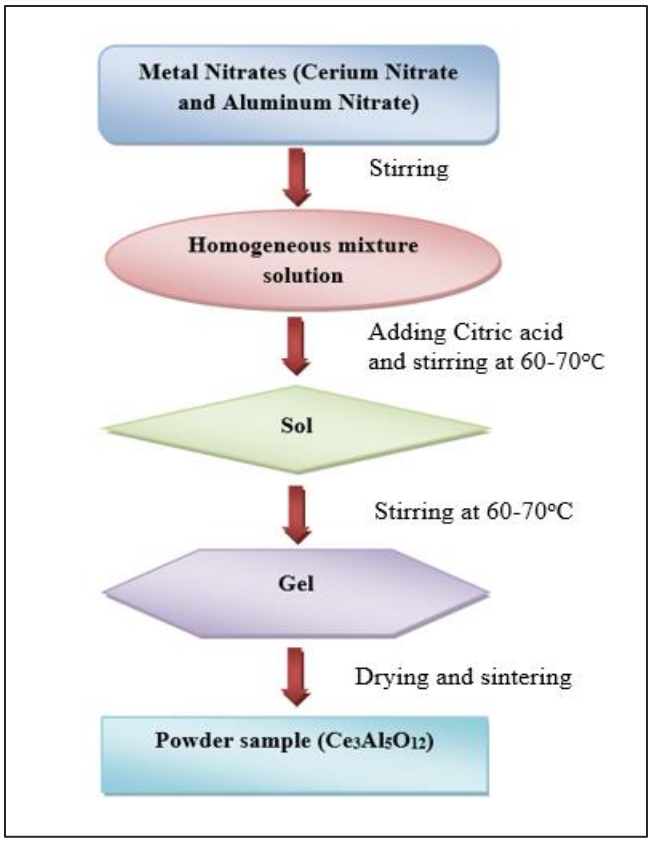

Fig 3.5. Flowchart representation of sequential steps in the synthesis of CAG by sol-gel method.

3.4.4. Synthesis of Chromium doped Cerium Aluminum Garnet (CAG: Cr) and Cobalt doped Cerium Aluminum Garnet (CAG: Co)

The preparation of CAG: Co and CAG: Cr followed a similar technique as used to employ for synthesis of the CAG host. However, for CAG: Cr Cerium nitrate, aluminum nitrate, and chromium nitrate were first individually dissolved in de-ionized water in an appropriate stoichiometric ratio. Similarly, CAG: Co was also synthesized using a similar technique by adding Cobalt nitrate in the place of Chromium nitrate. The samples were prepared with different concentrations of Chromium and cobalt shown in the table.

Table 3.3. CAG prepared samples with different doping concentrations of cobalt and chromium.

Sr. No	Concentration of Chromium /Cobalt (mol %)	Sample composition (CAG: Cr)	Sample composition (CAG: Co)	Sintering Temperature(^{o}C)
1	0.05	$Ce_{2.95}Cr_{0.05}Al_5O_{12}$	$Ce_{2.95}Co_{0.05}Al_5O_{12}$	1200
2	0.10	$Ce_{2.90}Cr_{0.10}Al_5O_{12}$	$Ce_{2.90}Co_{0.10}Al_5O_{12}$	1200
3	0.15	$Ce_{2.85}Cr_{0.15}Al_5O_{12}$	$Ce_{2.85}Co_{0.15}Al_5O_{12}$	1200
4	0.20	$Ce_{2.80}Cr_{0.20}Al_5O_{12}$	$Ce_{2.80}Co_{0.20}Al_5O_{12}$	1200

3.5. Characterization Techniques:

To explore the structural and optical attributes of all prepared GAG and CAG samples, a range of characterizations was conducted using various analytical tools, including XRD, FTIR, FE-SEM, TEM, UV-Vis Spectroscopy, and Fluorescence Spectroscopy.

3.5.1. X-Ray Diffractometer:

XRD is used to identify the phase of crystal material along with a couple of things like its crystallographic structure, chemical composition, and physical properties of prepared samples or material. It works on the principle of constructive interference of monochromatic X-ray and crystalline material. When subjected to incident X-rays, the sample interacts and generates diffracted rays that adhere to Bragg's law, indicating constructive interference. Bragg's law is

$$n\lambda = 2dsin(\theta) \ldots\ldots\ldots\ldots (3.1)$$

Where d is the spacing between the lattices λ denotes the wavelength of the X-ray, and the angle of diffraction is represented with θ. Lattice parameters like lattice constant, lattice strain, and crystal structure of garnets are calculated by using XRD data. XRD principle depends on the Braggs law.

Since the garnets have a cubic structure, a cubic crystal

$$\frac{1}{d^2} = \frac{h^2 + k^2 + l^2}{a^2}$$

$$\text{Thus, } a = \frac{\lambda}{2\sin\theta} (h^2 + k^2 + l^2)^{\wedge 2}$$

Where, 'a' is the lattice parameter, λ= 1.5405 Å and h k l are miller integers.

Now, crystalline size is considered by Scherer's equation:

$$D = \frac{k\lambda}{\beta cos\theta} \ldots\ldots\ldots\ldots (3.2)$$

Here, D represents the crystalline size, k is a constant (0.94), X-ray wavelength denotes by λ having value 1.5406 and β corresponds to the FWHM of peaks shown in the XRD pattern and θ is an angle between the incident and diffracted beams.

$$\delta = \frac{1}{D^2} \ldots\ldots\ldots\ldots\ldots\ldots (3.3)$$

Here δ denotes to the dislocation density which is the count of dislocation/displacement in a unit volume of crystalline material.

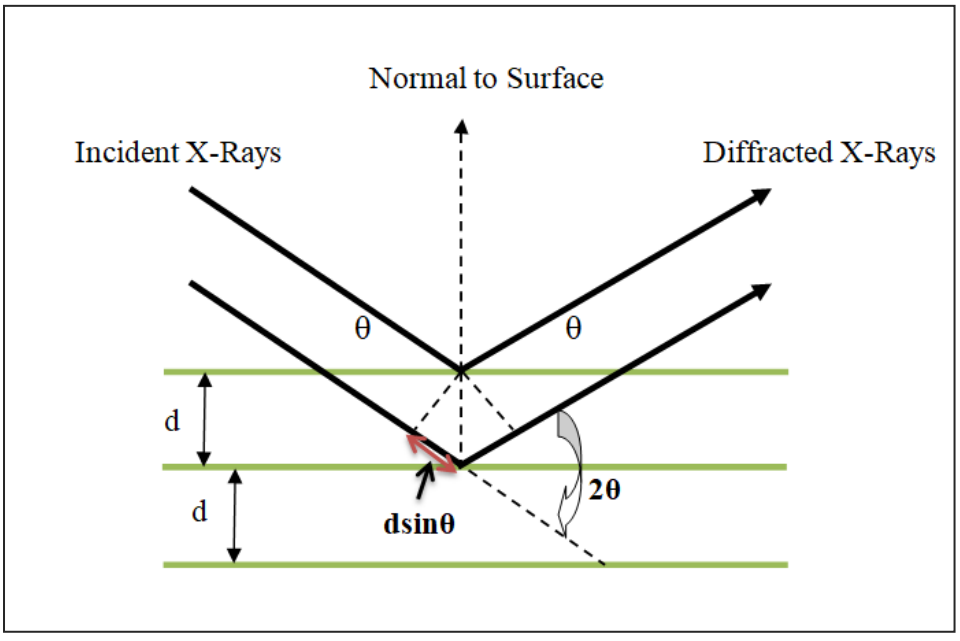

Fig 3.6. Working Principle of X-ray Diffraction.

XRD done with the Bruker Diffractometer in the range of 20°-80° using Cu-Kα radiations and Figure 3.7 shows the image of the Diffractometer and the typical XRD pattern obtained from the sample.

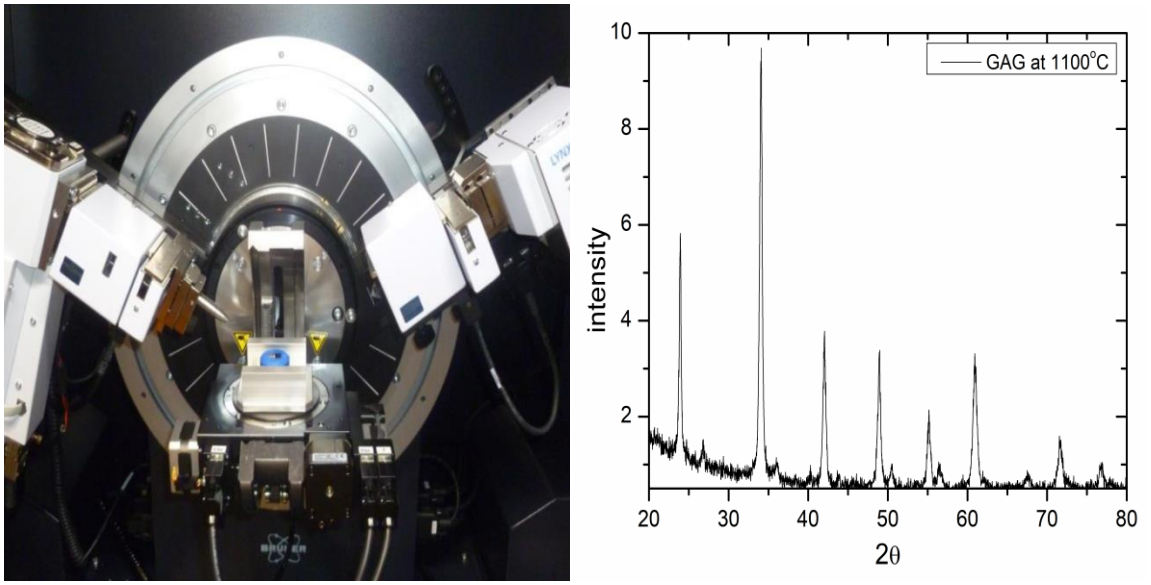

Fig 3.7.X-ray Diffractometer instrumental image and results of XRD pattern of GAG at 1100°C.

3.5.2. Fourier-Transform Infrared Spectroscopy (FTIR)

FTIR spectroscopy is utilized to get the IR spectra of emission or absorption of the sample and to identify the presence of the chemical functional groups, as well as the presence of unknown compounds in a sample. It operates on the principle that while the infrared (IR) radiations are used to pass through the sample, a portion of these radiations get absorbed by the sample, while the rest pass through the sample and are captured in the form of spectra.

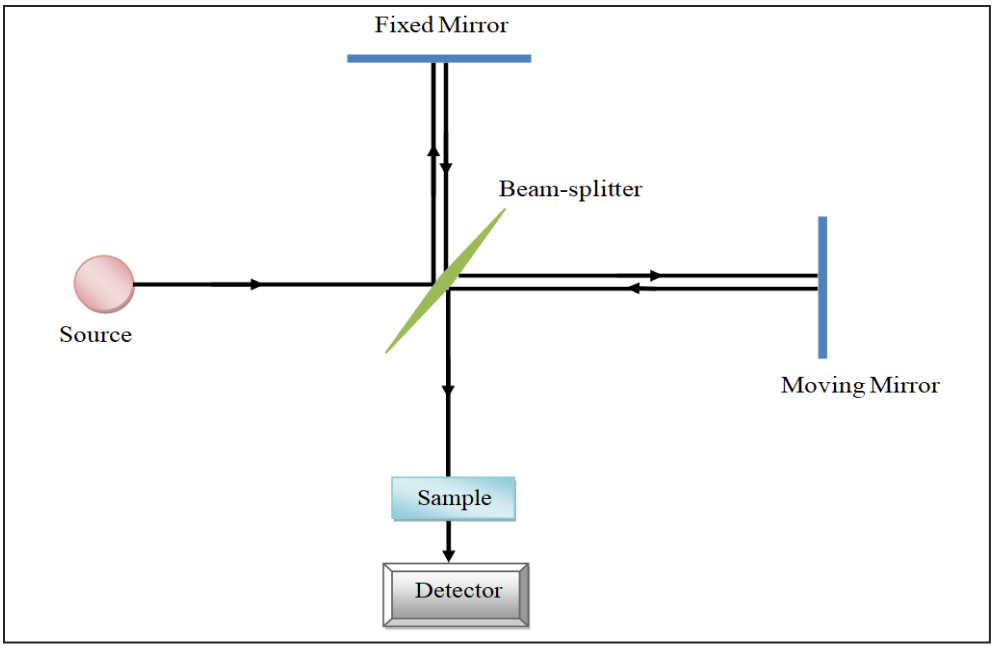

Fig 3.8. The pictorial representation for the working principle of FTIR.

The FTIR spectra were captured using PERKIN ELMER's spectrometer. A thin pallet of the mixture of sample and potassium bromide (KBr) was employed to examine the FTIR at room temperature and studies spanned under 4000 cm^{-1} to 400 cm^{-1}spectral range. The image of the spectrometer and spectra found from it are shown in the figure 3.9.

Table 3.4. Bonding or vibrations of functional group in FTIR spectra.

Sr. No.	Element Bonding/Vibration	Range (cm^{-1})
1	Gd-O	~423, 500, 556
2	Al-O	~598, 670, 648
3	Co-O	~492
4	H-O	~1400
5	C=O	~2344
6	Cr-O	~430-490
7	Ce-O	~836, 571
8	Nitrate vibrations	~1246,1330

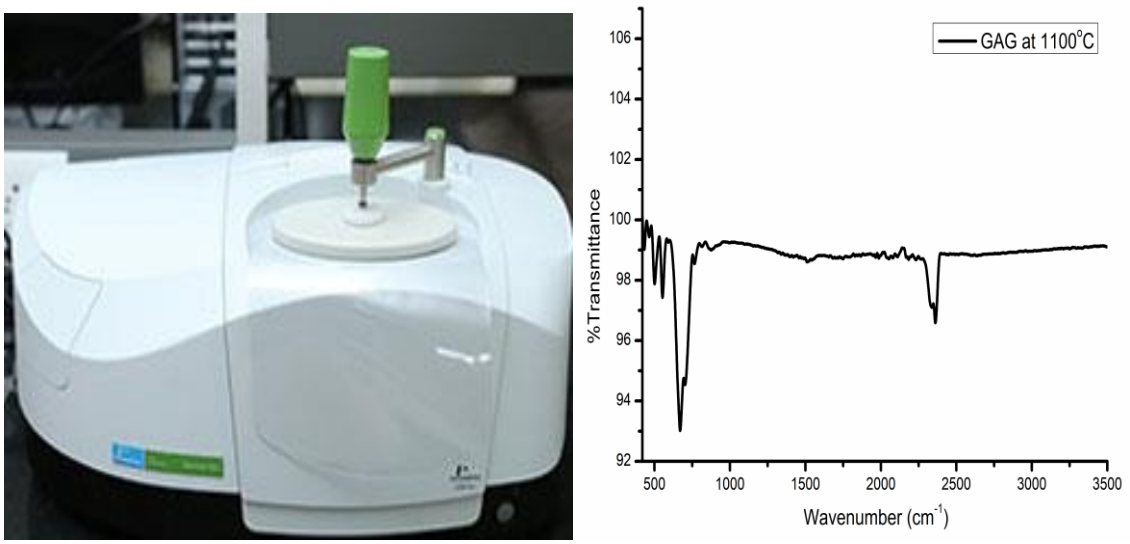

Fig 3.9.(a) Image of the FTIR (b) Typical FTIR spectrum of GAG at 1100°C.

3.5.3. Field Emission Scanning Electron Microscope (FESEM)

FESEM is an advanced technique used to capture the typical topographic image of the material with high magnification and unlimited depth of field and it produces a clearer and less distorted image of material with spatial resolution three to six times better than the conventional Scanning Electron Microscopy (SEM). Apart from this FESEM also can investigate contaminant spots with a reduced area at electron-accelerating voltages through Energy Dispersive Spectroscopy (EDX). EDX is also used for providing information on crystalline with a depth of a few nanometers of the material surface via an Electron Back Scattered Detection System (BDS) attached to a microscope.

The morphology of the prepared samples was analyzed using the JEOL JSM-7610F plus Field Emission Scanning Electron Microscope (FESEM), which has a magnification capability ranging from 25 to 1,000,000. The image of the FESEM instrument and the corresponding results of the material are given in the figure 3.10 below.

Fig 3.10. FESEM instrumental setup and view of results obtained from SEM.

3.5.4. UV-Vis Spectroscopy

When the radiations interact with matter (solid or liquid) the absorption or emission of atoms or molecules occurs, the absorption is typically measured with the UV- Vis spectrum. Light is the manifestation of energy, and when it is absorbed by matter, the atoms or molecules in the substance become energized. The incident photons from ultraviolet (UV) and visible light can lead to transitions between the various energy levels within specific molecules and atoms. The wavelength of absorbed light carries the requisite energy for elevating an electron by a lower energy level to a higher one. If the gap within these energy levels is larger, a higher amount of energy will be required for transition as Beer-Lambert's law asserts that the absorbance of light is directly proportional to both the path length and the concentration of the sample.

$$\alpha = \varepsilon L c$$

Where α is the amount of light absorbed, ε is the proportionality coefficient, L is the path length i.e. light covered a distance through the matter and c is the amount of sample or the concentration of absorbing species. The UV has an energy range of 200-400 nm and a visible range from 400-800 approximately.

The Wood-Tauc method as well as the Kubekla-Munk function (derived from the theory of P. Kubelka and F. Munk) utilized to determine the optical band gap. According to Wood-Tauc formula:

$$\alpha = \frac{A(h\upsilon - E_g)^n}{h\upsilon} \quad \ldots\ldots\ldots\ldots\ldots (3.4)$$

by equation the α denotes the linear absorption coefficient, E_g stands for optical band-gap energy and A is the constant. The type of transition determined by the value of "n" is, such as if value is ½ then, it is direct transitions, and for indirect it is 2. Now according to the Kubekla-Munk function:

$$R) = \frac{K}{S} = \frac{(1-R_\infty)^2}{2R_\infty} \ldots\ldots\ldots\ldots (3.5)$$

By substituting the F (R) in equation (1) in place of α, we get:F(R)or $\alpha = \frac{A(h\upsilon - E_g)^n}{h\upsilon}$

$$\alpha h\upsilon = A(h\upsilon - E_g)^n \ldots\ldots\ldots (3.6)$$

The plot of F(R)hυus hν used to calculate the optical band gap of the material.

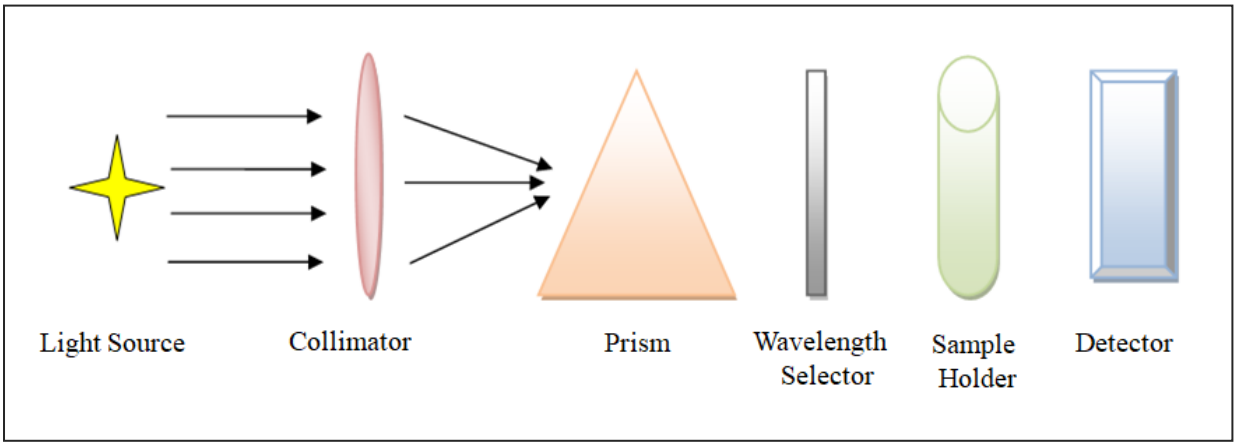

Fig 3.11. Working principle of UV-Vis absorption detector.

The Shimadzu UV-Vis Spectrophotometer was used for the UV-vis spectroscopy characterization of all the samples. The Image of the apparatus and its corresponding results are shown below.

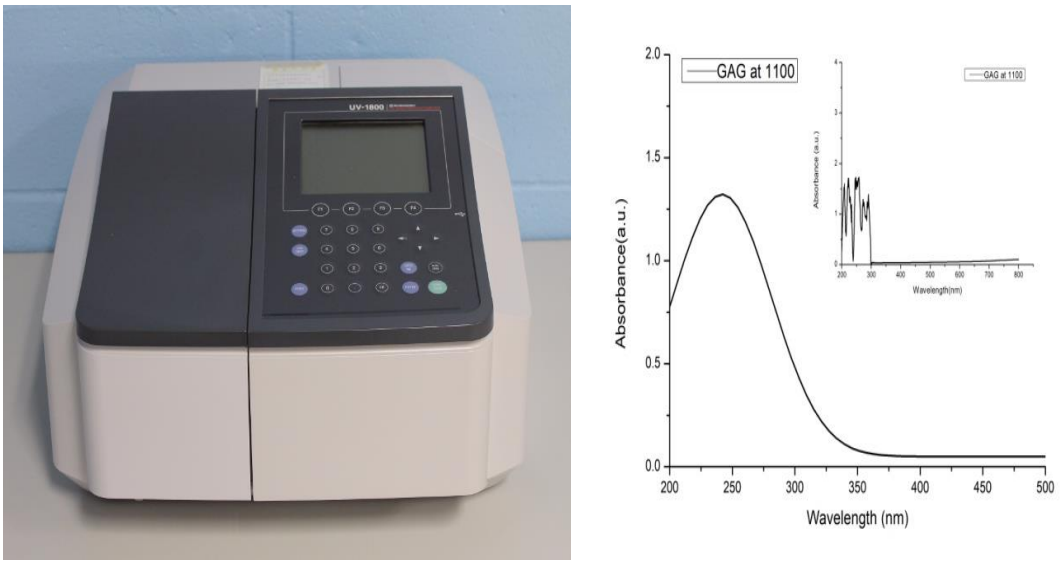

Fig 3.12. Image of apparatus of UV-vis spectroscopy and absorption spectra obtained for GAG at 1100°C.

3.5.5. Fluorescence Spectroscopy

Fluorescence spectroscopy is electromagnetic spectroscopy that is used to investigate the fluorescence properties of the material and it involves the beam of light falling on the material to excite the electron in a molecule that causes the emission of light. The principle of fluorescence spectroscopy depends upon the Jablonski's diagram shown in the figure 3.13.

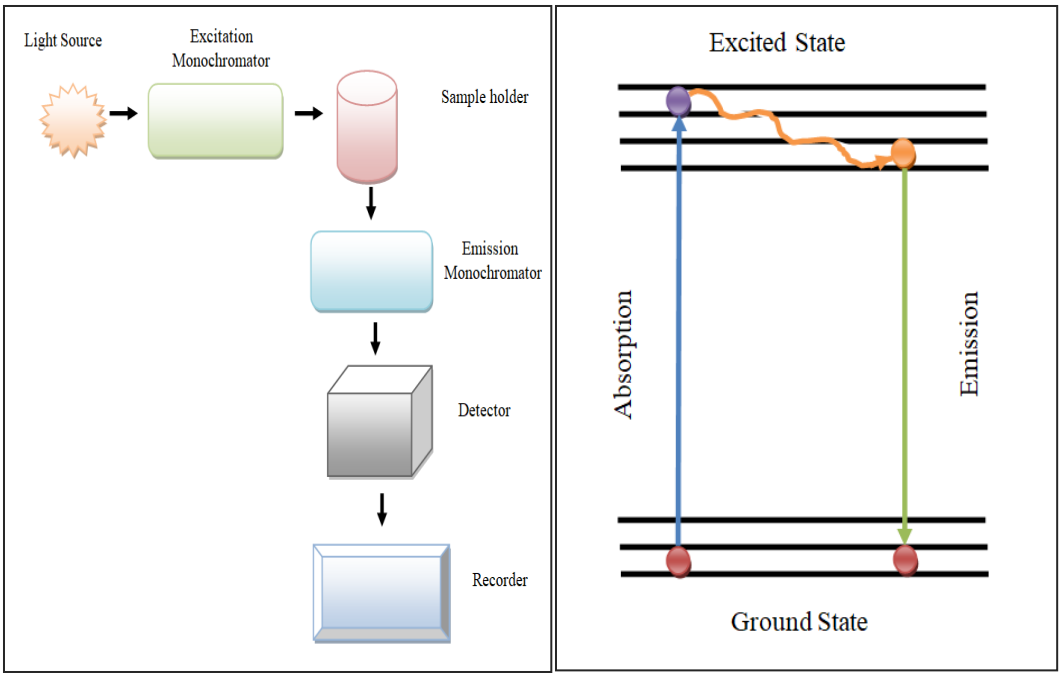

Fig 3.13. (a) Working principle of fluorescence spectroscopy and (b) Jablonski's diagram.

The characterization of fluorescence has been done for all the prepared by using a PERKIN ELMER spectrometer (xenon lamp) with 200-900 nm excitation as well as emission range. The image of the apparatus and the results obtained are shown in the figure 3.14 below.

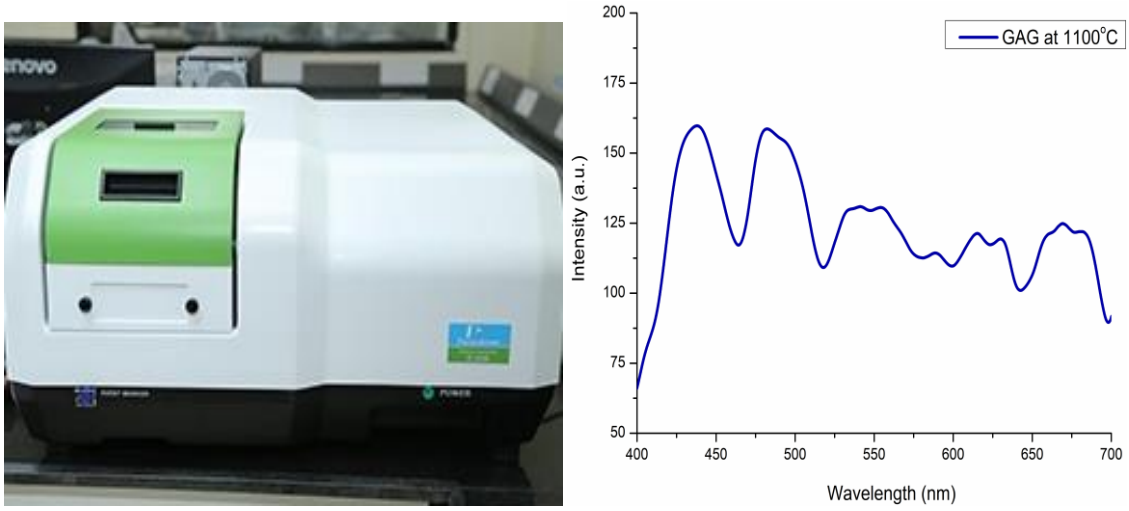

Fig 3.14. Fluorescence spectrometer and obtained spectra for GAG at 1100°C.

Chapter 4

Transition Metal Doped Gadolinium Aluminum Garnet (GAG)

4.1. Gadolinium Aluminum Garnet (GAG)

Gadolinium Aluminum Garnet (GAG or $Gd_3Al_5O_{12}$) exhibits a cubic crystal structure with a space group of Ia3d and a general formula of $Gd_3Al_5O_{12}$, showcasing favorable physical, chemical, and optical properties, as outlined in Chapter 1. The current research focuses on exploring the application of GAG in Solid-State Light Sources (SSLS), particularly White Light Emitting Diodes (WLEDs). In the ongoing study detailed in Chapter 3, GAG powders doped and co-doped with cobalt (Co) and chromium (Cr) were prepared through the sol-gel technique. Subsequently, these powders underwent sintering at various temperatures, with a maximum of 1100°C, facilitated by a temperature-controlled, muffle furnace. Doping concentrations ranging from 0.2 to 1.0 were investigated, and a series of GAG samples—pure host, doped, and co-doped with chromium and cobalt were scrutinized for structural and optical characteristics. Characterization of the prepared samples involved techniques such as XRD, SEM, TEM, EDX, FTIR, and fluorescence spectroscopy. The systematic analysis aims to provide insights into the structural and optical properties of GAG under various doping conditions, contributing to the understanding of its potential applications in Solid-State Light Sources.

4.1.1. X-Ray Diffraction

Bruker Diffractometer was used to analyze the X-ray diffraction (XRD) of the powder sample. Figure 4.1 illustrates the XRD spectra for Gadolinium Aluminum Garnet (GAG) recorded between 0^o to 70^o of Bragg's angle (2θ) that were sintered at 500^0C,700^0C, 900^0C, and 1100^0C temperatures. In Figure 4.1, no diffraction peaks were observed at 500^0C and 700^0C, indicating the amorphous nature of the material. At 900^0C, the crystalline phase started developing and consisted of two crystalline phases: Gadolinium Aluminium Garnet

($Gd_3Al_5O_{12}$, GAG) and Gadolinium Aluminate Perovskite ($GdAlO_3$, GAP). The XRD pattern is in excellent concurrence with the reference data for $Gd_3Al_5O_{12}$ (JCPDF -32-383) and $GdAlO_3$ (JCPDF -46-395).

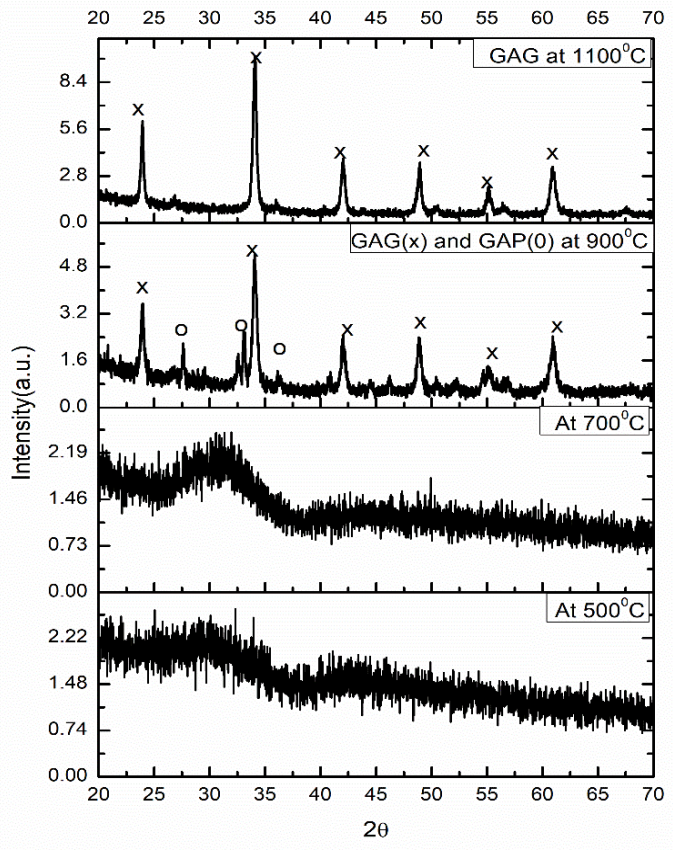

Fig. 4.1 Typical powder XRD pattern of $Gd_3Al_5O_{12}$ sintered at 500, 700, 900, and 1100 °C.

At a temperature of 1100^0C, the pure phase of garnet was found and peaks could be directly indexed to the cubic phase with no intermediary phase. So, these results designate that garnet configurations appear to be an established phase. Table 4.1 shows the crystalline size (D), d-spacing (d), and lattice constant at 900ºC and 1100ºC. The d-spacing and crystalline size was calculated by using Bragg's Law and Scherer's formula in equations (3.1) and (3.2). Crystallite size increase with an increase in temperature indicates improvement in the crystalline phase of the sample. The full crystalline phase was

developed at 1100ºC. [1-3] The results of crystalline size, d-spacing and lattice constant depicts in table 4.1.

Table 4.1. Summaries the Crystallite size (D), d-spacing, and lattice constant (a) of GAG at 900 and 1100^0C.

Sr.No.	Temperature (^{0}C)	2Ɵ (degrees)	(hkl)	D (nm)	d-spacing (Å)	Lattice constant(a)
1.	900	23.9	(220)	11.93	3.7173	10.5141
	1100	23.9		20.80	3.7175	10.5149
2.	900	34.0	(420)	17.17	2.6293	11.7587
	1100	34.0		20.52	2.6299	11.7613
3.	900	42.0	(521)	19.38	2.1471	11.7605
	1100	42.3		20.69	2.1479	11.7650
4.	900	48.8	(611)	21.38	1.8612	11.4738
	1100	48.9		21.80	1.8605	11.4692
5.	900	55.0	(640)	13.10	1.6661	12.0150
	1100	55.1		22.41	1.6638	11.9980
6.	900	60.9	(651)	16.18	1.5188	11.9595
	1100	60.9		17.21	1.5189	11.9598

4.1.2. Fourier Transform infrared spectroscopy (FTIR)

FTIR spectroscopy was carried out by using Perkin Elmer Fourier Transform Spectrometer in the range of 400cm^{-1}-4000 cm^{-1} and GAG was sintered at 500^0C ,700^0C ,900^0C, and 1100ºC as shown in figure 4.2. In FTIR, absorption peaks were found at lower regions i.e. around 400cm^{-1}-700 cm^{-1} is a pure metal-oxide bond i.e. Gd-O metal-oxygen and Al-O metal bonds established for GAG.

Peaks at 2922 cm^{-1} and 2975 cm-1 were due to the presence of water in the sample and the absorption peak at 1330 cm^{-1} was indicated as a nitrate peak i.e. C=N. With the increase in temperature, the concentration of water and nitrate in the GAG reduced and peaks diminished. The absorptions around 598cm^{-1} and 670cm^{-1}occurred as the presence of

stretching frequency Al–O vibrations (M: metallic elements) [4,5] and absorption peaks 423cm^{-1}, 499cm^{-1}, and 556cm^{-1} were due to stretching and vibrations of Gd-O bond in GAG [6].

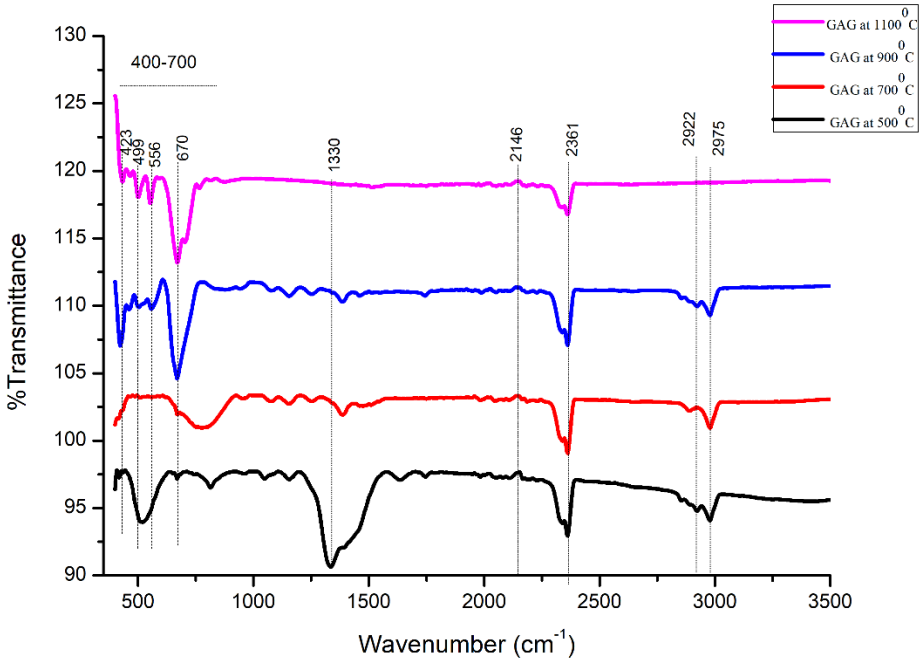

Fig 4.2. FT-IR spectra of GAG sintered at different temperatures recorded in the range of 400 cm-1 to 3500 cm−1.

4.1.3. UV-Vis Spectroscopy

UV-Vis spectrum was carried out to examine the typical emission of GAG with the increase of temperature shown in figure 4.3 and around the 200-350 nm absorption peaks were observed. The broad emission spectra observed in the UV graph from 200-350 nm were due to the defect states. As the temperature increased the area under the curve and FWHM both found increased which signifies the increase in defect states.[5] The band gap (Eg) for GAG was calculated by $(\alpha h\nu)^2/h\nu$ and the formula used, that shown in equation 3.6.

Where α is the linear absorption coefficient; h is Planck's constant; ν is the frequency of light; A stands for the proportionality constant; Eg band gap energy; n = 1/2 for direct band gap material. It was found that the band gap of the material decreases with the temperature rise i.e. 4.19 eV and 4.17 eV at 900^0 and 1100^0C respectively. [7]

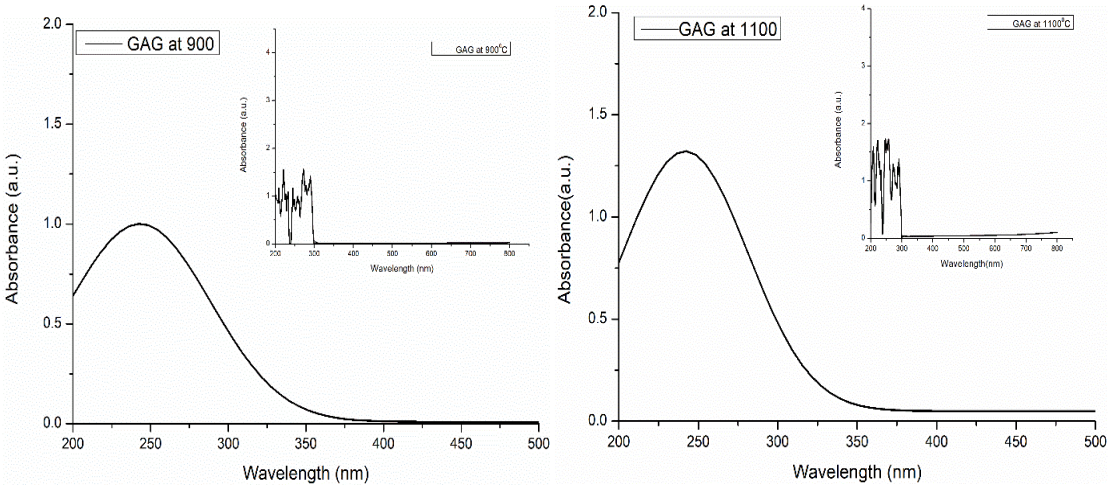

Fig. 4.3 Typical UV-visible absorption for GAG sintered at (a) 900° ,and (b) at 1100°C temperature.

4.1.4. Fluorescence Spectroscopy

Figure 4.4 (a,b,c) shows the fluorescence spectra of GAG sintered at 900ºC and 1100ºC excited by 256,291 and 391 nm corresponding to $^6I_{7/2}$,$^6D_{9/2}$, and $^6G_{7/2}$transition from state $^8S_{7/2}$ as shown in table 4.2 [8,9]. Down conversion (DC) visible emission spectra had been produced with UV excitation. Visible emission from GAG was attributed to F centers. The F centers were due to electrons trapped at oxygen vacancy. These F centers usually produced visible and UV bands attributed to the recombination of electrons (donor) and holes (acceptor) on the deep host lattice defects center. F centers were produced when the sample is heated at a high temperature.

The sharp emission peak around 450 nm might be due to aluminum ions and the peak near 533 nm due to the presence of Gadolinium ions in the base compound. Figure 4.5 is the bar graph showing integrated intensities versus excitation wavelength at 900ºC and 1100ºC. At 900ºC it has been observed that intensity increases with increases in excitation energy, it may be due to the participation of more F states at higher energy excitation. Non-

radioactive transition plays a major role in DC emission. The emission in 400ºC -700 ºC was found due to $^{8}S_j$ to $^{6}I_j$ (Gd^{3+}) transition also. [10]

Table 4.2 Transition line of Gd^{3+} [26].

	Type	Wavelength (nm)	Transition
1	Absorption	391	$^{8}S_{7/2}$ to $^{6}P_J$
2	Absorption	290	$^{6}I_J$ to $^{8}S_{7/2}$
3	Absorption	256	$^{6}P_J$ to $^{6}G_{7/2}$
4	Emission	400-700	F centres

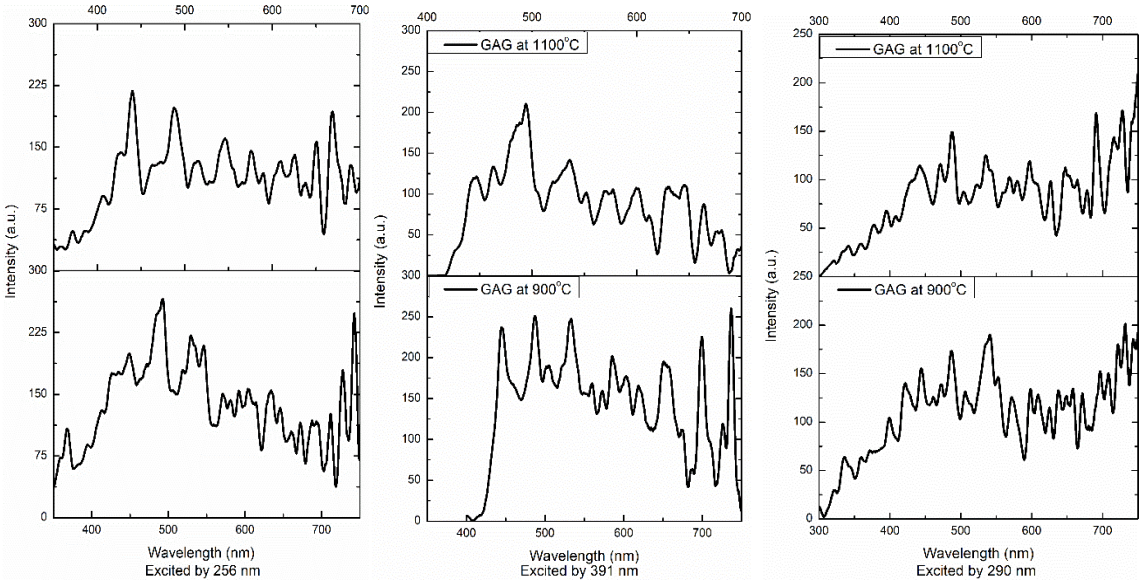

(a) (b) (c)

Fig4.4. Fluorescence spectra for GAG at 900^0C and 1100^0C excited by (a) 290 nm, (b) 391 nm, and (c) 256 nm.

At 1100ºC, integrated intensity is almost independent of excitation wavelength (very small decrease). At 1100ºC integrated intensity decreases with an increase in temperature which may be due to the increase in the crystalline nature i.e. decrease in defect centers [11-12].

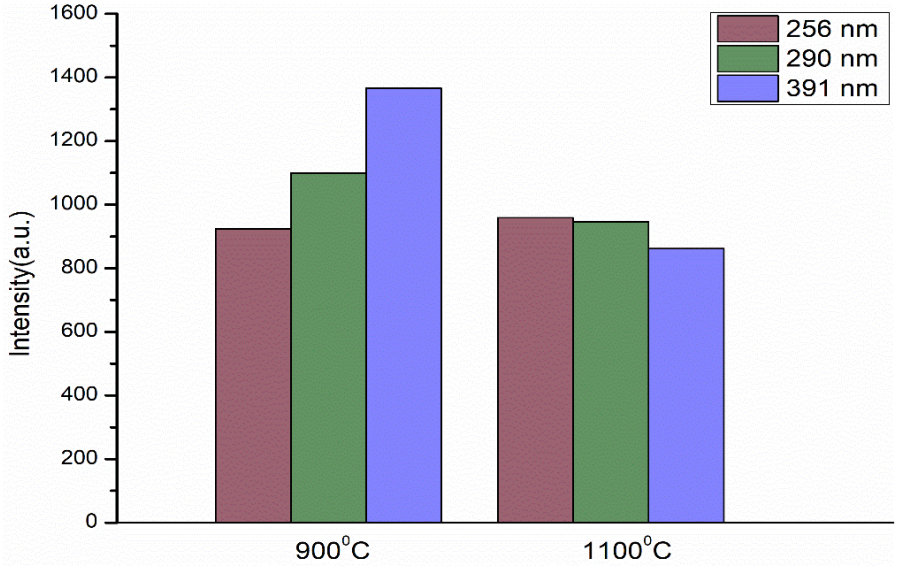

Fig. 4.5 Integrated intensity in 300-800 nm region for various excitation wavelengths at 900 °C and 1100 °C.

Figure 4.6 illustrates the International Commission on Illumination (CIE) coordinates on the chromaticity diagram (0.31, 0.31), (0.32, 0.32), and (0.30, 0.34) for GAG calcined at 1100^0C on different excitations of 256nm, 290 nm, and 391 nm respectively. These coordinates showed the mixed-color components. Color Purity (CP), Correlated Color Temperature (CCT), and CIE coordinates were calculated for the prepared GAG sample. The color purity of GAG was calculated by using equation 1.5. Color purity value can lie between 0-100 and it is a unit-less number describing the purity of color of the light that the source gives. CCT and Color purity and value of GAG can be calculated by using equations (1.4) and (1.5) correspondingly. According to equation (x_s, y_s) stand for the coordinates of GAG, ($x_{i,}$ $_{Yi}$) are illuminate points of the 1931 CIE standard source with coordinates, and (x_d, y_d) are the coordinates of the dominant wavelength. [13,14]

Consequently, the values of color purity of GAG were calculated as 11.7%, 4.02%, and 10.3% for 256 nm, 290 nm, and 391 nm respectively. CCT values calculated for GAG at 256 nm, 290 nm, and 391 nm excitation were 6451.61, 6016.05, and 6956.48, respectively.

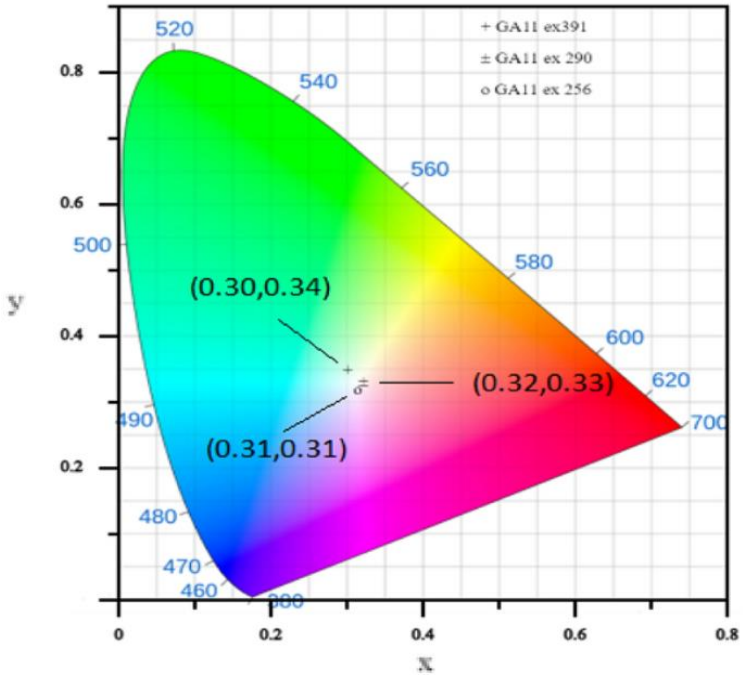

Fig. 4.6 Chromaticity diagram with CIE color coordinates (x, y) of GAG for 256 nm, 290 nm, and 391 nm excitations.

4.2 Gadolinium Aluminum Garnet Doped with Chromium

As study investigates Gadolinium Aluminum Garnet (GAG) with a focus on varying sintering temperatures to examine its structural and optical properties. Successful development of the GAG phase is observed at 1100°C, resulting in a pure garnet phase with visible region emissions, suggesting potential for white light generation. However, to enhance these properties and address limitations in the host material can be doped with a suitable dopant. Thus, this research emphasizes the strategic doping of GAG with transition metals and rare earth ions, aiming to stabilize the crystal structure and produce effective red phosphors. The study specifically explores the introduction of Chromium (Cr3+) into GAG phosphors to enhance the red component emission. Chromium doping is expected to influence the energy levels and transition lines of Cr3+ and facilitate energy transfer between Cr3+ and Gd3+. Chromium (Cr3+) doping is chosen due to its significant transition in the far-red region. The introduction of Chromium is expected to improve red component emission by influencing energy levels and transition lines, as characterized

through XRD, FTIR, SEM, and fluorescence measurements in this comprehensive investigation.

4.2.1. Structural characterization X-ray diffraction

The X-ray diffraction (XRD) of the prepared powder sample was characterized by a Bruker Diffractometer. Figure 4.7 shows the XRD pattern of GAG: Cr powders sintered at 1100 °C and it was compared with the XRD pattern of host GAG. Observed XRD pattern of GAG: Cr confirmed the formation of cubic phase and diffraction peaks are well indexed with JCPDS file No. 01-071- 4644. The Cr3+ addition does not alter the crystal structure of the GAG garnet.

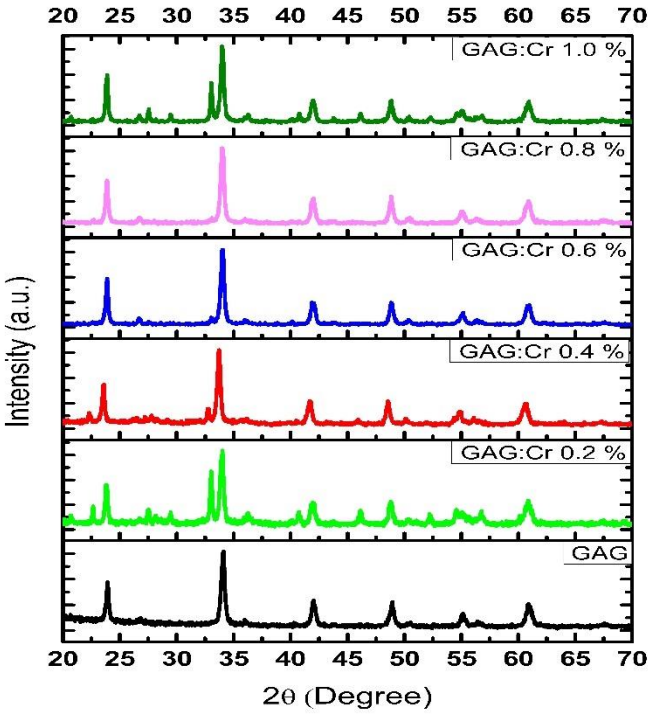

Fig. 4.7 XRD patterns of the GAG and GAG: Cr precursor powder samples with different concentrations of Cr^{3+} sintered at 1100 °C .

In Fig. 4.7, peaks marked with the symbol “x” signify the garnet phase and also there are some additional peaks at 0.2 and 1.0% which may be due to impurity or defect induced by Cr^{3+} doping marked with the symbol “o”. The Diffraction peak shift of plane (420) has

been observed toward the lower angle as mentioned in Table 4.3, which may be due to the doping of Cr^{3+}. Also, dopant ionic size is different from host cation i.e. Gd (3+), Al (3+), and Cr (3+) have ionic radii of 107.8 pm, 57 pm, and 75 pm, respectively. The average crystallite size was calculated by the well-known Scherer's Formula given in Equations (3.1) and (3.2) which is around 20.57 nm at 1100 °C for un-doped GAG and changes with the doping concentration of chromium in GAG [15,16].

The dislocation density of samples is calculated using Eq. (3.3), where δ is the dislocation density and D is the size of the crystallites. Dislocation density reduces as the value of crystallite size increases. A further observation was that the peak intensity and crystalline size of the material increased and the diffraction peaks became narrow with the increase in the doping concentration of chromium in GAG because absolute destructive interference arises at angles to some extent above and below the Bragg angle. The peak appears to be shifted towards the lower angle of the graph which leads to the tensile strain after doping. Moreover, lattice volume and d-spacing were found to increase with doping concentration which may be due to the incorporation of large Cr^{3+} ion at the lattice position of Al^{3+} ion. Hence, the shift towards lower angles in the XRD pattern on doping in the host material can also be attributed due to lattice expansion that caused by the incorporation of larger ions, strain effects, and formation of impurity phases.

The x-ray density, bulk density, and porosity were calculated by using Equations (4.1), (4.2) and (4.3) given below:

$$\rho_x = \frac{nM}{NV} \quad \text{..... (4.1)}$$

$$\rho_m = \frac{m}{\pi r2\, h} \quad \text{..... (4.2)}$$

$$P = 1 - \frac{\rho m}{\rho x} \quad \text{.....(4.3)}$$

Porosity, a critical material property, is influenced by variables like n (atoms per unit cell), M (molar mass), N (Avogadro's number), V (unit cell volume), m (mass), r (radius), and h (pellet thickness) [17]. Controlled by factors such as preparation method, processing

conditions, and doping, porosity plays a crucial role in determining a material's physical and mechanical characteristics. In materials like GAG garnet, reduced porosity positively impacts luminescence by preventing light trapping, and enhancing emission intensity, and overall emission properties.

Table 4.3. The Crystallite size (D),d-spacing, lattice constants (a), cell volume (V),lattice strain, peak shift, X-ray density (ρx), bulk density (ρm), porosity (P), of GAG: Cr at 1100°C.

Parameter	x=0	x=0.2	x=0.4	x=0.6	x=0.8	x=1.0
Crystallites size, D (nm)	20.52	23.58	23.80	22.76	22.61	24.33
Dislocation Density(m^2) $\times10^{-15}$	2.37	1.79	1.76	1.93	1.95	1.68
d-spacing(Å)	2.629	2.637	2.656	2.633	2.634	2.635
Lattice Constant (a)	11.76	11.79	11.88	11.77	11.78	11.78
Lattice Volume (a^3)(nm^3)	1626	1638	1676	1630	1635	1634
Lattice Strain($\times10^{-3}$)	6.02	5.25	5.24	5.43	5.47	5.08
Peak shift	0	0.090	0.035	0.033	0.064	0.082
X-ray density(ρ_x ,g/cm^3)	4.890	4.843	3.156	3.240	3.234	3.229
Bulk density(ρ_m ,g/cm^3)	1.395	1.380	1.329	1.976	1.302	1.616
Porosity (P, %)	0.72	0.71	0.59	0.40	0.59	0.50

4.2.2. Fourier transform infrared spectroscopy

The interpretation of the Fourier transformation infrared spectroscopy (FTIR) spectra of GAG: Cr can provide valuable information about the crystal structure, the coordination environment of the dopant ions, and the local symmetry of the crystal lattice. The FTIR spectra of GAG: Cr typically show characteristic absorption bands at specific wave numbers, which correspond to different vibrational modes of the atoms in the crystal lattice. These bands can be assigned to various chemical bonds such as O–H, Al–O, Gd–O, Cr–O, and Cr–O–Gd, depending on their location in the spectrum and their intensity. The Perkin Elmer Fourier Transform Spectrometer was utilized to investigate the functional groups in the precursors, within the range of 400–4000 cm^{-1}. Figure 4.8 shows GAG doped with various concentrations of Chromium, sintered at 1100 °C.

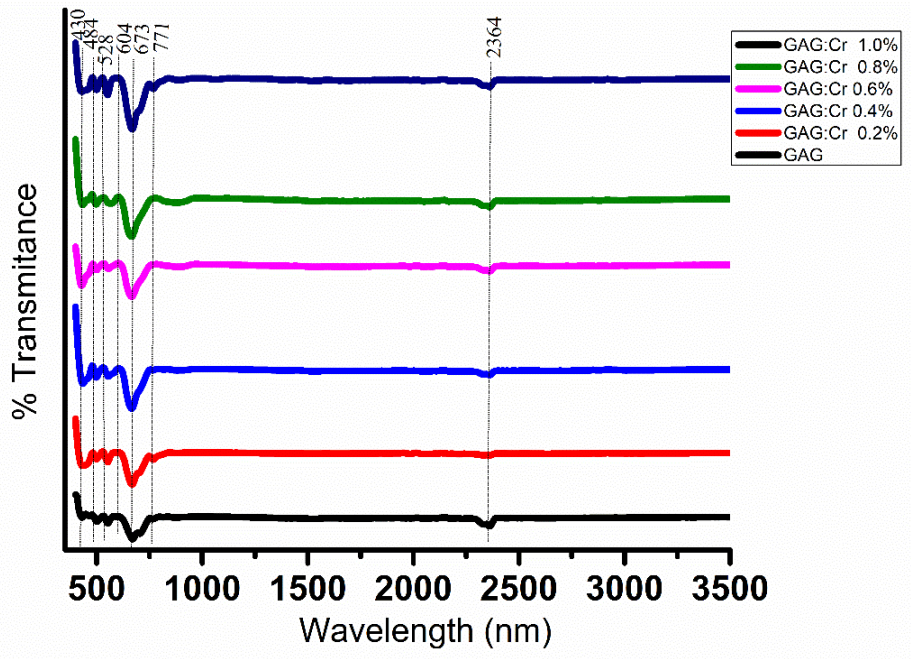

Fig. 4.8 FTIR spectrum of the GAG: Cr precursor at 1100 °C with different concentrations of dopant.

The position and shape of absorption bands in the spectra can provide information about the presence of defects or impurities in the lattice, or changes in the crystal structure due to the doping process. The FTIR spectrum of GAG and GAG: Cr in Fig. 4.8 exhibit the same main spectral features, indicating that the crystal structure remains unchanged after the doping of Cr^{3+}. In the spectra from 400 to 800 cm^{-1}, the metal–oxygen (Al–O, Gd–O, Cr–O, and Cr–O–Gd) vibrations in the tetrahedral garnet structure are observed. The Cr–O bond appears at around 430–490 cm^{-1}. The band at approximately 484 cm^{-1} may be linked to oxygen vacancy or oxygen deficiency, which may result in an enhanced green emission. The characteristic bands for Gd–O and Al–O bonds are observed at 528 cm^{-1} and 604 cm^{-1}. It is worth noting that Gd–O vibrational modes are relatively weak and can overlap with other peaks in the FTIR spectrum, making their identification challenging. The strong absorption band from 665 to 730 cm^{-1} is assigned to C=C bending. The shallow absorptions near 2344 cm^{-1} arise from surface-adsorbed CO_2 and can be assigned to the C=O vibrations [18, 19]

4.2.3. Scanning electron microscopy

Figure 4 shows the typical scanning electron microscopy (SEM) image of the GAG and Cr (1.0) doped GAG. As seen in Figure 4.9 a, b, the powder sample of the Cr (1.0) doped GAG and GAG was composed of spherically shaped particles along with some large-size particles, which might be due to the occurrence of agglomeration in particles. The average particle size was around 26 and 28 nm which was close to the crystallite size calculated from XRD data. This indicates that the sample was well dispersed and less agglomerate at high temperatures as shown in Figure 4.9 c, d for the GAG and Cr (1.0) doped GAG respectively.

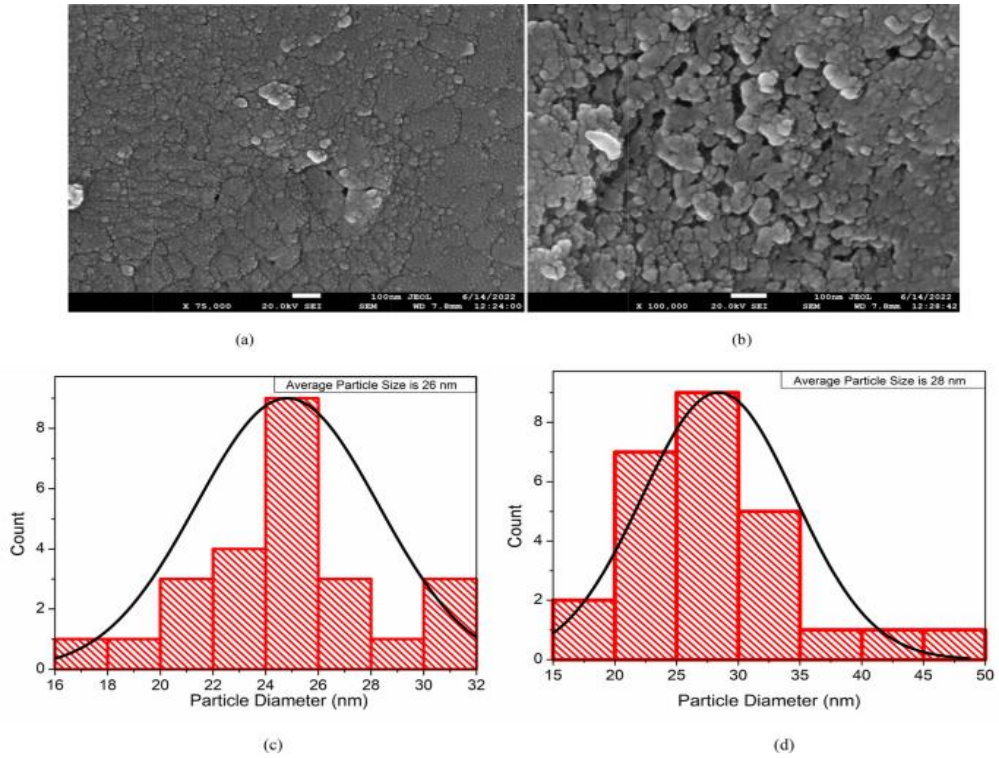

Fig. 4.9 SEM micrograph (a, b) and particle size distribution (c, d) GAG and GAG: Cr (1.0)powder sample sintered at 1100 °C.

In Fig. 4.10 a, b EDX element mapping in SEM mode of Gd, Al, O, and Cr showed, and during EDX different areas of samples were exposed. The peaks of Gd, Al, O, and Cr

confirm the formation of GAG and Cr^{3+} doping shown in Fig. 4.10 c. The weight% and atomic % are mentioned in Table 4.4

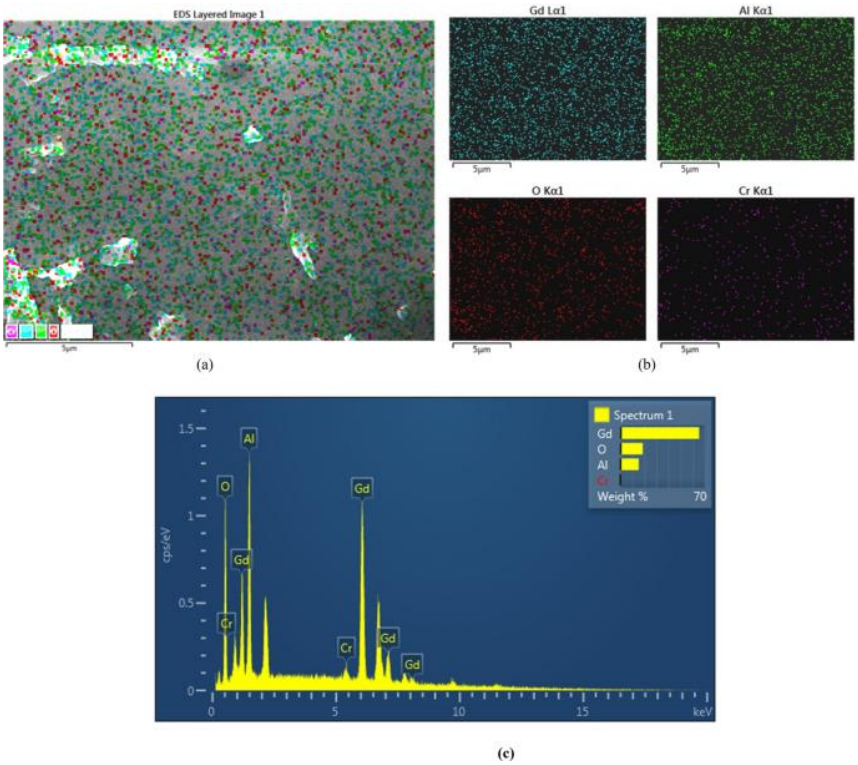

Fig. 4.10 a, b EDX element mapping in SEM mode of Gd, Al, O, and Cr and c EDX spectra of GAG: Cr 0.1wt%.

Table 4.4.EDX weight (%) and atomic (%) for area exposed for sample GAG: Cr 1.0Wt%.

Element	Weight %	Atomic %
Gd	65.46	19.96
Al	16.88	29.99
O	16.27	48.77
Cr	1.39	1.28

4.2.4. UV spectroscopy

Figure 4.11 shows the UV–visible spectra of Cr-doped GAG nano phosphors of samples that show strong absorption region around 270–285 nm. The plot of $(\alpha h\nu)^2$ versus hν for GAG: Cr at different concentrations of Cr is shown in Figure 4.11 and the optical Band-

gap (Eg) has been calculated by the intersection point of tangents drawn on curves. For Cr: The GAG value of Eg decreases with the increase of doping concentration of Cr. The change in Eg can depend on numerous things like grain size, carrier concentration, lattice strain, etc. Figure 4.12 shows how crystalline size and Optical band gap vary for the doping concentration of Cr^{3+} in GAG [20,21]

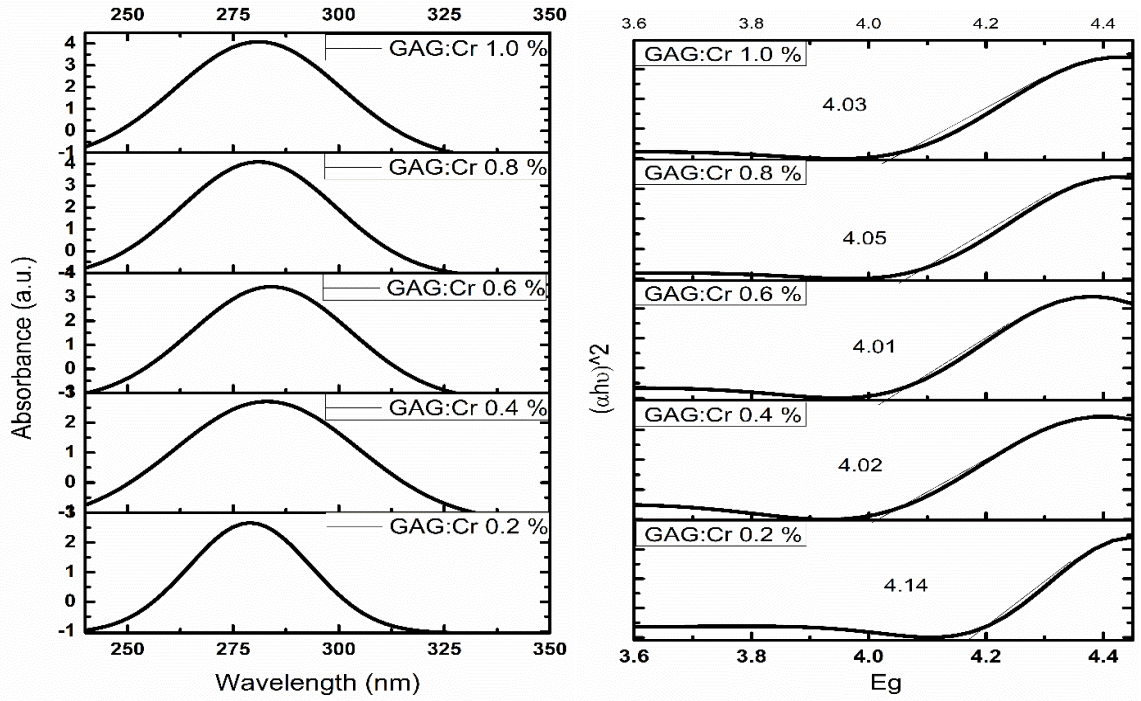

Fig 4.11 (a) UV- visible absorption and (b) Energy band gap for GAG: Cr sintered at 1100°.

The crystallite size and band gap of a material are often interrelated. The crystallite size can affect the band gap of a material due to quantum confinement effects. As the crystallite size decreases to the nanoscale, the energy levels of the electrons can become quantized, leading to changes in the band gap and the resulting optical and electronic properties of the material.

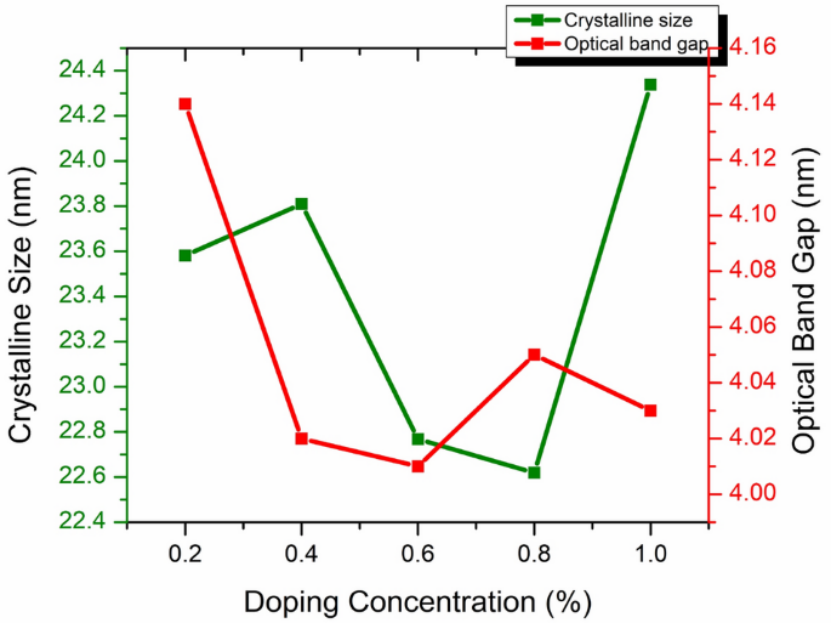

Fig. 4.12 Variation of Crystalline size and band gap at different doping of chromium in GAG.

4.2.5. Fluorescence spectroscopy

This investigation focuses on the fluorescence spectra of GAG: Cr, denoting the measurement of emitted fluorescent light from gadolinium aluminum garnet (GAG) doped with chromium (Cr) under UV light excitation (depicted in Figure 4.11). Fluorescence spectroscopy, a potent tool for probing material electronic structure and dynamics, highlights GAG: Cr potential applications in optical devices and scintillators. Figure 4.14 illustrates the integrated area of chromium-doped GAG at varying concentrations in the 300-800 nm range. The fluorescence spectra exhibit sharp emission peaks in the visible spectrum, their positions and intensities contingent on dopant concentration and excitation wavelength. Interpretation of GAG: Cr fluorescence properties involve analyzing the energy levels of Cr^{3+} ions within the garnet lattice and their interactions with the host lattice. Gadolinium, a lanthanide series element, showcases distinctive magnetic properties due to its seven unpaired electrons in the 4f sub-shell.

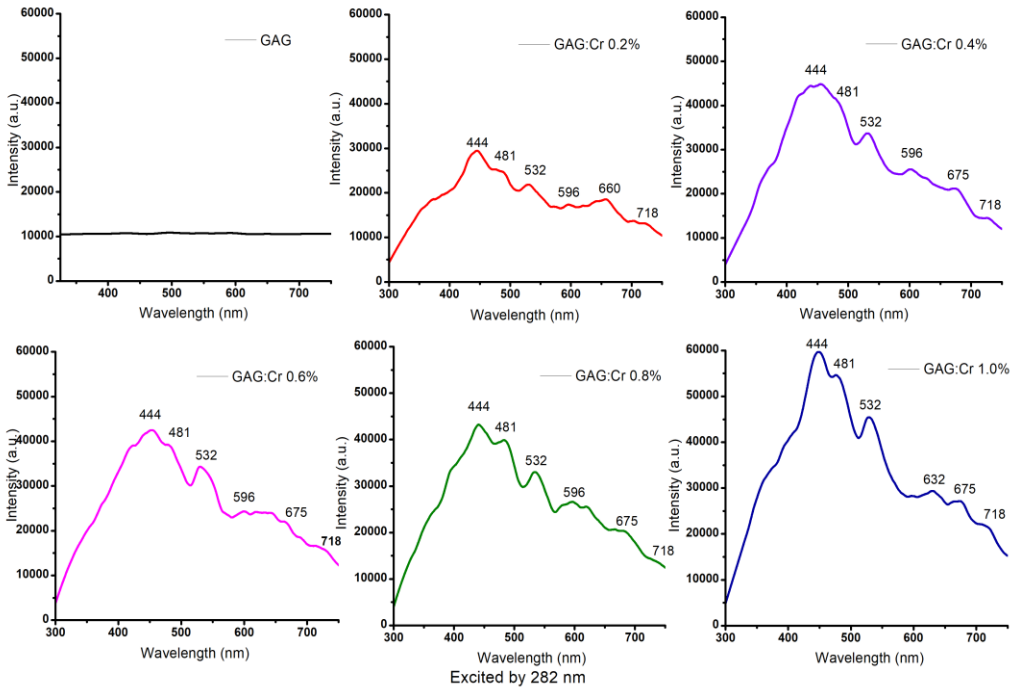

Fig. 4.13 Fluorescence spectra of GAG: Cr (Different concentration) excited by 282 nm sintered at 1100 °C.

The most prominent line in the electronic spectra of chromium is the red line at 690.7 nm, which corresponds to the transition from the 4F excited state to the ground state. Other prominent lines in the chromium electronic spectra include the blue line at 425.4 nm, the green line at 520.6 nm, and the violet line at 438.4 nm. In addition to the sharp lines in the visible region of the spectrum, chromium also exhibits several lines in the ultraviolet and infrared regions. These transitions correspond to the excitation of electrons from the lower energy levels of the 3d sub-shell to the higher energy levels. Overall, the electronic spectra of chromium exhibit several sharp lines corresponding to the transitions of electrons from the excited states to the ground state.

The FL emission spectra were traced by using a Xe lamp ranging from 350 to 750 nm shown in Figure 4.13 excited by 282 nm wavelengths and show the typical emission spectra. The emission spectra for all doping concentrations of Cr in GAG have mostly the same spectral positions whereas observed a considerable change in intensity pattern. From the spectra following results were observed.

a) In the FL spectra of the GAG, the host found a peak at 430 nm, and after doping of Cr^{3+} in GAG peak was found at 445 nm at all the doping concentrations i.e. 0.2, 0.4, 0.6, 0.8, and 1.0. As the doping concentration of Cr increases the intensity of the peak increases and the observed peak is due to the $^4A_2 \rightarrow {}^4T_1$transition of Cr^{3+} [22]
b) Similarly, the intensity of peaks around 532 nm and 610 nm was also found to increase with the increase in the doping concentration of Cr^{3+} in GAG, and these broad and weak peaks observed between 525 and 650 nm are consequently by $^4A_2 \rightarrow {}^4T_2$ of Cr^{3+} [18]
c) A peak was observed in the red region around 712 nm caused by transition $^4T_2 \rightarrow {}^4A_2$ of Cr^{3+}. There found energy transfer in Gd^{3+} and Cr^{3+} shown in figure 4.15. The intensity of the peak increased as it found 14,187 a.u. at 0.2 mol% of GAG: Cr and with the increase of doping concentration intensity reached 25,142 a.u. at 1.0 mol% of GAG: Cr [23,24]. Moreover, as the doping concentration of Cr increases insignificant blue shift of absorption is seen near 480 nm. The intensity of the fluorescence spectra increases when the Cr-doping concentration is increased from 0.2 to 1.0 mol%, which is expected as increases in the number of emitting centers with doping concentration.

Figure 4.14 illustrate the integrated area of chromium-doped GAG at different concentration and a bar graph plotted for three regions i.e. UV (300–400 nm), visible (400–700 nm), and IR (700–800) region. The area of the visible region increased with the rise in the doping concentration of Cr in GAG. At 1.0 concentration of chromium GAG had maximum integrated area for the visible region and for the white light emission, visible light is required. So, a 1.0 concentration of GAG: Cr is optimized.

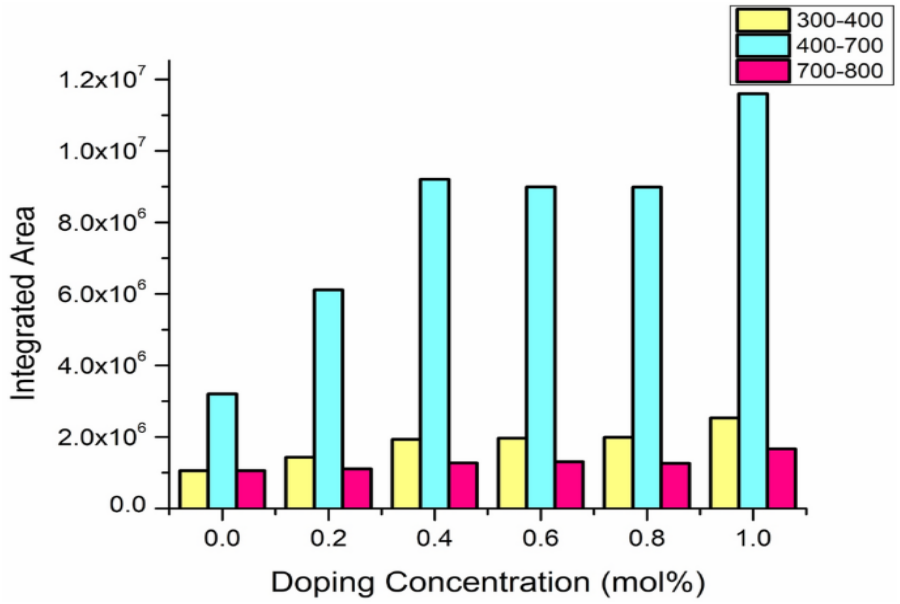

Fig. 4.14 Integrated areas of GAG: Cr with different doping concentrations of Cr sintered at1100 °C.

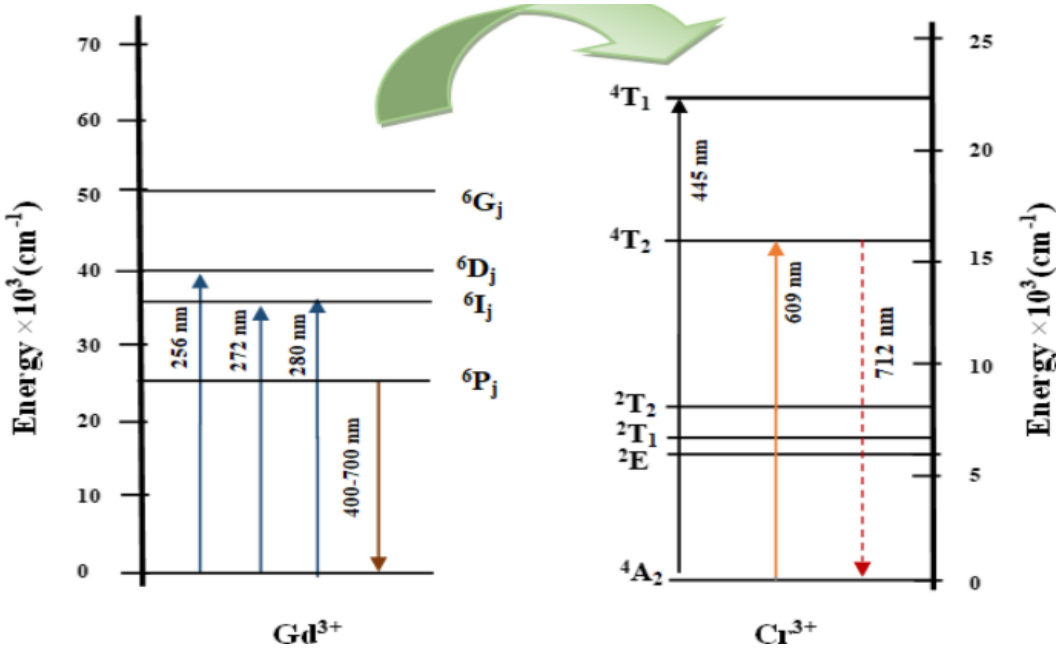

Fig. 4.15 Schematic Energy level diagram of energy levels of Gd^{3+} and Cr^{3+} ions in GAG: Cr.

4.2.6. Quantum yield

Fluorescence Quantum Yield (QY) is a good luminescent property that is useful for the appliance of luminescence techniques. By definition, QY is calculated by evaluating the fluorescence emission of the sample to that of the reference standard of the known quantum yield. There are optical and non-optical ways to measure quantum yield. Non-optical techniques include calorimetric approaches such as Photo-Acoustic Spectroscopy (PAS), and thermal lensing for assessing the indirect conversion of excitation energy into heat and its dissipation to the solvent. These techniques need specialized setups and thus are typically used to ascertain the quantum yield of significant standards. Thus, optical measurements of quantum yield either using the relative or absolute method are most frequently used. The absolute method includes an integrating sphere that detects all sample fluorescence to get the quantum yield directly. On the other hand, with the relative approach, the quantum yield of an unknown sample is determined by correlating its fluorescence intensity to that of a standard sample [25-27].

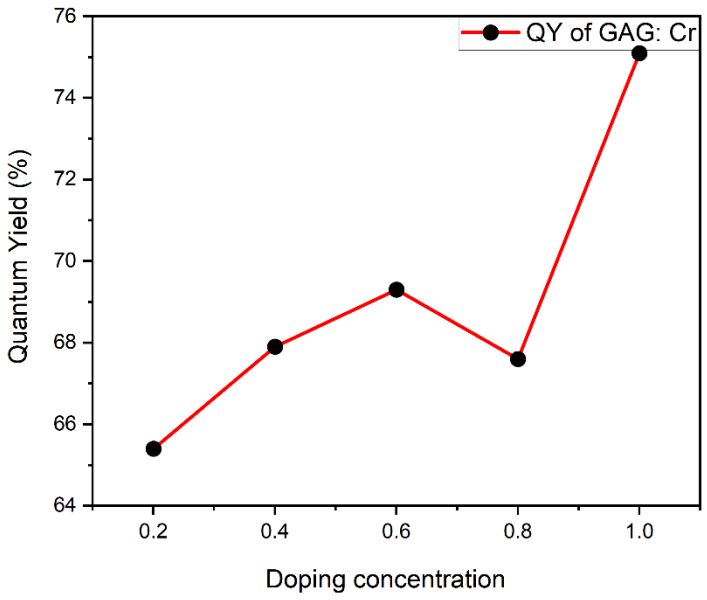

Fig. 4.16 Quantum Yield with doping obtained for GAG: Cr sintered at 1100 °C.

In this work, QY is calculated by the relative method. The quantum yield of the sample is determined using Eq. (1.2) by comparing the emission spectra of the sample with the reference standard under similar excitation conditions. The Quantum yield of GAG: Cr is calculated for different doping and increases with the increase of doping concentration of Cr3+ in GAG shown in Fig. 4.16. [28].

4.2.7. Fluorescence Lifetime

To investigate the luminescent lifetime of the garnet synthesized in this study, the decay behavior was analyzed using GAG: Cr sample sintered at 1100 °C shown in Figure. 4.17. The inset given away in the figure is the lifetime for GAG: Cr emission spectra obtained with excitation 282 nm, plotted aligned with the temperature. The decay curve for GAG: Cr can be fitted to a single exponential function according to the following equation 1.1 Where, as per equation I = relative intensity, x is decay time, t is fluorescence lifetime and A and B are constants. The calculated results displayed in table 4.5 below [29,30].

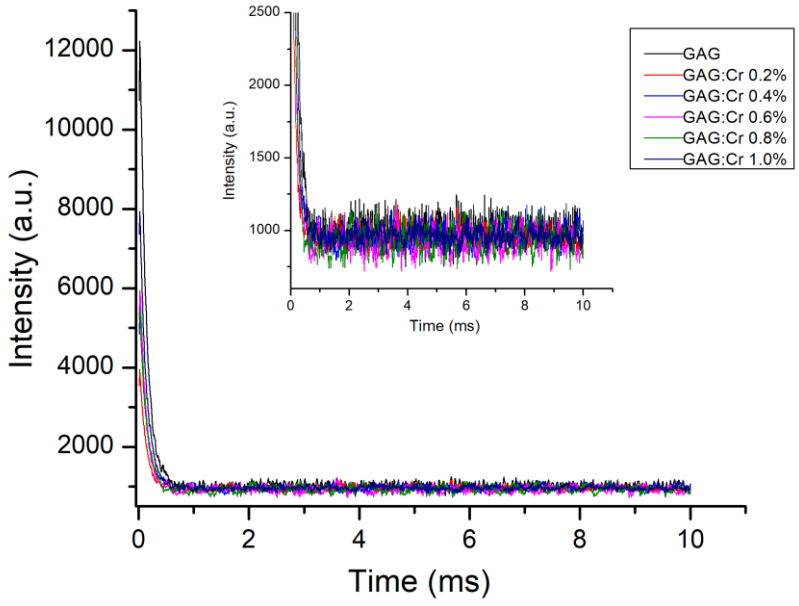

Fig. 4.17 Fluorescence Decay times obtained for GAG: Cr sintered at 1100 °C

Carrier lifetime and decay time, crucial parameters in material science, characterize charge carrier behavior in different contexts. Carrier lifetime, detailing recombination in electronic

devices, typically diminishes with doping, indicating increased recombination. In contrast, decay time, relevant in luminescence, tends to rise with doping due to additional recombination centers. Understanding these effects is vital for optimizing semiconductor performance. In the case of GAG with 0.2 doping of Cr^{3+}, maximum decay time and minimum lifetime are observed, contrasting with pure GAG. This insight aids in tailoring semiconductor materials for enhanced electronic and optoelectronic applications.

Table 4.5. Summarize Decay times and a lifetime of chromium-doped GAG.

	A	B	t (lifetime)	Decay time(ms), x
0	12782.746 ± 70.229	1010.941 ±3.739	0.126	0.160
0.2	3333.023 ± 37.359	954.610 ± 1.929	0.120	0.223
0.4	5009.289 ± 45.491	956.863±2. 433	0.121	0.201
0.6	5812.669± 55.126	923.777 ± 2.881	0.122	0.186
0.8	5173.410 ± 52.842	936.729 ± 2.803	0.125	0.202
1.0	7869.679 ± 37.664	961.989 ± 1.997	0.126	0.178

4.2.8. Colorimetry

Colorimetry is a scientific field that involves measuring color and expressing it in numerical terms. CRI, CCT, and CIE are three important concepts related to color science and lighting. The human eye has specialized cells called cones, which are responsible for color vision. There are three types of cones in the human eye, each sensitive to different wavelengths of light. This is known as the three-color cone theory or trichromatic theory of color vision. The trichromatic theory of color vision is a well-established theory that explains how humans perceive color. It suggests that the human eye has three types of color receptors, which work together to produce the full spectrum of colors we see. CRI (Color Rendering Index) is a measure of how well a light source can accurately reproduce the colors of objects in comparison to a reference light source.

CIE (Commission Internationale de L'Eclairage): CIE is an international organization that sets standards for color measurement and communication. The CIE was established in 1931

and has developed several color models and systems that are widely used today. These include the CIE 1931 XYZ color space, which provides a mathematical representation of color based on three color coordinates, and the CIE Lab color space, which is designed to be perceptually uniform, meaning that equal distances in the space correspond to equal differences in perceived color. The CIE also developed the CIE standard illuminates, which are used as reference light sources for measuring the color properties of objects under different lighting conditions.

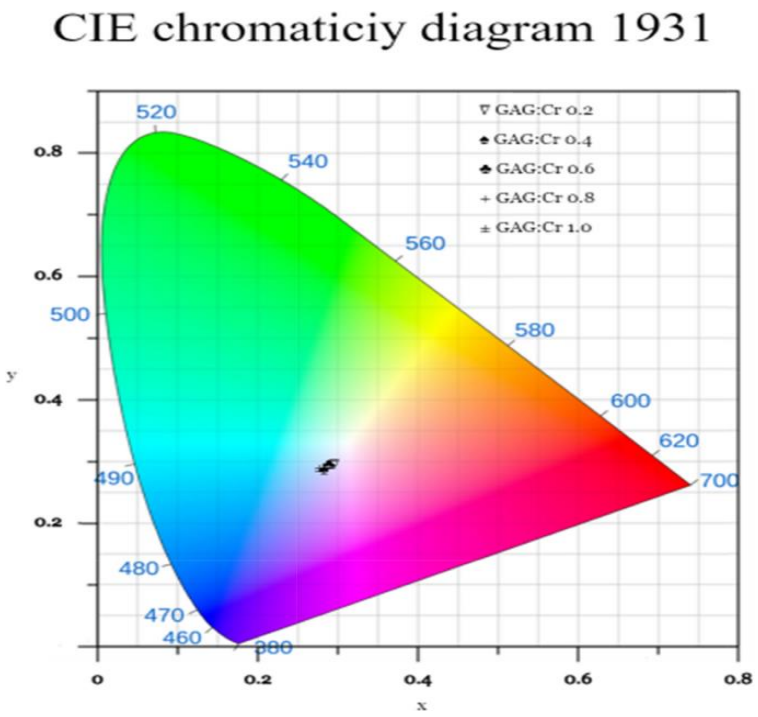

Fig.4.18 CIE chromaticity diagram with CIE color coordinates (x, y) of GAG: Cr sample under the 282 nm excitation.

CCT (Correlated Color Temperature): CCT is a measure of the color appearance of a light source, expressed in degrees Kelvin (K). CCT is based on the principle that a heated object predictably emits light depending on its temperature. For example, a piece of metal glows red when it's heated to a certain temperature and blue when it's heated to a higher temperature. Similarly, a light source with a low CCT (less than 3000 K) appears warm and yellowish, while a light source with a high CCT (above 5000 K) appears cool and

bluish. CCT is often used to describe the "color" of white light, with lower values corresponding to warmer (more yellow) colors, and higher values corresponding to cooler (more blue) colors.

Table 4.6. Summaries the CIE coordinates, CCT, color purity, and CRI values of chromium-doped GAG at excitation wavelengths 282 nm.

Doping conc.	CIE coordinates	CCT	Color Purity	CRI
0	(0.333,0.334)	5476	0.2%	96
0.2	(0.295,0.295)	8302	13.9%	90
0.4	(0.283,0.287)	9734	17.5%	94
0.6	(0.287,0.295)	9009	15.7%	94
0.8	(0.291,0.295)	8636	15.3%	94
1.0	(0.276,0.290)	10347	18.5%	96

The CRI scale ranges from 0 to 100, with higher values indicating more accurate color reproduction. A CRI value of 100 represents the maximum accuracy possible, which is achieved by using a reference light source that has the same spectral power distribution as natural daylight. A light source with a high CRI is often preferred for applications where accurate color rendering is important, such as in art galleries, clothing stores, and makeup studios.

The International Commission on Illumination -CIE chromaticity coordinates of GAG doped with different concentrations of Cr^{3+} observed by the excitation 282 nm were shown in Figure 4.18. It can be seen from the figure that the GAG: Cr transparent ceramic exhibits good CIE color coordinates close to the pure white light (0.33, 0.33). The observed fluorescence spectra of GAG: Cr is used to evaluate some optical parameters like Color Rendering Index (CRI), Correlated Color Temperature (CCT), and Color Purity (CP) are calculated by equations 1.3, 1.4 and 1.5 respectively and results are shown in Table 4.5. [31,32].

4.3. Gadolinium Aluminum Garnet doped with cobalt

The research delves into $Gd_3Al_5O_{12}$-based ceramics for solid-state light sources, leveraging the stability of the rare earth element Gadolinium in forming robust Garnet materials. The garnet formula for Gadolinium Aluminum Garnet (GAG) typically involves doping with transition metals, lanthanide elements, and rare earth ions. Cobalt-doped GAG, explored in this research, exhibits optical properties with potential applications in optical devices, and lighting technologies. The incorporation of cobalt aims to enhance GAG's properties. Ultimately, doped GAG garnets show promise for eco-friendly applications such as light devices and white LEDs. The investigation involves comprehensive characterization through XRD, FTIR, SEM, and Fluorescence measurements to elucidate the structural and luminescent properties of GAG: Co.

4.3.1. X-Ray Diffraction

The powder sample prepared for this study was analyzed using a Bruker Diffractometer to determine its X-ray diffraction (XRD) patterns. The XRD patterns of the GAG: Co precursors calcined at 1100°C were compared with those of pure host GAG phosphors, as depicted in Figure 4.19. The XRD spectra confirmed the crystal structure and were indexed with the JCPDS file no. 1-73-1371 [33]. Interestingly, no additional peaks were observed in the XRD patterns of GAG doped with different concentrations of Cobalt, indicating that the phase of the material remained the same after doping. However, the intensity and crystalline size of the material changed with increasing doping, as indicated by the results. The peak shifted towards a lower value of 2Θ, which suggests that the material underwent a tensile strain effect during the heating process due to the Cobalt doping.

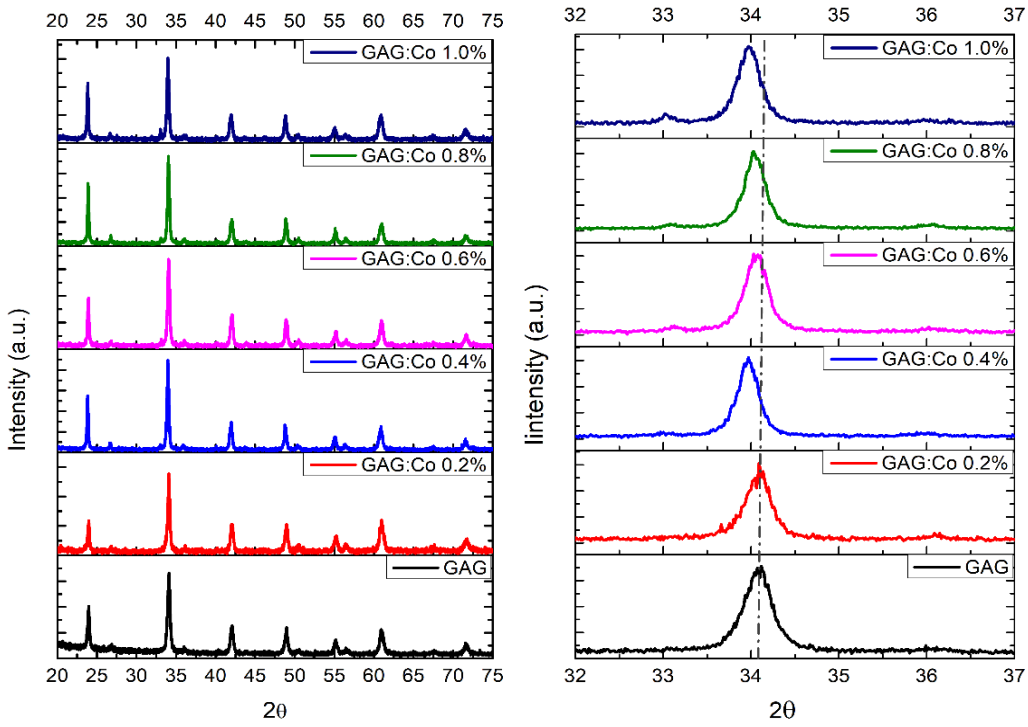

Fig.4.19 XRD patterns of the GAG: Co precursor powder samples annealed at 1100 °C with different concentrations of Co.

Table 4.7 Crystallite size (D), d-spacing, lattice constant (a), and peak shift of GAG: Co at 1100^0C.

Doping Cons.	2Θ(degree)	D (nm)	d-spacing (Å)	Lattice constant (a)	Lattice volume (a^3)	Peak shift
0	34.06	20.5	2.629	11.761	1622.523	0
0.2	34.09	24.0	2.627	11.750	1638.982	0.02
0.4	33.97	28.1	2.636	11.790	1627.381	0.10
0.6	34.06	26.1	2.630	11.762	1630.027	0.06
0.8	34.04	28.0	2.631	11.768	1638.982	0.07
1	33.97	26.4	2.636	11.790	1622.523	0.14

While the diffraction peaks shift or may expand when a crystal deviates somewhat from its perfectly ordered array. This might be caused by several things, including defects in crystalline, crystalline size, and lattice strain. Moreover, the thickness of the peak, its intensity, and the shift in its position may be caused by crystalline size as well as lattice

strain. The XRD results show the shift in peaks after doping of Cobalt (Co) in the GAG sample towards the lower angle of 2Θ. [34] Furthermore, a measurable shift in the peak position was observed when the XRD pattern of doped GAG: Co was compared to that of pure host GAG, implying that doping had altered the crystal structure of GAG. This was supported by an increase in the lattice volume and d-spacing with the rise in doping concentration. It's crucial to emphasize that due to the extremely small size of the nanoparticles, there's a possibility that not all of the added dopant has penetrated the host lattice. Some of it might be found on the surface or at the grain boundary.

XRD data analysis suggests that 0.2, 0.6, and 0.8 doping of Co might have entered the GAG unit cell at substitutional sites, while at 0.4 and 1.0, the migration of Co to the surface might have been the dominant process. The ionic radii of Gd (3+), Al (3+), and Co (3+) are 107.8 pm, 57 pm, and 75 pm, respectively. [35] The d-spacing, lattice parameters, and average crystalline size were calculated by the well-known Bragg's Law and Scherer's Formula given in equations (3.1) and (3.2), and crystalline size is around 20 nm at 1100^0C for host GAG and changes with the doping concentration of Cobalt in GAG [16][36-38]

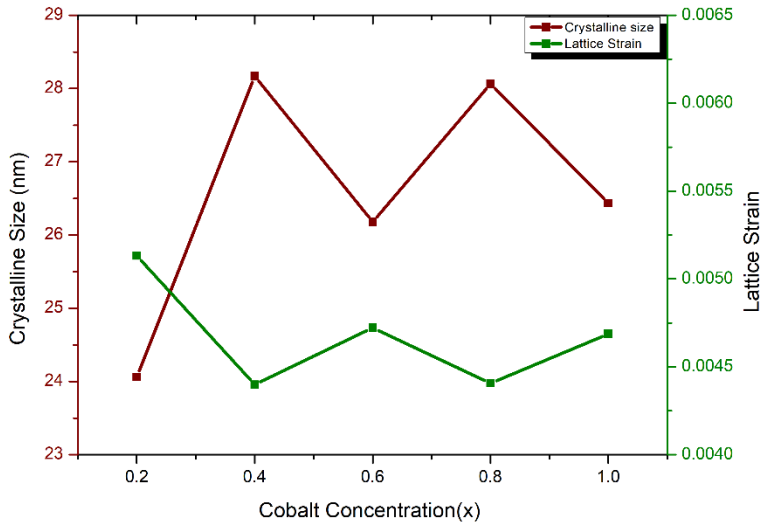

Fig.4.20 Variation of Lattice strain and crystallite size of GAG: Co with respect to doping concentration.

X-ray diffraction (XRD) is a potent method revealing crystalline size and lattice strain in materials, especially due to doping-induced deformation. In GAG, Figure 4.20 illustrates

an inverse relationship between crystallite size and lattice strain. Tensile strain impedes crystallite growth by pushing them apart, while compressive strain compacts crystallites, resulting in smaller sizes compared to unstrained samples.

4.3.2. Fourier transforms infrared spectroscopy:

The Perkin Elmer Fourier Transform Spectrometer was employed to conduct FTIR spectroscopy within the 400-4000 cm-1 range and GAG doped with various concentrations of Cobalt, was sintered at 1100°C as shown in figure 4.21. FTIR spectroscopy was performed to examine the functional group present in precursors.

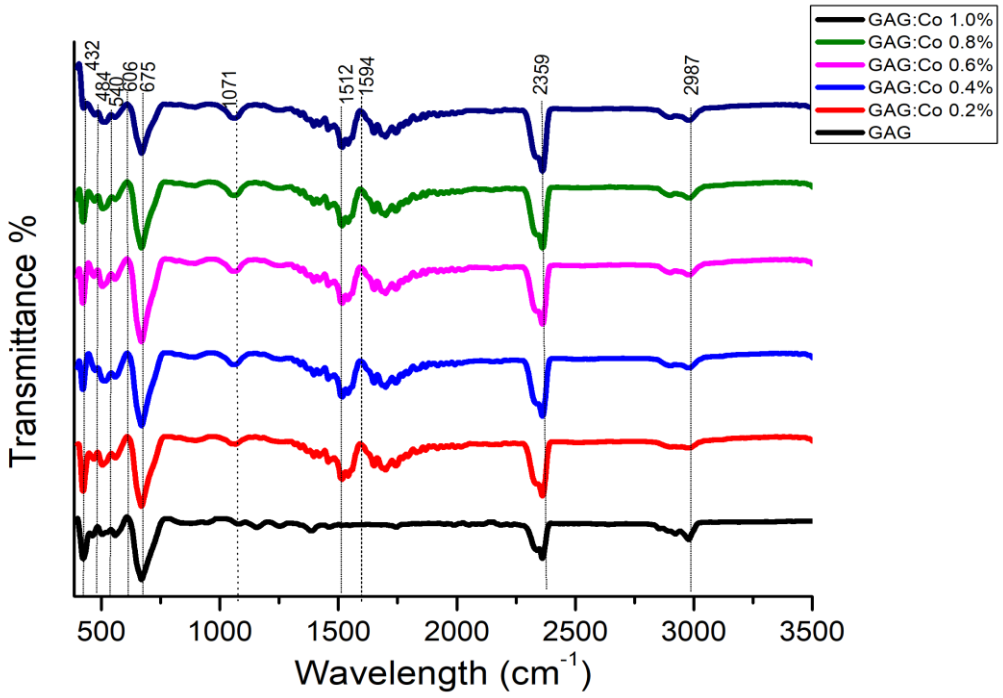

Fig 4.21 FTIR spectrum of the GAG: Co precursor at 1100 °C with different concentrations of dopant.

FTIR absorption peaks found at the region around 400-700 cm^{-1} were pure metal-oxide bonds i.e., Gd-O metal-oxygen and Al-O metal bonds established for GAG and these do not change with the doping of Cobalt [39]. Peaks at 2897 cm^{-1} were due to the presence of water in the sample. The absorptions peak near 2359 cm^{-1} due to starching of carbon dioxide (O=C=O).[4] around 1071 cm^{-1}, peak observed due to C-C starching bond. The

peaks in the range 1250-1560 nm absorption band were observed due to the 4A2 → 4T1 (4F) transition of the tetrahedral coordinated Co ions [40].

4.3.3. Field Emission Scanning Electron Microscopy; FE-SEM:

The Field Emission Scanning Electron Microscopy (FE-SEM) images of Co (1.0) doped GAG precursor, calcined at 1100^0C shown in Figure 4.22. The powder sample prepared by using the sol-gel method had a crystalline size between 50 to 200 nm. The powder sample consisted of particles with a spherical shape, and certain particles exhibited agglomeration. This agglomeration can be attributed to the presence of a cage network in the sample, which resulted from the addition of citric acid before the gel decomposition process. The precursor was found with an average particle size of around 30-35 nm.

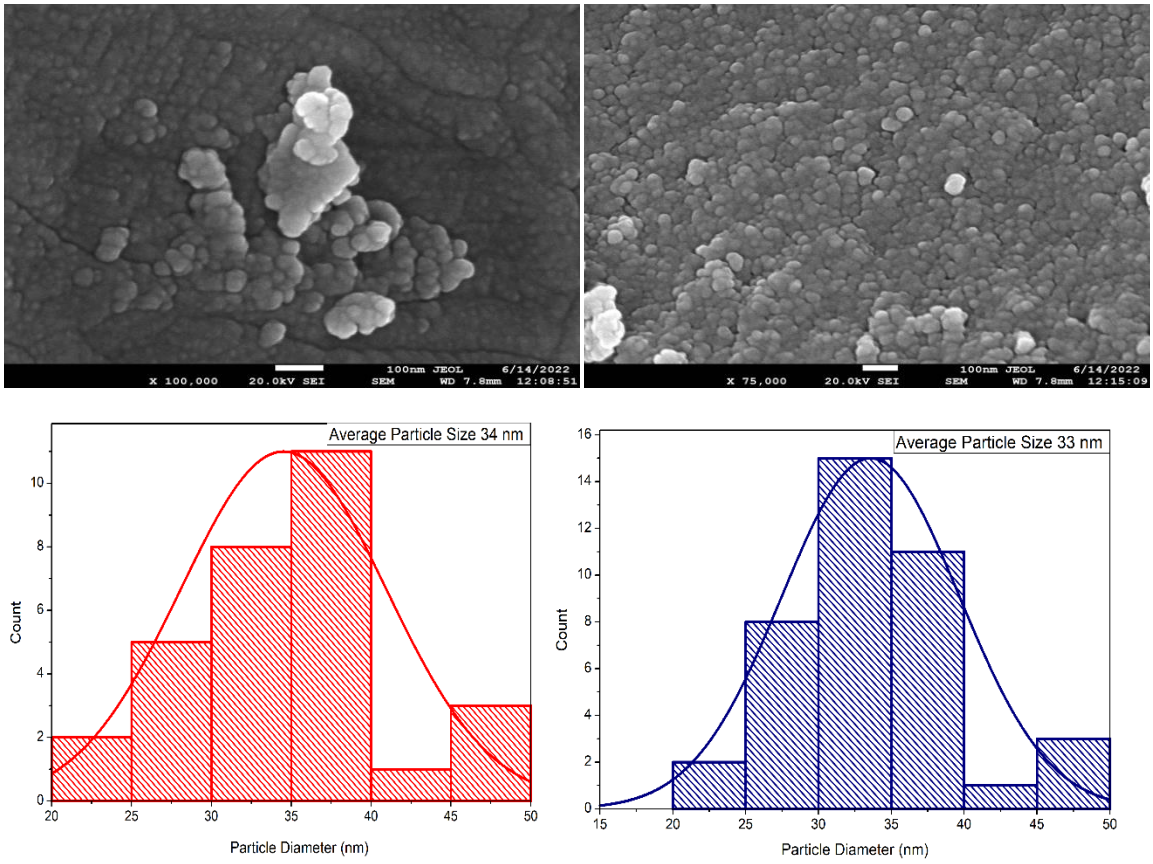

Fig 4.22 FESEM micrograph and histograms representing the particle size distribution of the GAG: Co (1.0) powder sample sintered at 1100 °C.

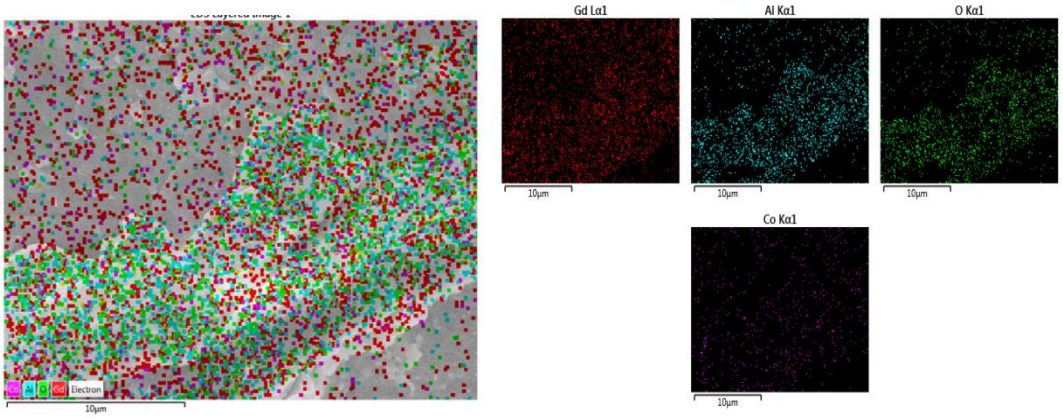

(a) (b)

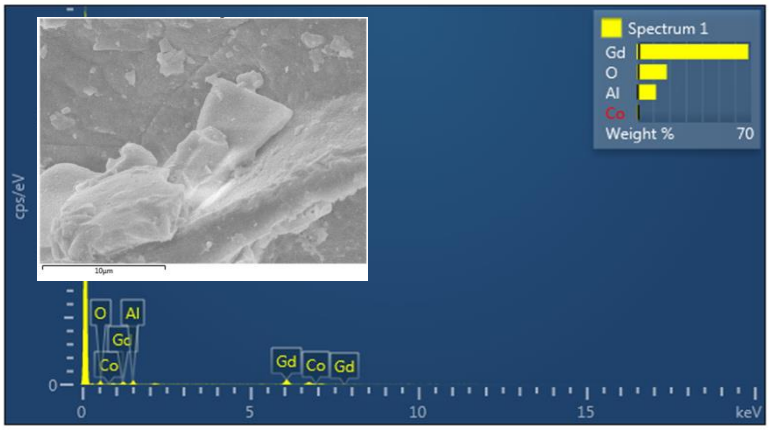

(c)

Fig. 4.23 (a,b) EDX element mapping in SEM mode of Gd, Al, O, and Co and (c) EDX spectra of GAG: Co 0.1 wt%.

In Figure 4.23(a,b) EDX element mapping in SEM mode of Gd, Al, O, and Co showed, and during EDX different areas of samples were exposed. The peaks of Gd, Al, O, and Co confirm the formation of GAG and Co doping shown in Figure 4.23(c).The weight and atomic % are mentioned in Table 4.8.

Table 4.8 EDX weight (%) and atomic (%) for the area exposed for the sample GAG: Co 1.0Wt%.

Element	Weight %	Atomic %
Gd	68.11	21.11
Al	11.81	21.34
O	18.45	56.21
Co	1.63	1.34

4.3.4. High-Resolution Transmission Electron Microscope (HRTEM)

High-Resolution Transmission Emission Spectroscopy (HRTEM) for GAG: Co (1.0) has been done with Tecnai G2 20 S-TWIN [FEI]. Figure 4.24 displays the HRTEM images for GAG: Co and shows that the cubic structure of material found from these images and HRTEM calculations indicate that the d-spacing of the material is around 0.28 nm. These findings are entirely confirmed by the XRD results and the images demonstrate that GAG: Co has good crystallinity.

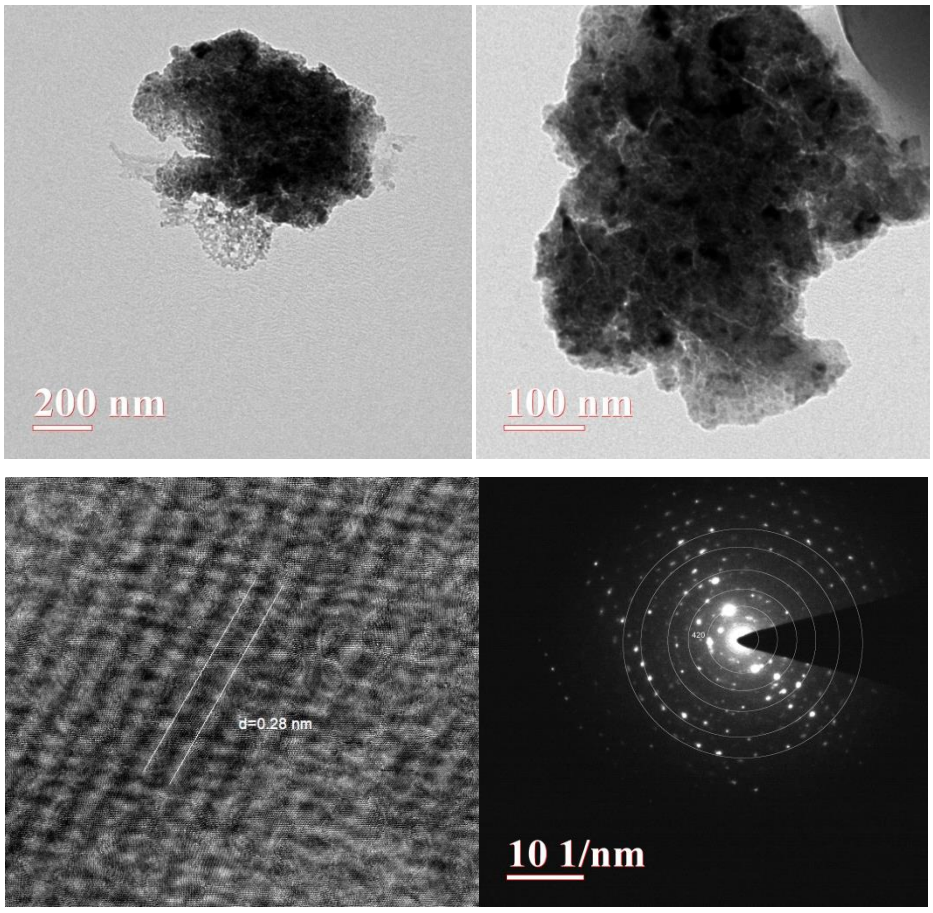

Fig.4.24 Typical HRTEM images of GAG: Co (1.0).

4.3.5. UV-Vis Spectroscopy

UV-Vis absorption spectroscopy is a useful tool for examining the effect of doping on the host lattice and its coordination location. To investigate the typical emission of GAG doped with cobalt, UV-Vis spectra were obtained for increasing concentrations of doping, as shown in Figure 4.25.

An absorption peak was observed around 200-400 nm. The broad emission spectra observed in the UV graph from 200-400 nm were attributed to defect states. As the doping concentration of Cobalt increased, both the area under the curve and full width at half maximum (FWHM) increased, indicating an increase in defect states. The band gap (Eg) for GAG was calculated using the formula 3.6. It was found that the band gap of the material decreases with the increase in doping concentration.

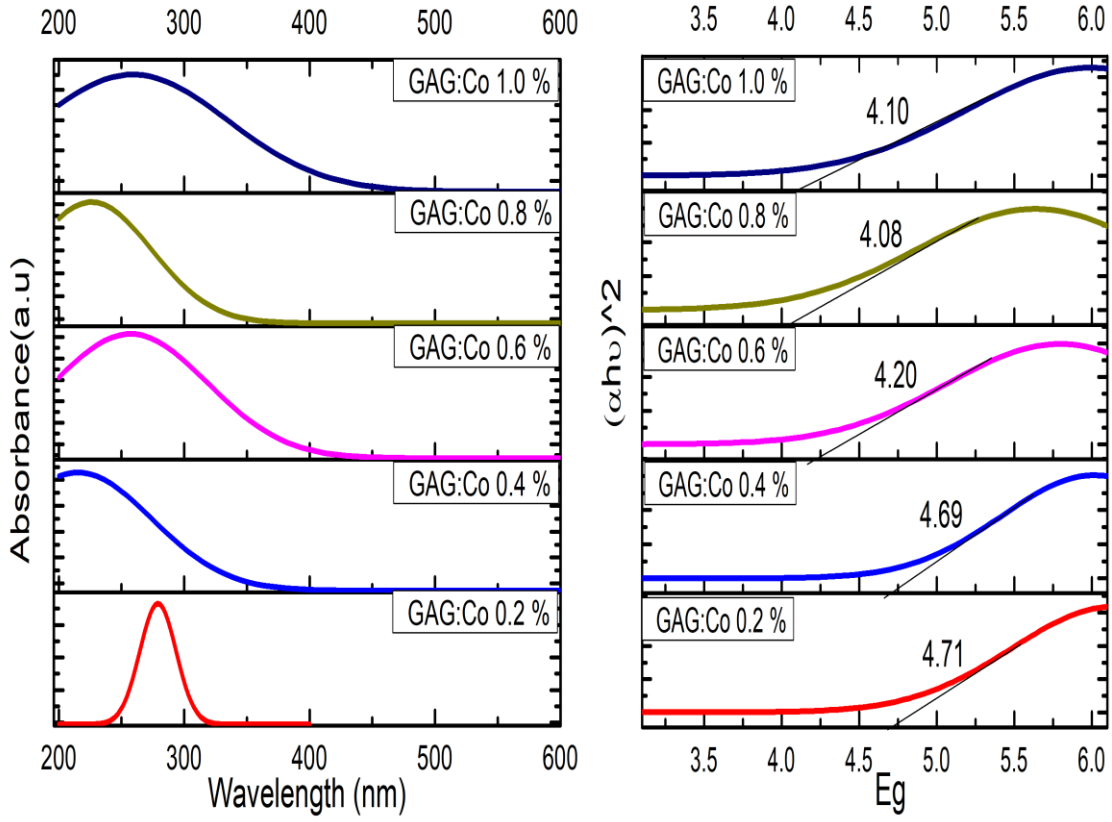

Fig.4.25 (a) UV- visible absorption and (b) Energy band gap for GAG: Co sintered at 1100^0.

Figure 4.26 shows the variation of the optical band gap and crystalline size of doped GAG and observed that the optical band gap of un-doped GAG is less than that of Co-doped GAG. Moreover, the increase in doping percentage in GAG found a reduction in the optical band gap. After approaching some reports, the reduction in the band can be explained based on exchange interactions of s-p electrons with the d-electron of dopant or it may be due to the presence of some mid-band gap states that results in a shift of optical band gap [41]. The crystalline size gets increased after doping. The absorbance intensity had increased with the increase of dopant since the crystallinity of the sample was increased.

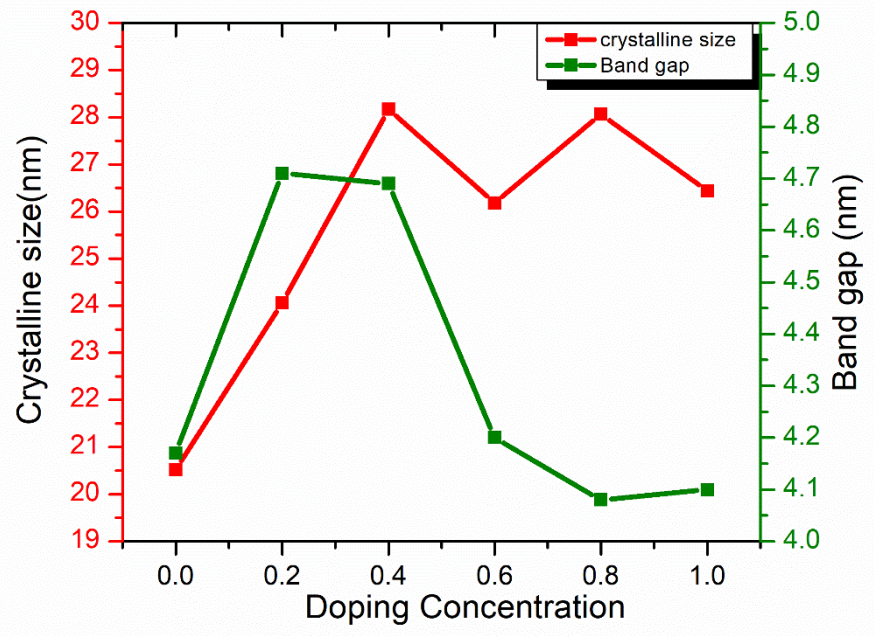

Fig.4.26 Variation in Crystalline size and band gap with different doping of cobalt in GAG.

4.3.6. Fluorescence Spectroscopy:

Gadolinium aluminum garnet (GAG) doped with cobalt shows exciting fluorescent properties that make it suitable for various applications such as light-emitting diodes (LEDs) and scintillators. Cobalt-doped GAG's fluorescence emission has been thoroughly investigated and its distinctive emission peaks have been established.

The fluorescence emission spectra of cobalt-doped GAG were measured using different excitation wavelengths 270nm and 282 nm shown in figure 4.27. Cobalt-doped GAG was discovered to have fluorescence emission peaks in the violet, blue, and green parts of the spectrum. While the blue and green emission peaks were seen in the area 450–550 nm, the violet emission peaks were seen at 420–445 nm. The violet emission peaks are defined as band edge emission that results from an indirect transition from the edge to the center that is helped by phonons. The peaks around 450 nm and 545 nm were due to the defect centers allied with oxygen vacancies, and defect centers originated due to the entrapping of one or more electrons in oxygen vacancies.

The 463 nm peak can be associated with the d–d transition Co from $^4T_1$ (F) to $^4T_1$ (P). The fluorescence intensity of cobalt-doped GAG was found to increase with the increase in the concentration of cobalt. The increase in the concentration of cobalt also led to an increase in the area under the curve and FWHM (full width at half maximum) of the UV-Vis spectrum, indicating an increase in defect states. Cobalt is a transition metal that displays several transition lines in its electronic spectra.

Cobalt's transition lines are of special relevance in the context of doped materials because they can provide important details about the material's electrical structure. The $^4T_1$ to $^4A_2$ transition line was observed in cobalt-doped Gadolinium Aluminum Garnet (GAG). This transition line is responsible for the peak observed around 601 nm in the fluorescence spectra of the material. It arises from the excitation of an electron from the ground state of the Co^{3+} ion ($^4T_1$) to an excited state ($^4A_2$) through the absorption of a photon of appropriate energy. The transition lines of cobalt are generally associated with the d-d transitions of the ion, where the valence electrons of cobalt transition between the 3d orbitals.

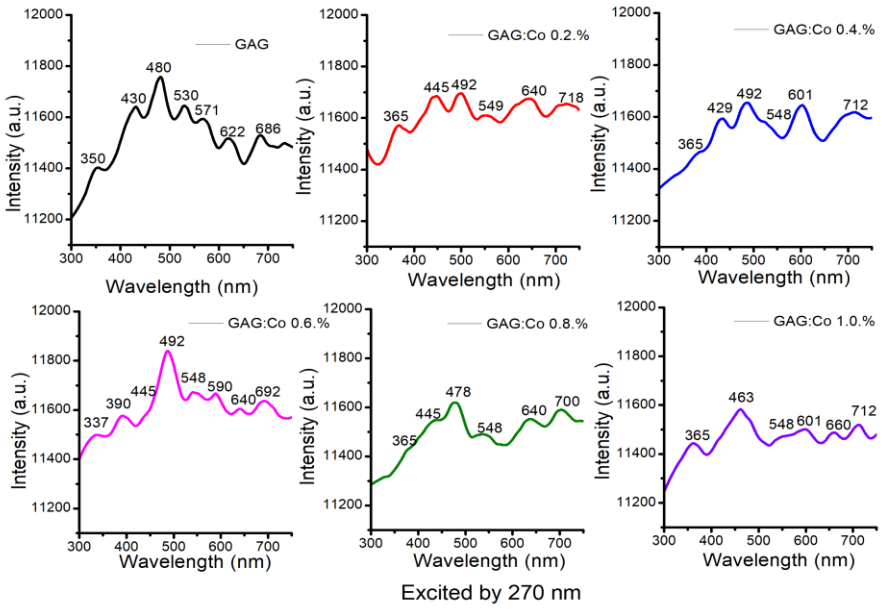

(a)

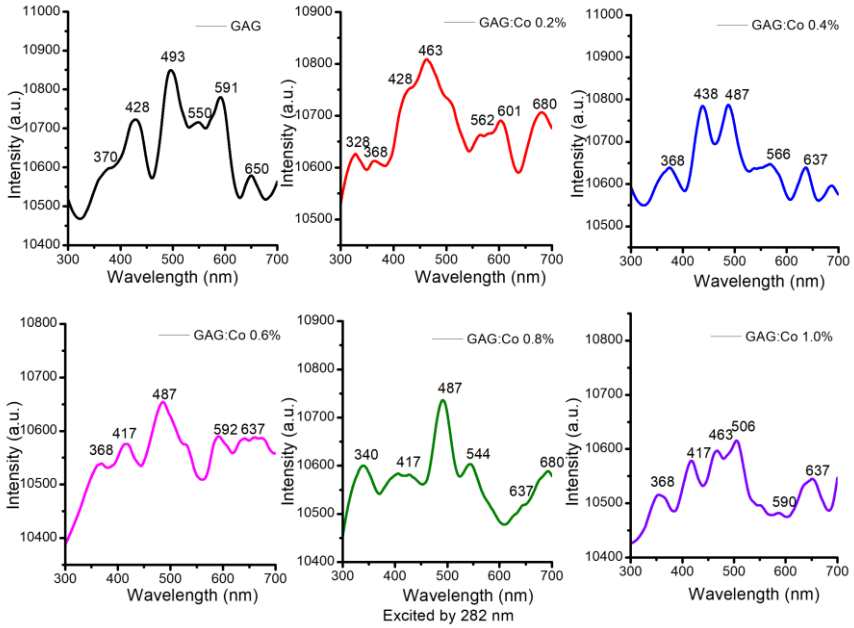

(b)

Fig. 4.27 Emission spectra of GAG: Co (Different concentration) at 1100^{0}C at excitation (a) 270nm and (b) 282 nm.

Cobalt-doped gadolinium aluminum garnet (GAG: Co) displays intriguing fluorescent characteristics upon excitation at 270 nm. This excitation induces violet emission peaks (420-445 nm) attributed to band edge emission, facilitated by phonon-assisted indirect transitions from the crystal edge to its center. Additionally, GAG: Co exhibits blue and green emission peaks (450–550 nm) resulting from defect centers linked to oxygen vacancies and trapped electrons. A distinct peak at 463 nm corresponds to the d-d transition of Co from $^4T_1(F)$ to $^4T_1(P)$, contributing to the vivid blue emission. Excitation at 282 nm reveals detailed fluorescence emission, with violet, blue, and green peaks. The blue and green emissions intensify with increased cobalt doping, indicating elevated defect center concentrations. This is corroborated by the widening of emission spectra, signifying a rise in defect concentration with higher cobalt doping levels. [42-45]

Overall, the fluorescence emission of cobalt-doped GAG excited by 282 nm is a result of various transitions involving cobalt ions and defect centers in the lattice, and it can provide valuable insights into the structural and optical properties of the material.

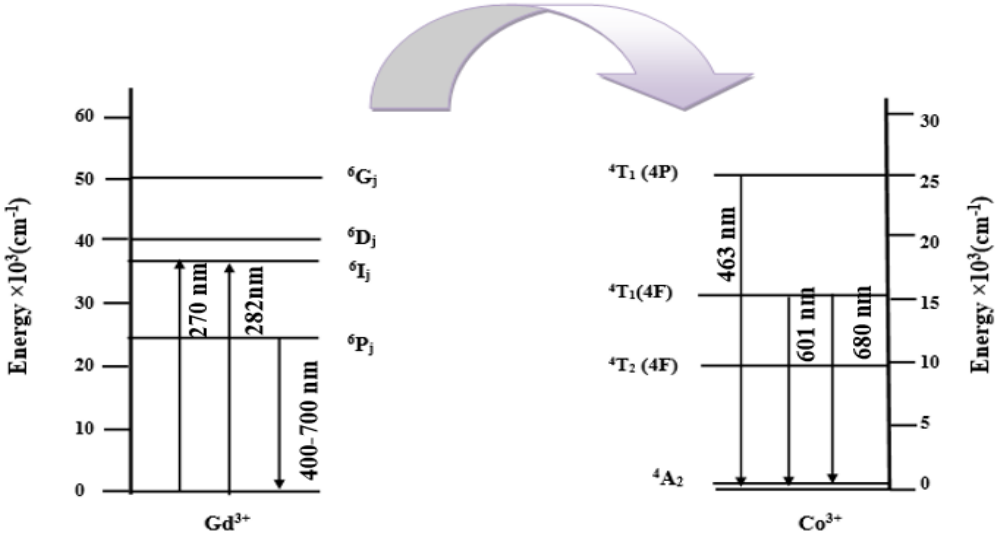

Fig. 4.28 Energy level diagram of Gd $^{3+}$ and Co3+ ion.

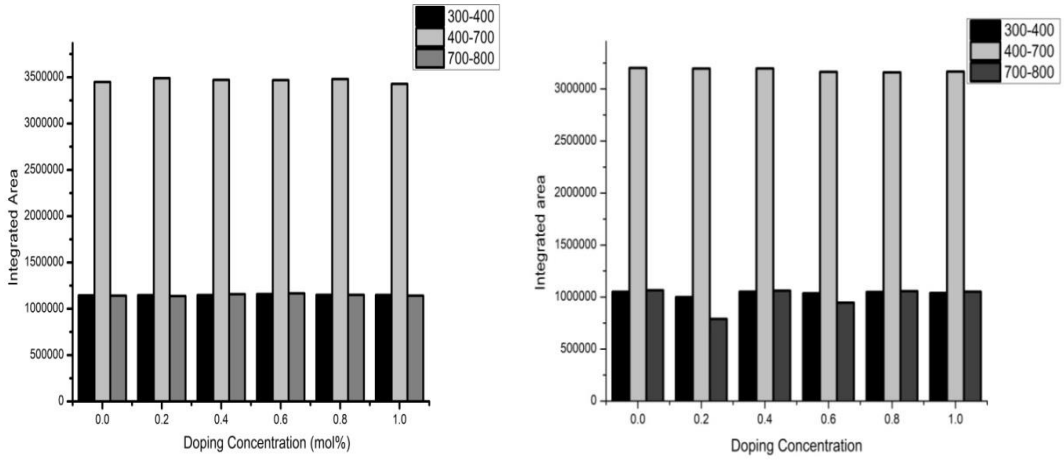

(a) (b)

Fig.4.29 Integrated intensity with a doping concentration of GAG: Co (Different concentration) at excitations (a) 270 nm and (b)282 nm.

Figure 4.29 shows the integrated area of cobalt-doped GAG at various concentrations and a bar graph plotted for the UV (300-400 nm), visible (400-700nm), and IR (700-800) regions. At 0.2 concentration of cobalt in the GAG integrated area for the visible region is maximum and for the white light emission visible light is required. So, 0.2 concentration of GAG: Co is optimized.

4.3.7. Fluorescence Lifetime

The fluorescence decay for $Gd_3Al_5O_{12}$ doped with cobalt was synthesized at 1100^0C shown in Figure4.30 The inset shown in the figure is the lifetime for GAG: Co of 270nm emission, plotted aligned with the temperature. The decay curve for GAG: Co was fitted in a single exponential function according to the following equation: I = A*exp (-x/t) + B. Where I= relative intensity, x is decay time, t is fluorescence lifetime and A and B are constants. The results of fitting are shown in table 4.9 [19][29,30][46]. Form results found that the lifetime decreases with the doping concentration of cobalt in GAG and decay time increases as the doping concentration increases.

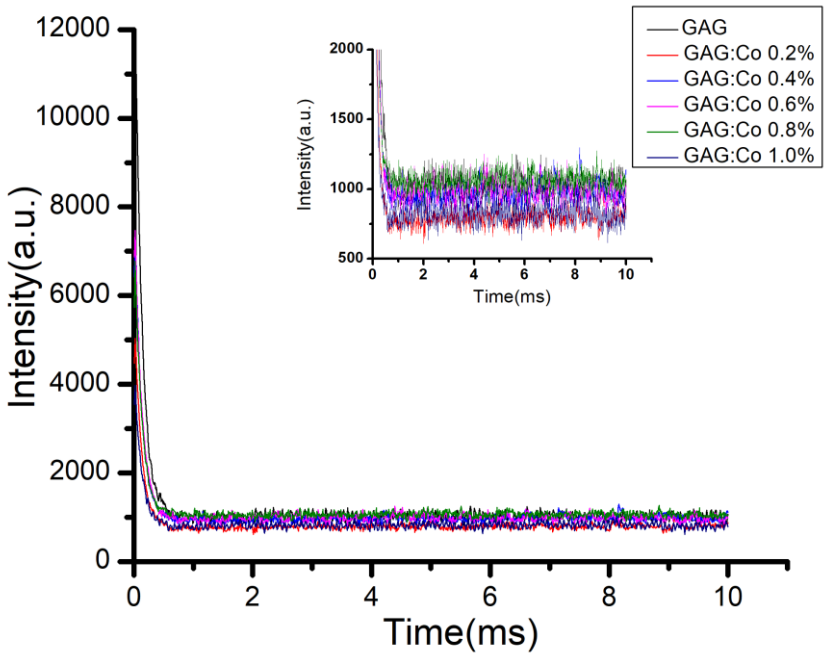

Fig 4.30 Fluorescence lifetime for GAG: Co sintered at 1100ºC.

Table 4.9 Decay time and lifetime of cobalt-doped GAG.

	A	B	t (lifetime)	Decay time(ms)
0	12782.746 ± 70.2	1010.9411 ±3.7	0.126	0.160
0.2	4859.151 ± 37.8	786.2143 ± 1.9	0.124	0.177
0.4	7239.052 ± 51.0	969.3645 ±2. 6	0.124	0.174
0.6	7316.133 ± 50.0	984.7285 ± 2.6	0.123	0.176
0.8	6350.672 ± 46.9	1059.5711 ± 2.4	0.124	0.180
1.0	3511.113± 41.7	817.8638 ± 2.1	0.123	0.196

4.3.8. Chromaticity

In Figure 4.31, the Commission Internationale de L'Eclairage (CIE) color coordinates (x, y) of GAG: Co (where Co = 0.2, 0.4, 0.6, 0.8, and 1.0) samples are calculated. The chromaticity diagram shows that coordinates shifted to the white area after doping of Cobalt in GAG. The color coordinates found for various doping were located in the white light area in the middle of the chromaticity diagram. So, tuned color with doping of Co3+

in GAG shows the application of the material in solid-state white light sources and also for a few other optical fields. The CCT ,and color purity of GAG-doped Cobalt were calculated by using equations (1.4) and (1.5) correspondingly and results are shown in the table 4.10.

Table 4.10 CIE coordinates, CCT, color purity, and CRI values of cobalt-doped GAG at excitation wavelengths 270 nm and 282. nm.

Doping conc.	**CIE coordinates**		**CCT**		**Color Purity**		**CRI**	
	270 nm	282 nm	270 nm	282 nm	270nm	282nm	270nm	282nm
0	(0.333,0.332)	(0.333,0.334)	5513	5476	0.3%	0.2%	95	96
0.2	(0.333,0.333)	(0.332,0.332)	5464	5498	0%	0.4%	95	95
0.4	(0.333,0.333)	(0.332,0.332)	5457	5508	0%	0.4%	95	95
0.6	(0.333,0.334)	(0.333,0.333)	5475	5460	0.3%	0%	96	95
0.8	(0.333,0.332)	(0.332,0.333)	5477	5504	0.2%	0.2%	95	95
1.0	(0.333,0.333)	(0.333,0.333)	5470	5488	0%	0%	95	95

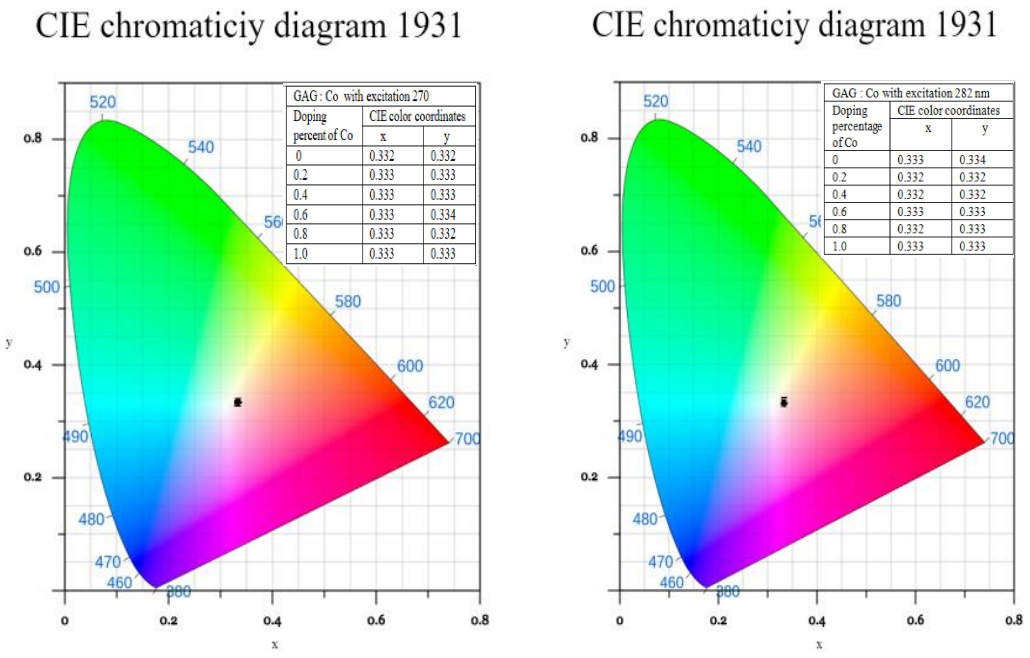

Fig. 4.31 CIE chromaticity diagram with CIE color coordinates (x, y) of GAG: Co sample under 270 nm and 282 nm excitation.

4.4. Gadolinium Aluminum Garnet co-doped with Chromium and Cobalt

Gadolinium aluminum garnet (GAG) has been extensively investigated for its optical and structural properties, particularly with single doping of cobalt and chromium. The observed positive impact of both dopants on the host GAG makes the material promising for applications in solid-state light sources. Building upon this, further co-doping of Cr3+ and Co3+ in GAG has been explored, anticipating energy transfer within the host and between the two dopants. The distinctive and impactful transition lines of Cr3+ and Co3+ suggest that the emission from the material should incorporate contributions from both, potentially yielding favorable results for achieving white light emission. In an extension of this research, the present study focuses on understanding the influence of Cr^{3+} and Co^{3+} co-doping on the structural and luminescent properties of GAG. The objective is to enhance emission characteristics, color rendering, and overall efficiency. The anticipated outcomes hold significant implications for diverse applications, including display devices, white light-emitting diodes (WLEDs), and solid-state light sources. This research seeks to contribute valuable insights into tailoring the properties of GAG for advanced optoelectronic applications.

4.4.1. X-ray Diffraction

X-ray diffraction analysis of Cr^{3+} and Co^{3+} co-doped GAG garnet deposited at various concentrations and sintered at 1100ºC is shown in Figure 4.32 (a). The figure represents the diffraction peaks belonging to the cubic structure of the GAG phase in conformity with JCPDS (no 01-073-1371) confirming the occurrence of a single garnet phase. This shows that no impurity peak was found in the XRD pattern after the co-doping in GAG. The (420) major peak of GAG: Co, Cr has the computed crystalline size, d-spacing, peak shift, lattice constant, and dislocation density. The changes in crystalline size, lattice strain, defects in the lattice, and unit cell expansion, may be due to replacing Al3+ or Gd3+ after doping of Cr3+ and Co3+ in GAG that causes. The d-spacing and the estimated crystalline size are calculated by Bragg’s law and Scherrer's formula respectively shown in equations 3.1 and

3.2. The crystalline size of pure host GAG is around 20 nm and after doping or co-doping it is found to increase since dopant enters a crystal lattice. Hence, for GAG: Co (0.2), Cr(0), and GAG: Co(0), Cr(1.0) crystalline size increase to 26 and 23 nm respectively, and GAG: Co(0.2), Cr(1.0) has around 24.7 nm. The Dislocation Density for the prepared sample was determined by using the relation given in equation 3.3 for the cubic phase structure of GAG: Cr, Co.

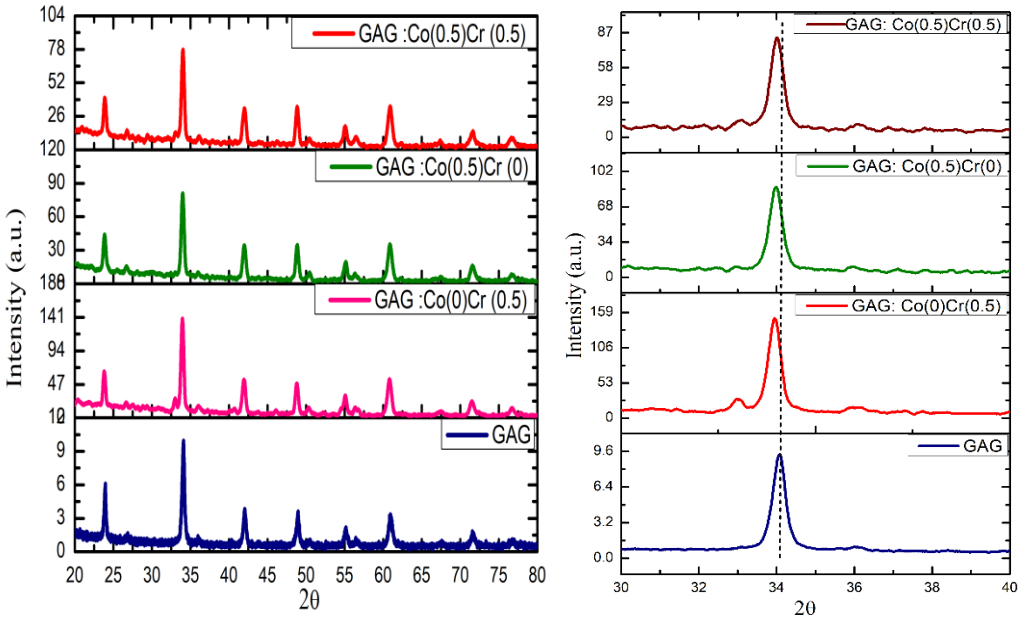

Fig 4.32. (a) Typical XRD spectra for GAG: Co, Cr sintered at 1100°C, (b) shift in diffraction peak with doping and co-doping of Co and Cr in GAG.

In comparison to the GAG host, the diffraction peaks of co-doped GAG get shifted towards the lower angle of 2θ seen in Figure 4.32(b). The peak position for pure host GAG at 34.19° of 2θ, but after doping for GAG: Co(0.5) and GAG: Cr the peak position was found at 33.96° and 33.98°, which means the peak gets shifted towards the lower angel of 2θ due to the lattice distortion or lattice strain induced by doping of Co(0.2) and Cr (1.0) in the GAG. Moreover, for co-doping of Co (0.2) and Cr (1.0) in GAG, the peak found shifted to the higher value of 2θ and the peak position observed at 34° which implies that Co-doping of Co and Cr reduces the distortion as compared to single doping in GAG.

4.4.2. Fluorescence Spectroscopy

Fluorescence spectroscopy is a significant technique for the analysis of the optical properties of material. It works on the principal excitation of an electron from the lower ground state to the excited state and after the instability of exited states gets back to the ground state. The spectra for GAG co-doped with Co3+ and Cr3+ are shown in Figure 4.33.

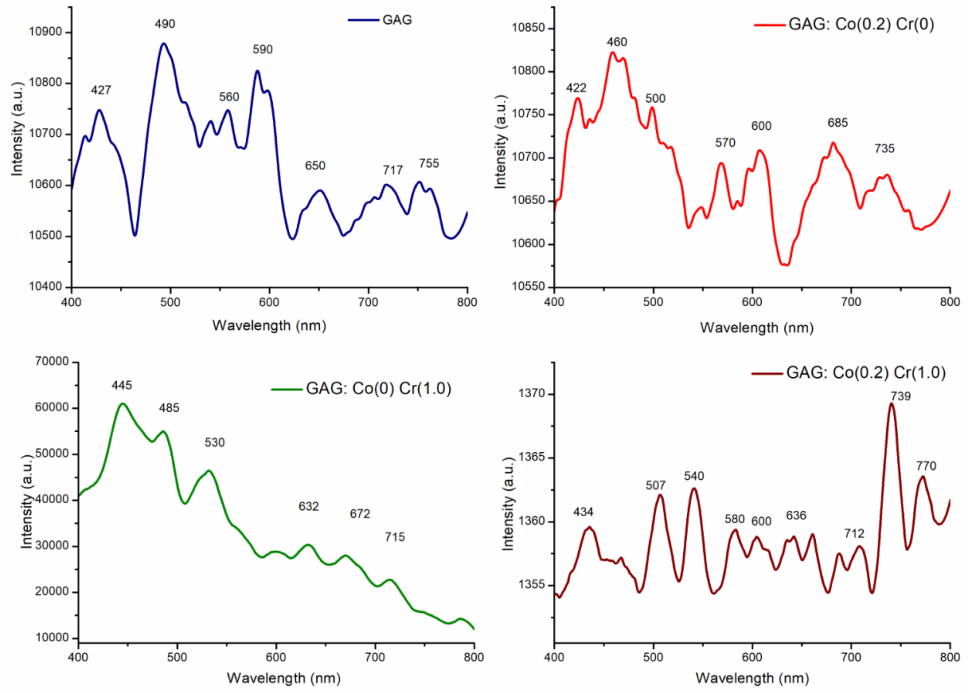

Fig 4.33. Fluorescence spectra for excitation 282 nm of GAG: Co, Cr sintered at 1100°C.

The spectra were observed by examining under the excitation 282 nm and the spectra of pure host GAG show the multiple emission in the visible region due to the Gd3+ transition lines and defect states. The peaks centered at 590 nm and 650 nm correspond to 4f→4f transitions of Gd3+, being the $^6G_{7/2} \rightarrow {}^6P_{7/2}$ and $^6G_{7/2} \rightarrow {}^6P_{3/2}$ transitions, respectively. After doping of Cobalt and Chromium in GAG the energy is transferred within host and dopant. [49,50] The emission spectra of GAG: Co (1.0) observed peaks at 460 nm, 500 nm, and 685 nm due to the Co3+ transition. Apart from these peaks around 445 nm, 530 nm, and 632 nm are also due to the $^4A_2 \rightarrow {}^4T_1$ and $^4A_2 \rightarrow {}^4T_2$ transition of Cr3+.

The International Commission on Illumination (CIE) chromaticity diagram and coordinates for the host, singly and co-doped samples are shown in figure 4.34. The CIE color coordinates (x,y) for all samples have been calculated and listed in Table 4.11. Herein, a change in CCT, CRI and CP values has been detected with the incorporation of doping. Moreover, the values are found enhanced and improved in case of double doping of Cr^{3+} and Co^{3+} in GAG.

Table 4.11 Shows the value of CIE, CCT, CRI, and Color Purity of co-doped GAG with Cr and Co.

Sample Code	CIE coordinates	CCT	Color Purity	CRI
GAG	(0.333,0.334)	5476	0.2	96
GAG: Co (0.2)	(0.332,0.332)	5498	0.5	95
GAG: Cr(1.0)	(0.276,0.290)	9353	18.0	94
GAG: Cr(1.0) Co(0.2)	(0.333,0.333)	5457	0.1	96

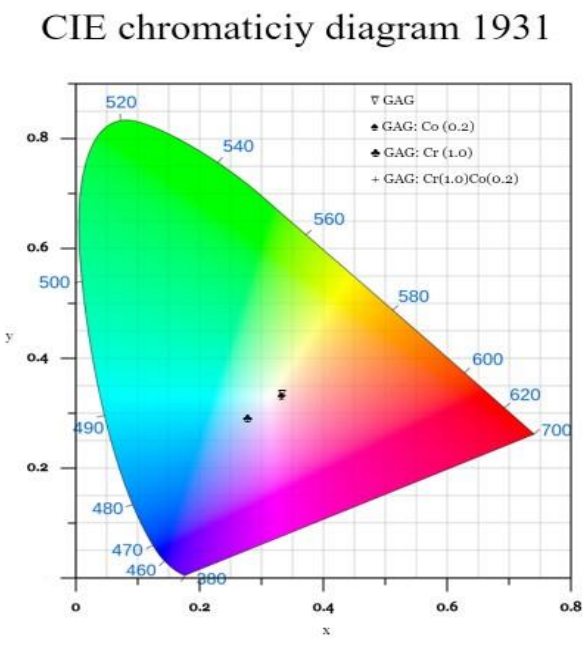

Fig. 4.34. Shows the CIE coordinates of Chromium and Cobalt co-doped GAG.

References:

1. E. Garskaite, S. Sakirzanovas, A. Kareiva, J. Glaser, and H. J. Meyer, "Synthesis and structure of europium aluminium garnet (EAG)," J. Inorg. Genral Chem., vol. 633, no. 7, pp. 990–993, 2007.
2. M. Uemura, T. Yamagishi, S. Ebisu, S. Chikazawa, and S. Nagata, "A double peak of the coercive force near the compensation temperature in the rare earth iron garnets," Philos. Mag., vol. 88, no. 2, pp. 209–228, 2008.
3. J. Y. Choe, D. Ravichandran, S. M. Blomquist, K. W. Kirchner, E. W. Forsythe, and D. C. Morton, "Cathodoluminescence study of novel sol–gel derived $Y_{3-x}Al_5O_{12}$: Tbx phosphors," J. Lumin., vol. 93, p. 119, 2001.
4. J. Li, J. G. Li, Z. Zhang, X. Wu, S. Liu, X. Li, X. Sun, Y. Sakka, "Crystal structure stabilization via Lutetium doping and properties of the $(Gd_{1-x}Lux)_3Al_5O_{12}$ Solid Solutions (x= 0–0.5)," J. Am. Ceram. Soc., vol. 95, no. 3, pp. 931–936, 2012.
5. J. A. Gadsden, "Infrared spectra of minerals and related inorganic compounds," Infrared Spectra Miner. Relat. Inorg. Compd., vol. 40, no. 313, p. 277, 1976.
6. I. Lanez, B. Rekik, M. Derbal, and A. Chaib, "Structural study and the effect of ionic size of the systems," J. Fundam. Appl. Sci., vol. 11, no. 2, pp. 857–874, 2019.
7. M. A. Hameed, O. A. Ali, and S. S. Al-Awadi, "Optical properties of Ag-doped nickel oxide thin films prepared by pulsed-laser deposition technique," Optik, vol. 206, p. 164352, 2020.
8. P. S. Peijzel, P. Vermeulen, W. J. M. Schrama, A. Meijerink, M. F. Reid, and G. W. Burdick, "High-resolution measurements of the vacuum ultraviolet energy levels of trivalent gadolinium by excited state excitation," Phys. Rev. B , vol. 71, no. 12, p. 125126, 2005.
9. G. Liu, B. Wang, J. Li, B. Cao, Y. Lu, and Z. Liu, "Research progress of gadolinium aluminum garnet based optical materials," Phys. B, vol. 603, p. 412775, 2021.
10. J. Kaur, S. Rani, and B. Lal, "Luminescence properties of Eu^{3+} doped gadolinium aluminum garnet phosphors," Optik, vol. 212, p. 164745, 2020.

11. J. Li, J. G. Li, Z. Zhang, X. Wu, S. Liu, X. Li, X. Sun, and Y. Sakka, "Effective lattice stabilization of gadolinium aluminate garnet (GdAG) via Lu^{3+} doping and development of highly efficient (Gd, Lu) AG: Eu^{3+} red phosphors," Sci. Technol. Adv. Mater., 2012.
12. T. M. Rekha, P. Kamala, B. Kumar, and K. V. R. Murthy, "Synthesis and photoluminescence study of Tb (1%) Eu (1%) Ge (1%) and Ce (1%) doped with $(YGd)_3Al_5O_{12}$," in Proceedings of the twenty second national conference, 2016.
13. Y. Shi, Y. Wen, M. Que, G. Zhu, and Y. Wang, "Structure, photoluminescent and cathodoluminescent properties of a rare-earth free red emitting β-$Zn_3B_2O_6$: Mn^{2+} phosphor," Dalton Trans., vol. 43, no. 6, pp. 2418–2423, 2014.
14. X. Wang, Z. Zhao, Q. Wu, C. Wang, Q. Wang, L. Yanyan, and Y. Wang, "Structure, photoluminescence and abnormal thermal quenching behavior of Eu^{2+}-doped $Na_3Sc_2(PO_4)_3$: a novel blue-emitting phosphor for n-UV LEDs," J. Mater. Chem. C , vol. 4, no. 37, pp. 8795–8801, 2016.
15. L. Alexander and H. P. Klug, "Determination of crystallite size with the X-ray spectrometer," J. Appl. Phys., vol. 21, pp. 137–142, 1950.
16. S. Rani, B. Lal, S. Saxena, and S. Shukla, "Modifications in the structural and optical properties of ZnO nanophosphor on doping with tb," J. Nanosci. Nanotechnol., vol. 9, pp. 353–361, 2019.
17. M. J. Iqbal and M. N. Ashiq, "Physical and electrical properties of Zr–Cu substituted strontium hexaferrite nanoparticles synthesized by co-precipitation method," Chem. Eng., vol. 136, pp. 383–389, 2008.
18. Y. Tang, S. Zhou, X. Yi, S. Zhang, D. Hao, and X. Shao, "The Cr-doping effect on white light emitting properties of Ce: YAG phosphor ceramics," J. Am. Ceram. Soc., vol. 100, pp. 2590–2595, 2017.
19. J. Li, J. G. Li, Z. Zhang, X. Wu, S. Liu, X. Li, X. Sun, and Y. Sakka, "Effective lattice stabilization of gadolinium aluminate garnet (GdAG) via Lu^{3+} doping and development of highly efficient (Gd, Lu)AG: Eu^{3+} red phosphors," Sci. Technol. Adv. Mate., 2012.

20. N. Pushpa and M. K. Kokila, "Effect of cobalt doping on structural, thermo and photoluminescent properties of ZnO nano powders," J. Lumin., vol. 190, pp. 100–107, 2017.
21. V. Lisitsyn, L. Lisitsyna, A. Tulegenova, Y. Ju, E. Polisadova, E. Lipatov, and V. Vaganov, "Nanodefects in YAG: Ce-based phosphor microcrystals," Crystals, vol. 9, p. 476, 2019.
22. H. Hua, X. Wang, H. Ding, Q. Du, S. Feng, H. Jiang, J. Jiang, H. Jiang, Z. Zhang, and H. Qin, "Preparation and luminescent properties of highly transparent Y3Ga5O12: M3+ (M = Dy, Cr) ceramics," J. Eur. Ceram. Soc., vol. 39, pp. 5345–5349, 2019.
23. A. Zabiliūtė-Karaliūnė, H. Dapkus, R. P. Petrauskas, S. Butkutė, A. Žukauskas, and A. Kareiva, "Cr3+ doped yttrium gallium garnet for phosphor-conversion light emitting diodes," Lith. J. Phys., vol. 55, 2015.
24. A. Yamaji, S. Kurosawa, A. Suzuki, J. Pejchal, K. Kamada, Y. Yokota, and A. Yoshikawa, "Optical and scintillation properties of Cr doped Y3Ga5O12 crystal for infrared scintillators," Key Eng. Mater., vol. 616, pp. 92–95, 2014.
25. C. Würth, M. Grabolle, J. Pauli, M. Spieles, and U. Resch-Genger, "Relative and absolute determination of fluorescence quantum yields of transparent samples," Nat. Protoc., vol. 8, pp. 1535–1550, 2013.
26. A. M. Brouwer, "Standards for photoluminescence quantum yield measurements in solution (IUPAC technical Report)," Pure Appl. Chem., vol. 83, pp. 2213–2228, 2011.
27. M. Levitus, "Tutorial: Measurement of fluorescence spectra and determination of relative fluorescence quantum yields of transparent samples," Methods Appl. Fluoresc., vol. 8, p. 033001, 2020.
28. M. Nyman, L. E. Shea-Rohwer, J. E. Martin, and P. Provencio, "Nano-YAG: Ce mechanisms of growth and epoxy-encapsulation," Chem. Mater., vol. 21, pp. 1536–1542, 2009.

29. X. Teng, W. Wang, Z. Cao, J. Li, G. Duan, and Z. Liu, "The development of new phosphors of Tb3+/Eu3+ co-doped Gd3Al5O12 with tunable emission," Opt. Mater., vol. 69, pp. 175–180, 2017.
30. L. Tian, L. Wang, L. Zhang, Q. Zhang, W. Ding, and M. Yu, "Enhanced luminescence of Dy3+/Bi3+ co-doped Gd3Al5O12 phosphors by high-efficiency energy transfer," J. Mater. Sci. Mater. Electron., vol. 26, pp. 8507–8514, 2015.
31. A. Bala and S. Rani, "UV excited emission spectra of gadolinium aluminium garnet," J. Opt., vol. 52, pp. 868–874, 2022.
32. A. Bala and S. Rani, "Down conversions excitation dependent luminescent properties of terbium aluminum garnet," J. Phys. Conf. Ser., vol. 2267, p. 012113, 2022.
33. X. Teng, J. Li, G. Duan, and Z. Liu, " Development of Tb3+ activated gadolinium aluminate garnet (Gd3Al5O12) as highly efficient green-emitting phosphors ", J. Lumin., vol. 179, p. 165, 2016.
34. S. K. Mishra, H. Roy, A. K. Lohar, S. K. Samanta, S. Tiwari, and K. Dutta, Mater. Sci. Eng., vol. 75(1), p. 012001, 2015.
35. L. Alexander and H. P. Klug, " Determination of crystallite size with the X-Ray spectrometer ",J. Appl. Phys.," vol. 21(2), p. 137, 1950.
36. P. Scherrer, "Bestimmung der Grösse und der inneren Struktur von Kolloidteilchen mittels Röntgenstrahlen," *Nachr. Ges. Wiss. Göttingen*, vol. 26, p. 98, 1918.
37. J. I. Langford and A. J. C. Wilson, " Scherrer after sixty years: a survey and some new results in the determination of crystallite size ",J. Appl. Crystallogr.," vol. 11, p. 102, 1978.
38. V. Uvarov and I. Popov, " Metrological characterization of X-ray diffraction methods at different acquisition geometries for determination of crystallite size in nano-scale materials ",Mater. Charact., vol. 85, p. 111, 2013.
39. J. A. Gadsden, *Butterworth, Newton, MA.*, 1975.

40. A. Szysiak, K. Leśniewska-Matys, H. Węglarz, P. Gołębiewski, D. Podniesiński, and A. Kozłowska, "Journal of the American Ceramic Society," vol. 104(3), p. 1204, 2021.
41. B. Choudhury and A. Choudhury, " Luminescence characteristics of cobalt doped TiO2 nanoparticles." J. Lumin.," vol. 132(1), p. 178, 2012.
42. A. M. Malyarevich, I. A. Denisov, K. V. Yumashev, O. S. Dymshits, and A. A. Zhilin, " Optical absorption and luminescence study of cobalt-doped magnesium aluminosilicate glass ceramics " JOSA B, vol. 19(8), p. 1815, 2002.
43. N. Serpone, " Is the band gap of pristine TiO2 narrowed by anion-and cation-doping of titanium dioxide in second-generation photocatalysts?" J. Phys. Chem. B., vol. 110(48), p. 24287, 2006.
44. W. Y. Wu, Y. M. Chang, and J. M. Ting, " Room-temperature synthesis of single-crystalline anatase TiO2 nanowires". Cryst. Growth Des., vol. 10(4), p. 1646, 2010.
45. N. M. Rasdi, Y. W. Fen, N. A. S. Omar, and M. H. M. Zaid, "Results in physics," vol. 7, p. 3820, 2017.
46. K. K. Rasu, D. Balaji, and S. M. Babu, " Photoluminescence properties of Eu3+: RbGd (WO4) 2 red phosphors prepared by sol–gel method" J. Lumin., vol. 170, p. 825, 2016.
47. B. V. Kumar, B. W. R. Kumar, P. Kamala, T. M. Rekha, and K. V. R. Murthy.
48. J. Y. Park, H. C. Jung, G. S. R. Raju, B. K. Moon, J. H. Jeong, S. M. Son, and J. H. Kim, "Opt. Mater.," vol. 32(2), p. 293, 2009.
49. I. Adell, R. M. Solé, M. C. Pujol, M. Lancry, N. Ollier, M. Aguiló, and F. Díaz, "Single crystal growth, optical absorption and luminescence properties under VUV-UV synchrotron excitation of type III Ce3+: KGd (PO3) 4, a promising scintillator material," Sci. Rep., vol. 8, no. 1, p. 11002, 2018.
50. I. Khan, G. Rooh, R. Rajaramakrishna, N. Sirsittapokakun, H. J. Kim, J. Kaewkhao, and K. Kirdsiri, "Energy transfer phenomenon of Gd3+ to excited ground state of Eu3+ ions in Li2O-BaO-Gd2O3-SiO2-Eu2O3 glasses," Spectrochim. Acta A Mol. Biomol. Spectrosc., vol. 210, pp. 21-29, 2019.

Chapter 5

Transition Metal Doped Cerium Aluminum Garnet (CAG)

5.1. Cerium Aluminum Garnet (CAG)

In recent times, researchers have been captivated by the exceptional qualities of newly synthesized garnets, specifically their outstanding structural, chemical, and optical characteristics, coupled with an impressive color rendering index. Garnets have found diverse applications spanning LEDs, display panels, lasers, field emission displays (FEDs), luminescent solar concentrators (LSCs), and more. Several well-known rare-earth garnets, including Yttrium Aluminum Garnet ($Y_3Al_5O_{12}$), Terbium Aluminum Garnet ($Tb_3Al_5O_{12}$), Lutetium Aluminum Garnet ($Lu_3Al_5O_{12}$), and Gadolinium Aluminum Garnet ($Gd_3Al_5O_{12}$), have become staples in research applications. However, certain lanthanide aluminum garnets, such as $Ce_3Al_5O_{12}$, $Pr_3Al_5O_{12}$, $Nd_3Al_5O_{12}$, $Dy_3Al_5O_{12}$, and $Er_3Al_5O_{12}$, have not yet undergone synthesis using the sol-gel method, based on current knowledge.

Despite this wealth of information, the synthesis of Cerium Aluminum garnets (CAG) via the sol-gel method has not been reported to date. Thus, the primary objective of the ongoing research study is to create and characterize CAG using the sol-gel technique at various temperatures. The cubic symmetry of garnets, along with their face-centered lattice structure and space group la3d, contributes to their unique properties. The intricate cation positioning within unit cells further enhances their distinctive characteristics. Notably, the luminescence properties of garnets undergo variation through the substitution of different elements, such as rare earths, at sites A and B. In garnet structures, trivalent ions such as Al^{3+} and Ga^{3+} occupy octahedral sites (A) and tetrahedral sites, respectively, while larger rare earth ions like Y^{3+}, Gd^{3+}, and Tb^{3+} preferentially locate themselves in dodecahedral sites (B). The present investigation explores the possibility of Ce^{3+} occupying dodecahedral sites within the garnet structure. As the research progresses, the focus remains on understanding the optical and structural properties of Cerium Aluminum garnets, shedding light on their potential applications and paving the way for advancements in the field of

solid-state lighting. This chapter explores the structural and luminescent properties of CAG thorough characterization utilizing X-ray diffraction (XRD), Fourier-transform infrared spectroscopy (FTIR), Scanning Electron Microscopy (SEM), and Fluorescence measurements.

5.1.1 X-Ray Diffraction (XRD):

Figure 5.1 illustrates the XRD spectra meant for Cerium Aluminum Garnet (CAG) recorded by varying the range of the Bragg's angle (2θ) from 0^o to 80^o which sintered at 900^0C, 1000^0C, 1100^0C, 1200^0C, and 1300^0C temperatures. The XRD pattern confirmed the formation of poor crystalline CeO_2 and, probably, amorphous aluminum oxide (Al_2O_3) up to 1000 [1]. But at 1100 peak start traces of $Ce_3Al_5O_{12}$ could be detected in the XRD pattern. The positions of diffraction peaks were found similar and compatible with the conventional cubic structure of other garnets at 1200^0C, which indexed with JCPDS-00-067-0123. The peaks identified in the XRD pattern for CeO_2 are marked with 'o', peaks of Al_2O_3 marked with the symbol 'x', and peaks that show the phase of CAG garnet marked as 'G'. It suggested that the homogeneous phase of CAG can be achieved at 1200^0C. [2-4]

Meanwhile, crystalline size can be calculated by Scherrer's formula (equation 3.2), and found that as calculations temperature rises crystallinity of the material increases. This means grain size increases with the increase of sintering temperatures.

The peak intensity of CAG was found to increase with temperature which indicates that the crystalline quality of material increased with the rise of temperature and the material became more crystalline with the rise of temperature. The lattice volume and dislocation density of GAG seem to be decreased with the temperature rise.

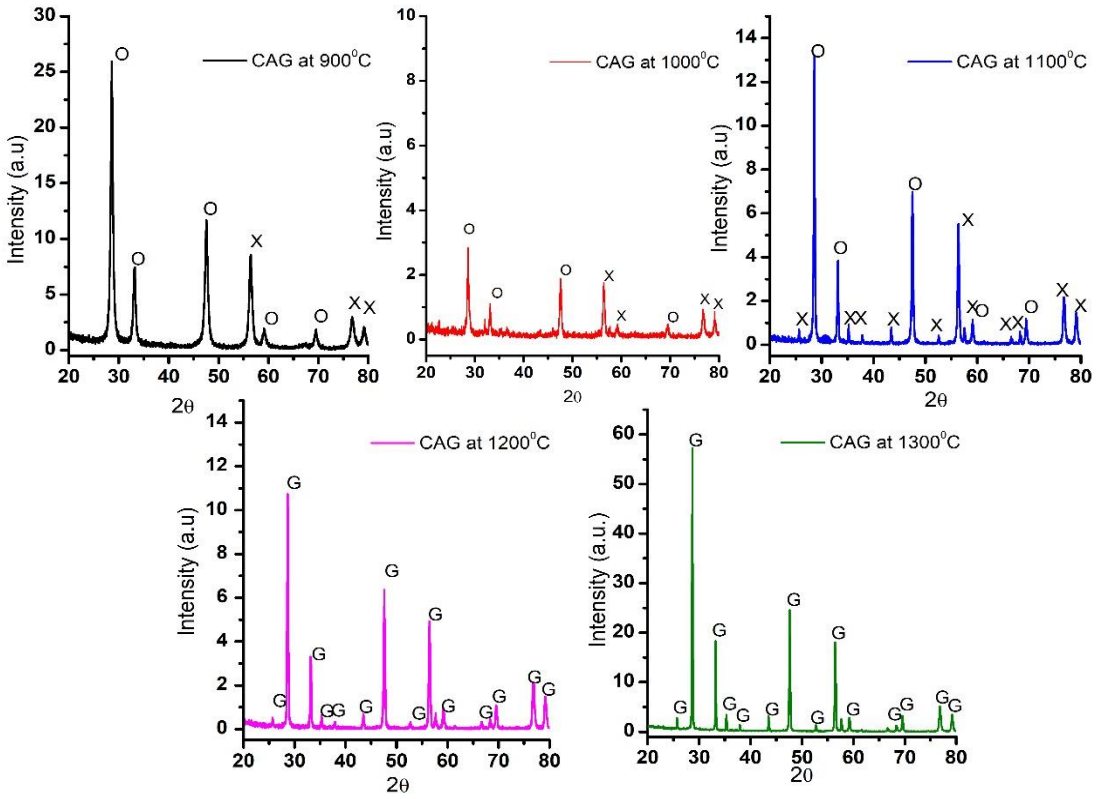

Fig.5.1 Typical XRD pattern of the CAG precursor powder samples sintered at different temperatures.

Porosity, in the realm of material science, measures the number of voids present within a material. This property is significant because it influences the material's physical and mechanical properties. Several factors, such as preparation method, sintering temperature, processing conditions, and the inclusion of dopant may be manipulated to regulate porosity. Calculated results indicate that the porosity of CAG seems to decrease as the sintering temperature rises. So, it may indicate that as the temperature increases the space or voids of the lattice of CAG have decreased which causes a decrease of porosity.

Table 5.1. The Crystallite size (D), d-spacing, lattice constants (a), lattice strain, and porosity (P), of CAG at 900°C, 1000°C, 1100°C,1200°C and 1300°C temperatures at hkl 321.

	900	1000	1100	1200	1300
2Θ	28.614	28.592	28.572	28.484	28.699
FWHM(β)	0.608	0.383	0.263	0.254	0.155
D	14.065	22.309	32.543	33.662	55.184
d-spacing	3.117	3.119	3.121	3.131	3.108
Lattice constant	11.663	11.671	11.679	11.715	11.629
Lattice Volume	1586.51	1590.10	1593.35	1607.92	1572.76
Dislocation Density($\times 10^{-3}$)	0.0050	0.0020	0.0009	0.0008	0.0003
Lattice strain	0.0104	0.0065	0.0045	0.0043	0.0026
Porosity	0.71	0.67	0.66	0.65	0.69

5.1.2 Scanning Electron Microscopy (SEM):

Scanning Electron Microscopy (SEM) pictures of synthesized CAG samples at various sintering temperatures are provided in Figure 5.2 to illustrate the nanostructure nature and morphology of the sample. It observed from the images that particle size and morphology of CAG changes with the temperature. The Nano powder of CAG has spherical morphology, along with it some larger particles (large grain size) were also seen which may be because of agglomeration and stress/stained in compass in the lattice structure. As the average particle size of CAG had been calculated from SEM appeared to grow with the rise in temperature like the crystalline size obtained from XRD. The particle sizes determined by SEM and XRD analysis are highly comparable and exhibit a similar pattern with temperature, as illustrated in the figure.

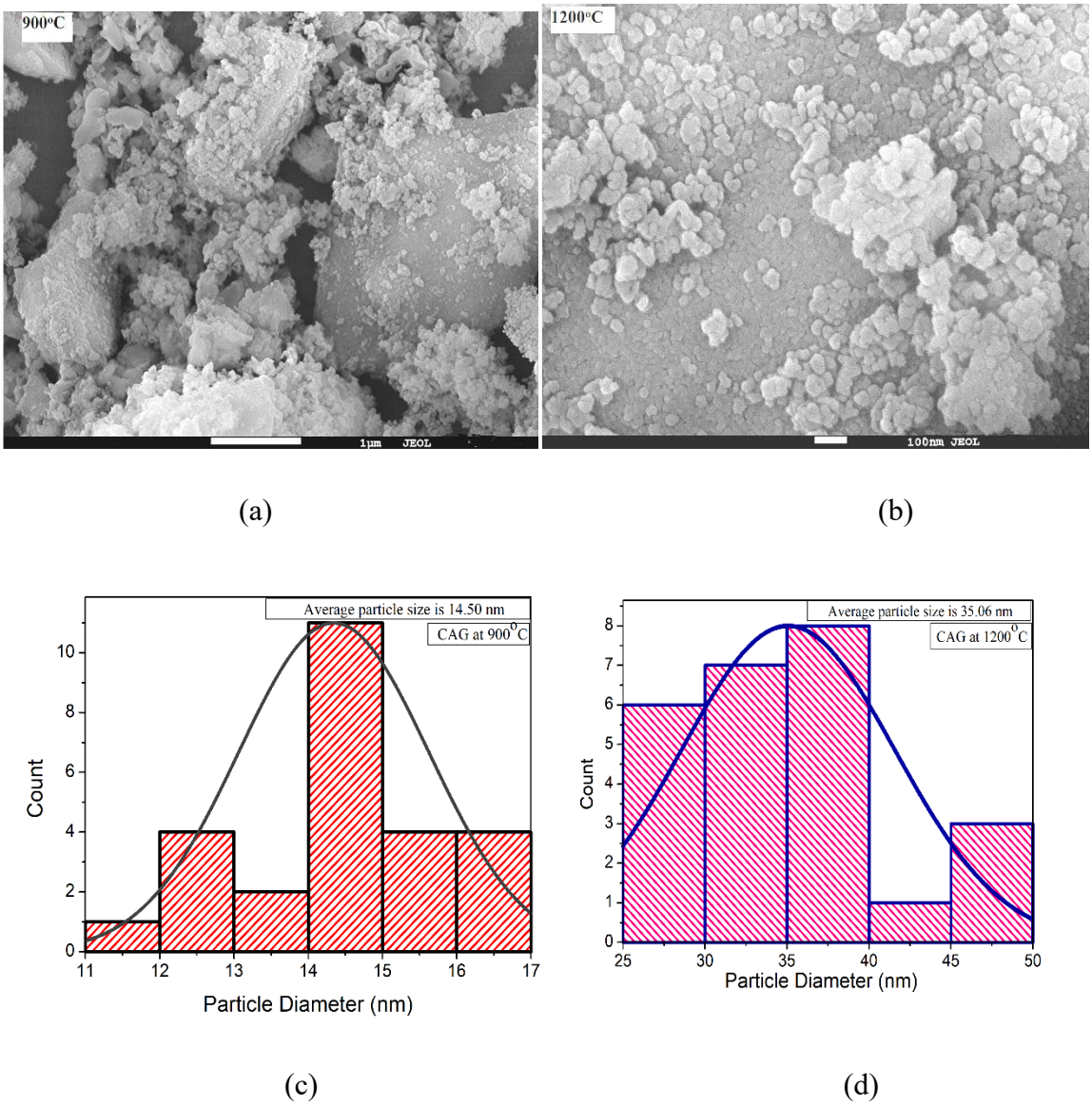

Fig 5.2. SEM micrograph at 900ºC and 1200ºC shown in a and b respectively and a bar graph(c,d) show particle size of the CAG powder sample synthesized at 900°C and 1200°C respectively.

5.1.3 Energy Dispersive X-ray (EDX):

The EDX for the prepared sample of CAG sintered at 1200ºC is shown in Figure 5.3 and observed that without the presence of any extra or other elements (impurity), pure composition of required elements of CAG has been found which indicates the effectiveness of the synthesized method and purity of prepared material. Figure 5.3 (a,b) illustrates the

EDX element mapping in SEM of Ce, Al, and O shown, and through EDX different areas of samples were visible. The peaks of Ce, Al, and O verify the configuration of CAG shown in Figure 5.3 (c). The weight and atomic % are mentioned in Table5.2.

Table 5.2. EDX weight (%) and atomic (%) for area exposed for sample CAG at 1200°C.

Element	Weight %	Atomic %
Ce	62.74	19.72
Al	19.88	35.45
O	17.38	47.83

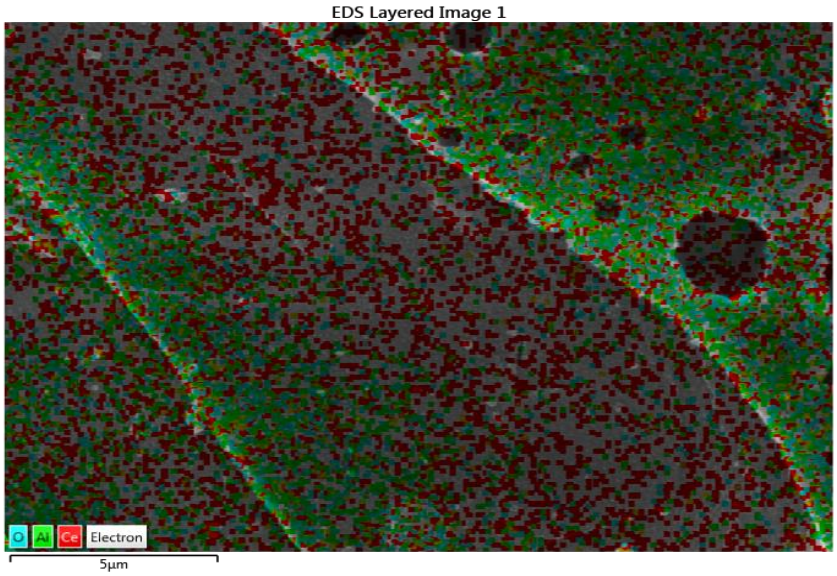

(a)

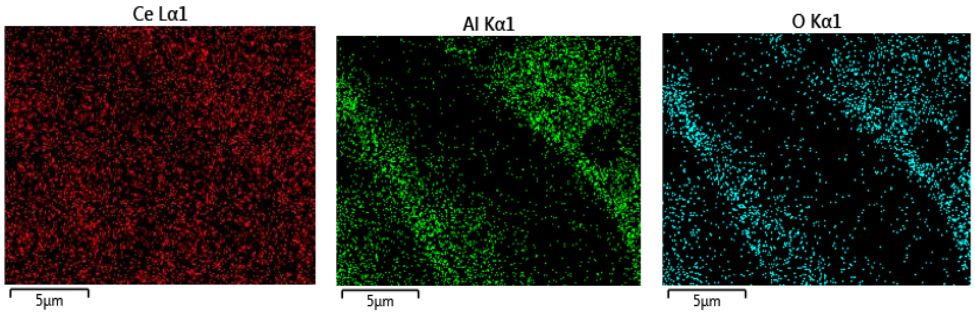

(b)

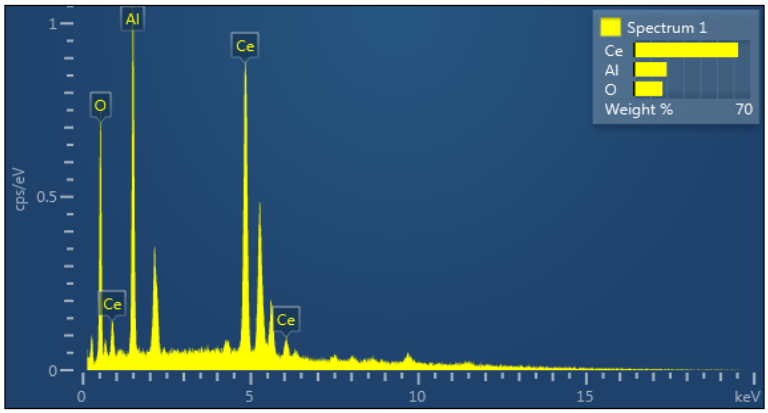

(c)

Fig. 5.3 (a,b) EDX element mapping in SEM mode of Ce, Al, O and (c) EDX spectra of CAG.

5.1.4 Fourier Transform Infrared Spectroscopy (FTIR):

Figure 5.4 illustrates the FTIR spectroscopy results for CAG sintered at temperatures ranging from 900°C to 1300°C. The FTIR spectrogram revealed absorption peaks within the 400-800 cm^{-1}range, signifying the presence of pure metal-oxide bond specifically Ce-O metal-oxygen and Al-O metal bonds, which are recognized for CAG.

Notably, peaks at 639 and 437 corresponded to the Al-O absorption, while 836 and 571 peaks were indicative of Ce-O absorption. The bonds due to the presence of moisture or water are identified as O-H vibrations that were observed at 2980 and 2901 $cm^{-1}$for the samples and absorption peaks at 1401 and 1246 cm^{-1}indicated OH bending and C=N bonding respectively. Therefore, the IR results support the conclusions made by XRD measurements. [5,6]

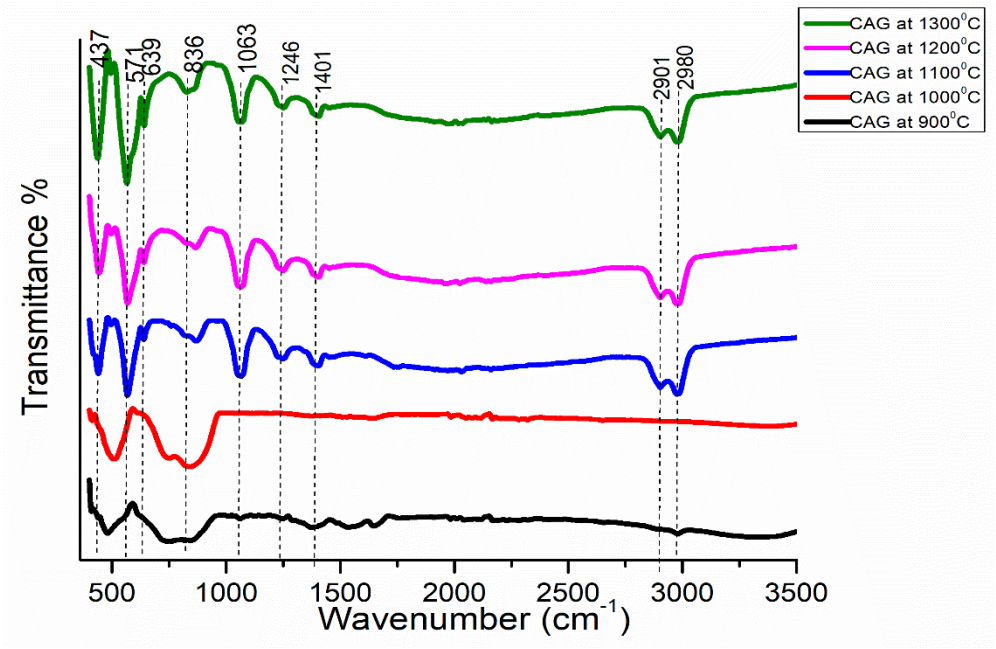

Fig 5.4 FTIR spectrum of the CAG precursor at various temperatures.

5.1.5 UV- spectroscopy

The absorption properties of the prepared CAG sample that sintered at 1200°C were studied via UV-vis spectroscopy. The resulting absorption spectrum is depicting in Figure 5.5 which consists of broad absorption region from 200-450 nm, this may indicate the presence of defects states between the bands. The absorption near 350-400 nm is caused by the 4f-5d transition of Ce. [7,8] The material's band gap was manually computed via a formula in equation 3.6 and plotting a graph of $(\alpha h\nu)^2$ v/s hv.

Where in this formula α stands for the coefficient of linear absorption, ν denotes the frequency of light, hrefer the Plank's constant, A denotes the proportionality constant, Eg stands for the band gap energy, and the value of n is 1/2 for a material with a direct band gap. From results observed that the band gap is 2.35 eV for the prepared material sintered at 1200^0C.[2][9]

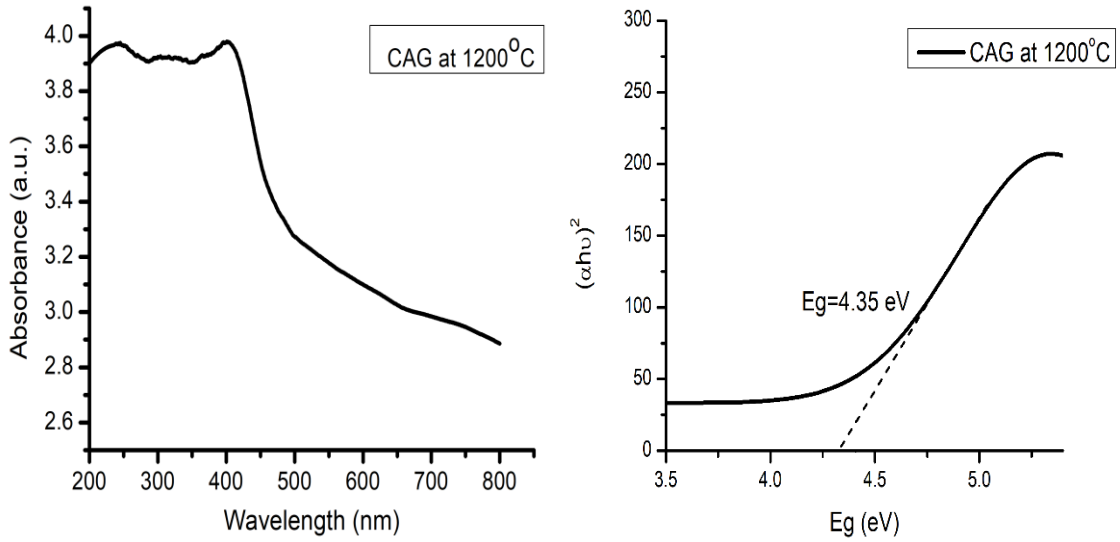

(a) (b)

Fig 5.5 (a)UV- visible absorption spectrum recorded for CAG sintered at 1200^0 and (b) Energy band gap for CAG sintered at 1200^0.

5.1.6 Fluorescence Spectroscopy

Fluorescence spectroscopy is an investigative characterization technique that is used for quantitative measure or analysis the optical or fluorescence properties of a phosphor or any semiconductor material.

The cerium ion (Ce^{3+}) has quite a straight forward configuration of electrons in both ground as well as excited states. Spin-orbit coupling divides the $^4f_1$ ground state configuration into two levels, $^2F_{5/2}$ and $^2F_{7/2}$. There is a 2000 cm^{-1}difference in energy between the two levels. However, in exceptional cases, because of the strong coupling of vibrational lattice, these emission bands get prolonged as compared to 2000 cm^{-1}. [10,11]

Figure 5.6 shows typical Fluorescence spectra for CAG sintered by 1200ºC under the excitation of 227 nm and 278 nm and it consists of multiple broad peaks in the region 400-800 nm. Under the excitation of 227 nm spectra show the five peaks at 455nm, 490 nm, 530 nm, 585 nm, and 655 nm. The two major peaks around 455 nm and 530 nm observed due to the $4f^1$ ($^2F_{7/2}$) → $4f^05d^1$ and $5d^1$-$4f^1$ ($^2F_{5/2}$) transitions of Ce3+ ion respectively.

Further, peak at and 585 nm was observed due to the $5d^1$-$4f^1$ ($^2F_{7/2}$) transition of Ce^{3+} ion. [1][12]

Similarly, FL spectra of CAG excited by 278 nm shows same peaks but the intensity of peaks found less as compare. In the spectra of CAG, the Ce^{3+} ions responsible for the emission in yellow region, but the whole spectrum has numerous peaks in the visible range, indicating the suitability of CAG material for WLEDs and other white light sources.

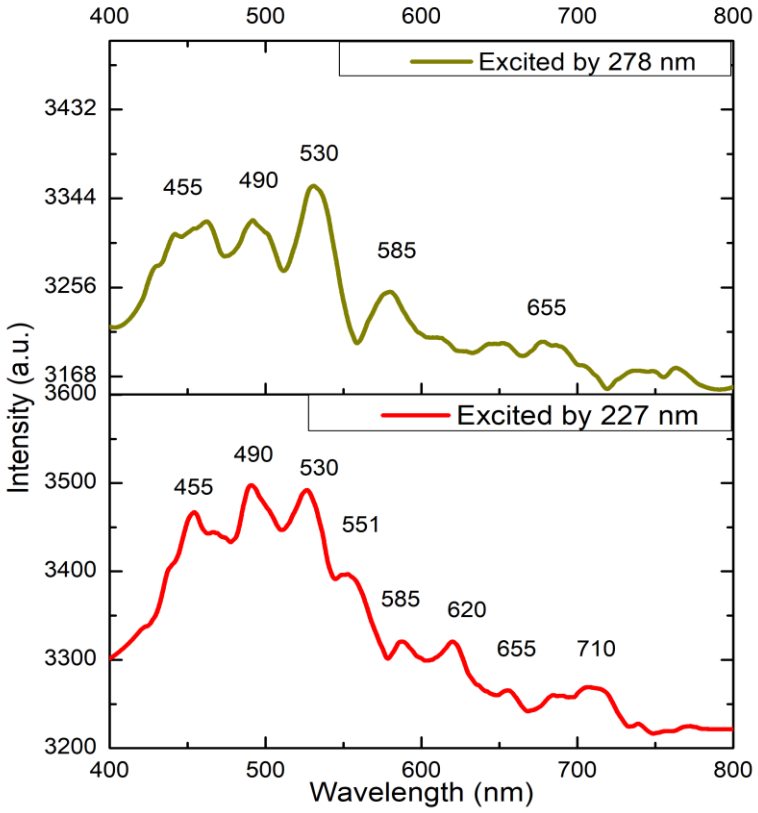

Fig.5.6 The fluorescence emission spectra of CAG sintered at 1200ºC at excitation 227 nm and 278 nm.

5.1.7 Fluorescence Lifetime:

The fluorescence lifetime is defined duration in which a fluorophore stays in its excited state prior to releasing a photon and going back to its ground state. Frequently, it is expressed in terms of time units, like nanoseconds (ns) or picoseconds (ps). It is a crucial feature of a precise fluorophore is its fluorescence lifespan, which varies greatly among

them. This characteristic is essential for many fluorescence-based methods and uses, including fluorescence spectroscopy and microscopy, since it tells us something about the behavior of the fluorophore. The time it takes for energy lost over fluorescence emission or other non-radiative processes to origin a population of excited fluorophores to shrink to around 37% of its initial size (N/e). In this framework, "lifespan" is often referred to the fluorophore population kinetics. It is closely associated with the lifespan of fluorescence of each individual fluorophore in the population.[13]

The fluorescence lifetime of the garnet investigated to check the decay behavior of the sample sintered at 1200°C shown in figure 5.7. The sample's decay curve can be modeled by employing a single exponential function outlined in equation 1.1. By equation, I stand for relative intensity, x denotes the decay time, t signify fluorescence lifetime and A and B considered as constants.[14] The lifetime and decay time of CAG sintered at 1200°C are 0.124 ms and 0.21 ms respectively.

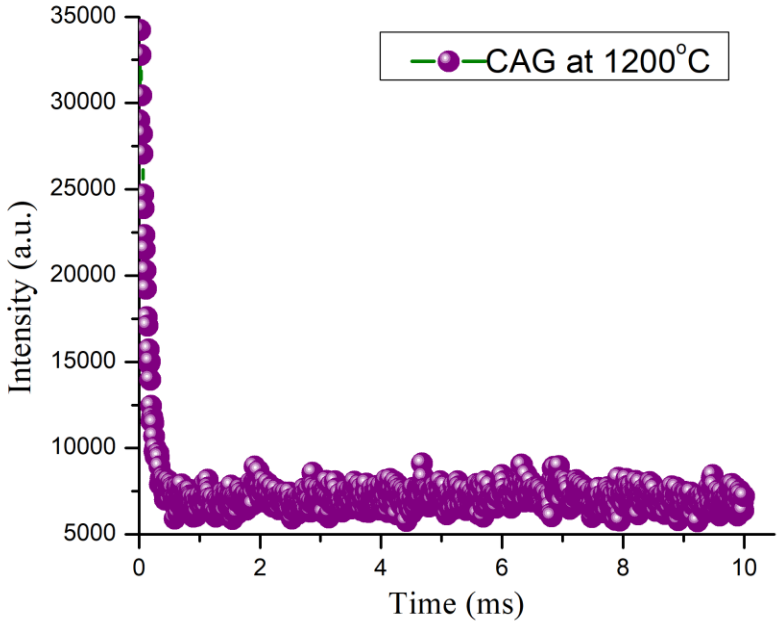

Fig 5.7 Fluorescence lifetime and Decay times for CAG sintered at 1200^0C.

5.1.8 CIE chromaticity analysis:

The fluorescence spectra have been used to calculate a few parameters like International Commission on Illumination (CIE coordinate), Color Coordinate Temperature (CCT), Color Purity (CP), and Color Rendering Index (CRI) to analyze lighting applications of prepared material (CAG). The CIE coordinates of CAG at excitation 227nm and 278 nm are shown in Figure 5.8.

Color Rendering Index (CRI)

The color rendering index parameter used to measure the capacity of fluorescence emission spectra of CAG that how much resemblance of color with the natural light source as likes sunlight. The value of CIR lies between 1-100 and if it is between 70-100 then considered as good or excellent quality of light source. In this study, the calculated value of CRI was found very near 100 which indicates that the material is highly applicable for a good white light source or solid-state light source. The value of CRI has been calculated by using equation 1.2.[15]

Color purity

The color purity value of CAG can be calculated by using equations (1.4). The computed value of CP for CAG is 1.2% and 0.5% for material excitations at 227 nm and 278 nm, respectively, as shown in the table. It indicates the pure white light emission.[16]

Correlated Color Temperature (CCT):

CCT, or Correlated Color Temperature, is a metric employed to gauge the perceived color of a light source. It relies on the concept that an object, when heated, emits light in a consistent manner according to its temperature, and this measurement is expressed in units of degrees Kelvin (K). The value of CCT tells about the warmness and coolness of light alike if material has a value below 3000K it will count as a warm source of light which give yellowish light and if the value if above 5000 K, then the source will shows bluish light which is cool light. In the case of this study, the value of CCT clearly indicates that

the material will be an applicable candidate for cool white light source. The CCT value can be calculated by using equation 1.3.[17]

CIE color coordinate is (0.329,0.334), color purity is 1.2%, CRI value is 96, and CCT value is 5635 for the CAG sample at excitation 227 nm and CAG at 278 nm excitation correspondingly has CIE color coordinate is (0.331,0.333), color purity is 0.5%, CRI value is 96, and CCT value is 5576.

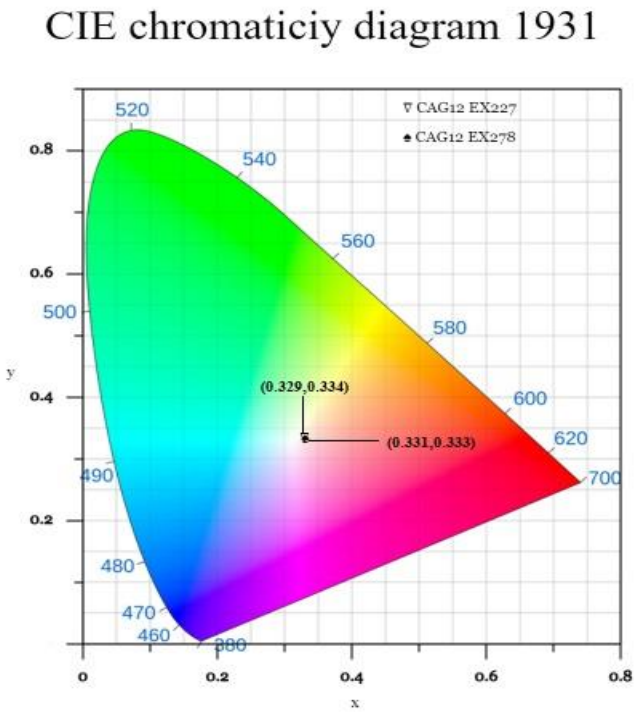

Fig 5.8 CIE chromaticity diagram for the CAG at excitation 227 nm and 278 nm.

5.2 Cerium Aluminum Garnet doped with cobalt

In prior investigations, cerium has demonstrated remarkable luminescent properties as a dopant. In the current study, cerium serves as the host for the preparation of $Ce_3Al_5O_{12}$ garnet. The luminescence behavior of Ce^{3+} ions is notable, involving both fluorescence and phosphorescence processes, contingent upon the specific energy levels engaged. As a rare earth element, cerium exhibits visible light emission through the broadband transition between its 5d and 4f energy levels, making it an excellent candidate for a host material capable of generating white light. To enhance the luminescent characteristics, the introduction of cobalt as a dopant into the $Ce_3Al_5O_{12}$ host has been chosen. Cobalt-doped materials are known for their luminescent properties, with cobalt displaying absorption in the blue and green regions due to its d_6 configuration, as well as absorption in the red or infrared (IR) region owing to its d_5 configuration. This study delves into the structural and optical properties of cobalt-doped $Ce_3Al_5O_{12}$ garnet (CAG), exploring its potential as a white light source based on considerations such as energy efficiency, Color Rendering Index (CRI), Correlated Color Temperature (CCT), and Color Purity (CP).

5.2.1 X-ray Diffraction (XRD):

The XRD study was conducted to investigate the phase and structure of all cobalt doped CAG samples. Figure 5.9 displays the obtained XRD pattern for CAG: Co sintered at 1200^{o}C. The positions of diffraction peaks were matched and consistent with the typical cubic phase of CAG (JCPDS-00-067-0123).It was clearly seen in figure that the phase of material remains unaltered even after doping of cobalt in CAG. Hence, it implies that no impurity peaks were found at all the doping concentrations of cobalt. The crystalline size, lattice volume, peak shift and lattice strain are calculated for the 220 hkl plane for all the doping concentrations of cobalt in CAG. The Scherrer's formula (equation 3.2) used to quantify crystalline size and it was found that the crystalline size decrease with the rise of doping concentration of cobalt.[15][18] With an increase in doping concentrations, the major peak's full width at the half-maximum (FWHM) rises, this can be ascribed to a reduction in crystalline size.

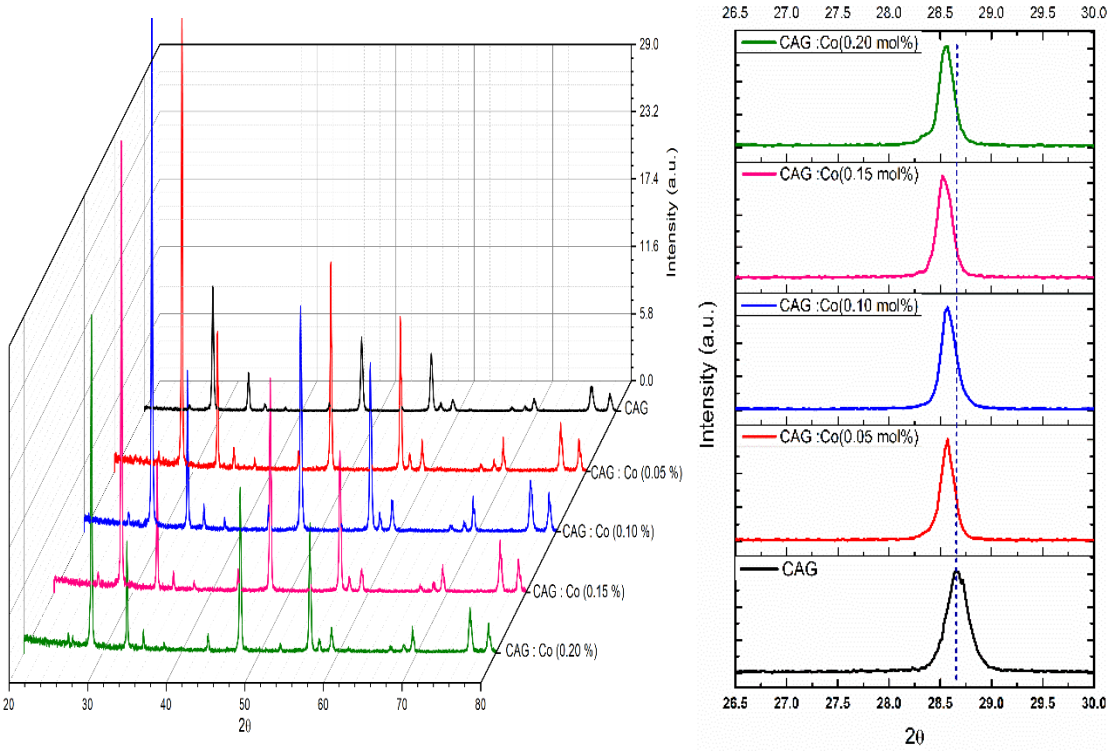

Fig 5.9 Typical powder XRD pattern of the CAG: Co powders calcined at 1200 °C.

Further observing that the XRD peaks shift towards the lower angle 2Θ using the (220) peak as shown in figure 5.9. The peak gets shifted might be caused by several factors like strain in lattice or change in lattice parameters and also because of occupation of the interstitial sites in host lattice by dopant and vice versa. The change in lattice parameters leads the change in diffraction angles that cause the shift in peaks. The strain in lattice leads to shift the peaks and makes them broad. It is observed that the crystalline size and strain are inverse shown in figure 5.10 and the strain of lattice increases as the doping concentration of cobalt increases in CAG: Co.

Table 5.3. Summarize crystalline size, d-spacing, lattice strain, lattice volume and dislocation density of CAG: Co sintered at 1200°C.

Doping Conc.	2Θ (degree)	Crystalline Size, D(nm)	d-spacing	Lattice Constant	Lattice Volume	Peak Shift	lattice strain (ε×10-3)	Dislocation density
0	28.66	33.8	3.111	8.800	681	0	0.00431	0.00087
0.05	28.56	50.8	3.121	8.830	688	0.09	0.00288	0.00038
0.10	28.58	47.4	3.120	8.826	687	0.10	0.00309	0.00044
0.15	28.54	48.1	3.124	8.838	690	0.13	0.00304	0.00043
0.20	28.55	48.6	3.122	8.832	689	0.11	0.00301	0.00042

The Williamson and Hall used to obtain the comparison of crystalline size and the strain in lattice of CAG: Co by considering the below formula:

$$\beta\cos(\theta) = \frac{\lambda}{D}.4\eta\sin(\theta)\ldots\ldots\ldots\ldots (5.1)$$

Where β denotes the Full Width Half Maxima and λ stands for X-ray wavelength and D is the crystalline size. In order to obtain strain and particle size component the graph plotted between $\beta\cos(\theta)$ on y-axis and $4\sin(\theta)$ on x-axis shown in figure 5.11.[19,20]

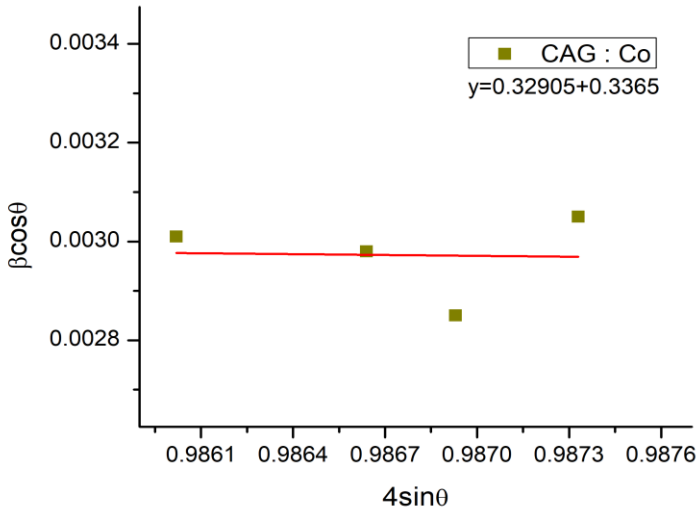

Fig 5.10 Williamson Hall plot for CAG: Co of (220) plane.

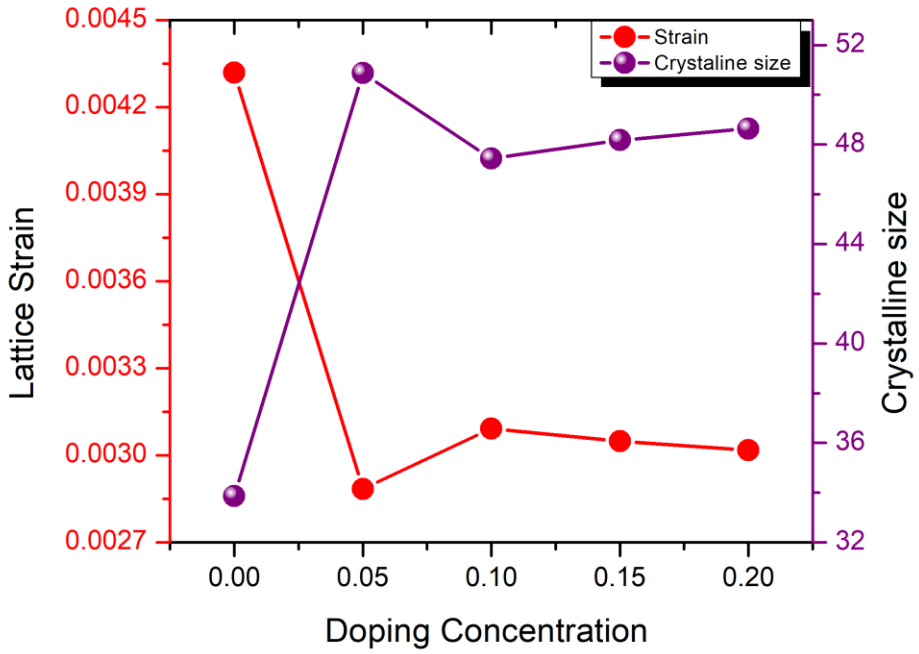

Fig 5.11 Comparison of the lattice strain and crystalline size corresponding to doping concentration in CAG: Co.

The radius variance (△) calculation can be used to check the doing position of Co^{3+} in CAG host. The formula for the radius variance given in equation below:

$$\Delta = \frac{R_H(CN) - R_D(CN)}{R_H} \times 100\% \text{.....(5.2)}$$

Where R_H and R_D are the ionic radius of host (Ce^{3+}) and ionic radius of dopant (Co^{3+}) respectively and CN is the coordination number [21]. By applying formula, the radius variance of Ce^{3+} with respect to Co^{3+} is 54% and the radius variance of Al^{3+} with respect to $Co^{3+}$is 1.8%. According to research the required radius variance of dopant ions and host ions must be below 15-20%. So, results show that the radius variance of Al^{3+} with Co^{3+} found favorable.

5.2.2 Fourier Transform Infrared Spectroscopy (FTIR)

To explore the presence of functional group composition in GAG: Co, the FTIR analysis was performed. Fig 5.12 displays the observed FTIR spectra of CAG: Co sintered at

1200ºC. The absorption bands centered at 842 cm^{-1} and 577 cm^{-1} were ascribed to the Ce-O (metal-oxide) absorption bonding. Moreover, the appearance of absorptions peaks near ~439 cm^{-1} and ~648 cm^{-1} were providing the evidence of Al-O metal-oxide bonding [5][22]. These absorption bands of metal oxide bonding gave the confirmation of structure of CAG: Co.

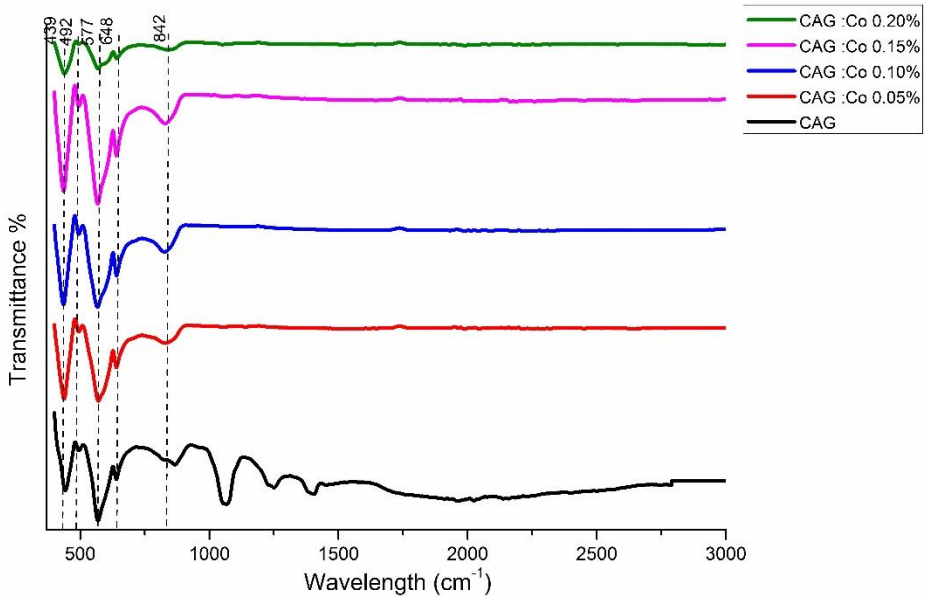

Fig 5.12 FT-IR analysis of CAG :Co precursor synthesized by different cobalt concentrations 0.05,0.10,0.15 and 0.20.

5.2.3 UV-Vis Spectroscopy

The absorption properties of prepared CAG: Co samples that sintered at 1200ºC were studied by UV-vis spectroscopy. UV spectra observed in the range of 150-400 nm for the CAG: Co was shown in Figure 5.13. The spectra show the broad absorption band between 200-300 nm and the absorption peaks centered in this region near 295 nm is attributed to the transition of Ce^{3+} ions. Similar absorption region was seen for all the doping concentrations of Cobalt in CAG.Apart from it the UV absorption spectra were also utilized to determine the optical band-gap of CAG: Co for various doping concentrations. The band gap is quantified via the Wood-Tauc formula shown in equation 3.4 [23] Where α stands for linear absorption coefficient, h is Plank's constant, ν is for the frequency of light, A

denotes the proportionality constant, and Eg is for the optical band gap energy, and n having value according to band gap, thus n is1/2 and 2 for direct and indirect band gap respectively. The garnets are material that shows the direct band gap. To calculate the optical band gap values for CAG: Co samples the plots of $(\alpha h\nu)^2$ v/s $h\nu$ at various concentrations of Cobalt and shown in figure 5.13.[24]

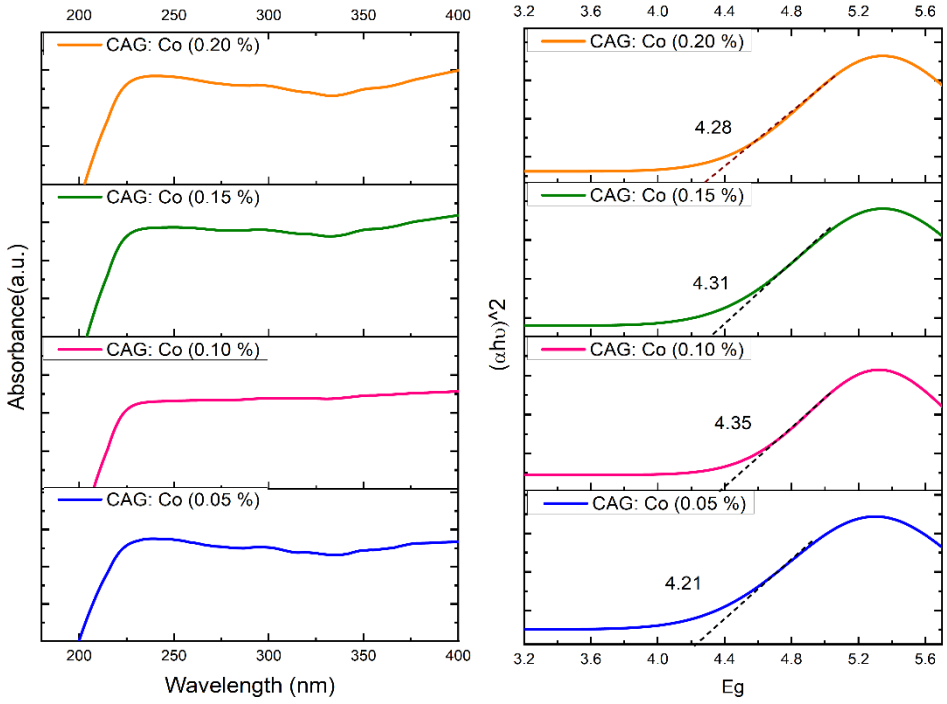

(a) (b)

Fig 5.13 (a)UV- visible absorption and (b) Energy band gap for cobalt doped CAG at various concentrations sintered at 1200^0 .

From the graph seen that the optical band gap seems increases with the rise in doping concentrations of Cobalt in CAG and the optical band gap was observed as inverse to the crystalline size of the material depicts in figure 5.14 in which crystalline size for different doping concentration of Cobalt in CAG found in XRD data compared with the Optical band gap of same material.

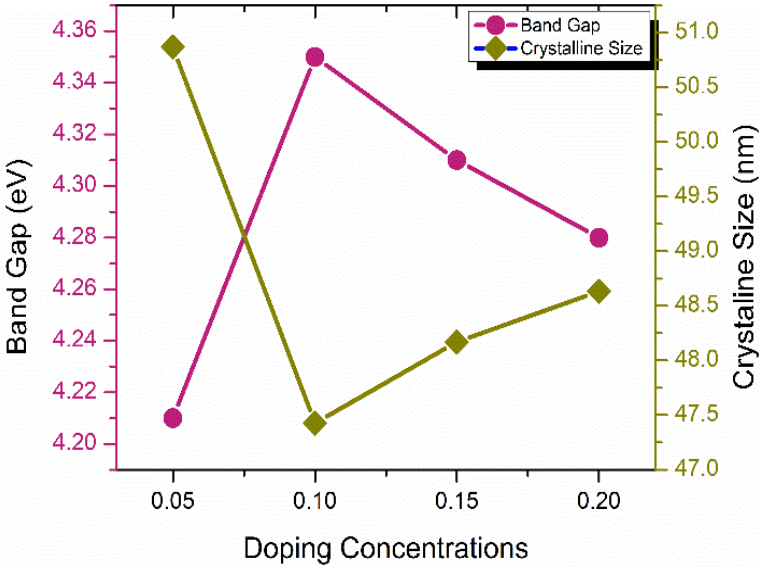

Fig 5.14 Variation in crystalline size and optical band gap with respect to doping concentrations of cobalt in CAG.

5.2.4 Fluorescence Spectroscopy

Figure 5.15 displays fluorescence spectra of CAG: Co sintered at 1200°C under the excitation wavelength 294 nm. The fluorescence spectroscopy was carried out to investigate the optical or fluorescence properties of prepared material CAG: Co at various doping concentrations. The Spectra had well-known peaks in the region 400-700, two major peaks around 450 nm due to the $4f^1$ ($^2F_{7/2}$) → $4f^0 5d^1$ and 533 nm observed $5d^1$-$4f^1$ ($^2F_{5/2}$) transitions of Ce^{3+} ion.[1][10-12]The emission peak at 530 nm caused by transition of Ce^{3+} shifted to the 580 nm after the doping of Co^{3+} in CAG because of the energy of Ce^{3+} gets transferred to the Co^{3+} .Therefore, peak at 580 nm was observed due to the $5d^1$-$4f^1$ ($^2F_{7/2}$) transition of Ce^{3+} ion. It has been seen that there are peaks at 450nm (blue emission peak) that is due to the transition of Ce^{3+} . Apart from it there found several peaks due to the cobalt transition alike emission peaks at 512 nm and 580 nm (yellow emission peak) were ascribed by the $^4T_2$ (F) → $^2T_1$ (G), $^4T_1$ (P) → $^4T_2$ (F) transition of Co^{3+}. Moreover, another emission peaks in the region 620-650 are identified because of the $^4T_1$(4P)-$^4A_2$(4F) transition of Co^{3+}. [25,26] Clearly seen from figure 5.15 the peaks in

the region 550 nm -800 nm found enhanced after the doping of cobalt in CAG due to the transition and energy enhancement of Co^{3+} ions. In the spectra of CAG: Co, the Ce^{3+} ions responsible for the emission in yellow region and Co^{3+} ions show the blue, green and red region, thus the whole spectrum has multiple peaks in the visible range that can produce the white light, hence indicating the suitability of CAG: Co material for WLEDs and other white light sources.

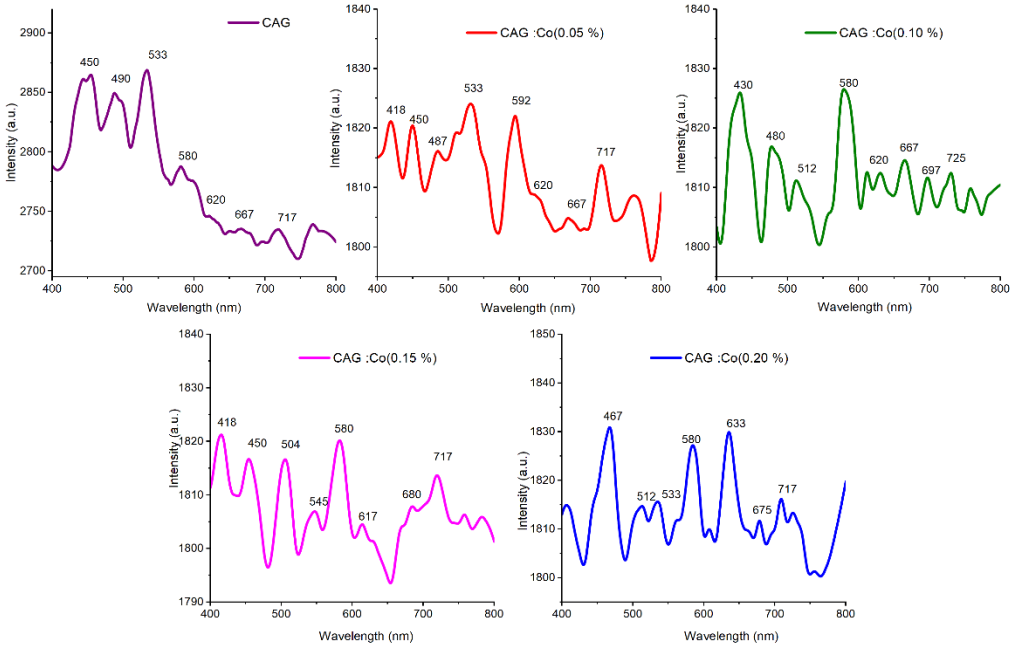

Fig 5.15 The fluorescence spectra of CAG: Co calcined at 1200 °C with different concentration of Co. The spectra observed at the excitation of 294 nm.

Figure 5.16 illustrates a bar graph displayed the combined area of cobalt-doped CAG at various concentrations within the visible range (400-700 nm), and the infrared range (700-800 nm). Therefore, it can be seen from graph that after doping of cobalt in CAG the integrated area in Visible and IR region at various doping concentration shows approximately close fluctuations. However, can be concluded that in contrast to other doping concentrations, 0.10 (mol %) of Cobalt doping concentration in CAG had highest

visible region and lowest area in IR region. Hence 0.10 doping concentration shows favorable results for CAG: Co material in order to be suitable for white light sources.

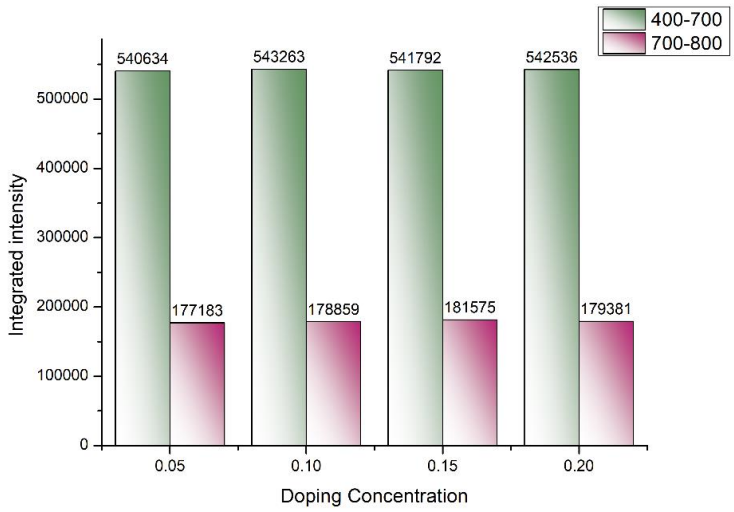

Fig 5.16 Bar graph of an integrated area at 294 nm with a different doping concentration of CAG: Co at 1200^0C.

5.2.5 Fluorescence Lifetime

Figure 5.17 depicts the fluorescence decay curves of CAG: Co samples with different Co^{3+} doping concentrations sintered at 1200ºC. These curves used to be fitted using single-exponential function i.e. I = A*exp (-x/t) + B. Here. I= relative intensity, x shows the decay time, t denotes the fluorescence lifetime and A and B are known as constants. The lifetime and decay time for the CAG: Co has been calculated and seen that both are in inverse relation, however as doping concentration of cobalt rises, the lifetime of the CAG: Co decreases.

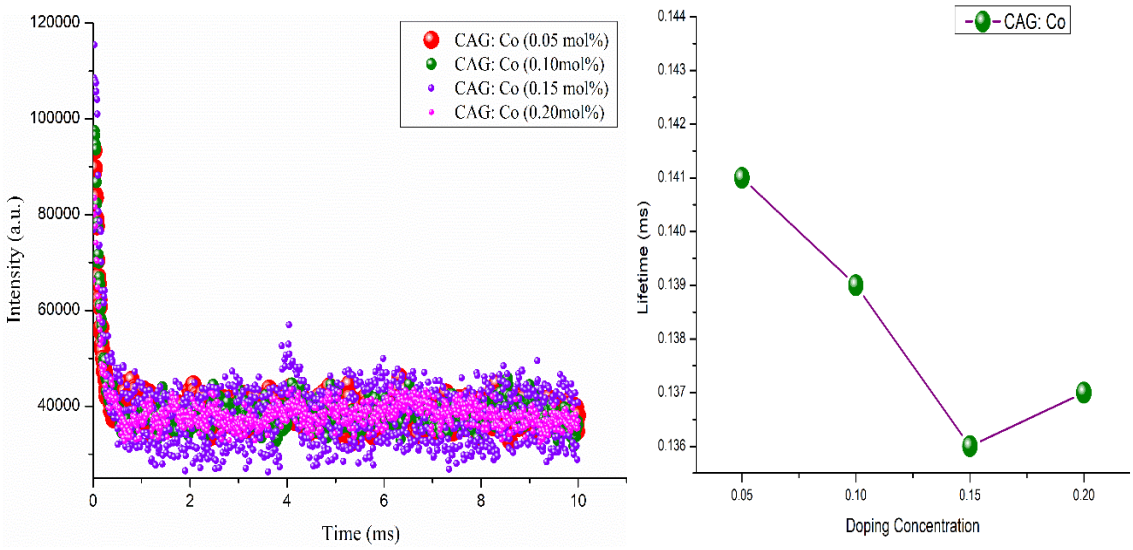

Fig 5.17 Fluorescence lifetime of CAG: Co at various doping concentrations.

5.2.6 Calorimetry

Figure 5.18 depicts the CIE chromaticity coordinates and color temperature of CAG: Co calcined at 1200ºC. It has been clearly seen from figure the value of CIE coordinates for different doping concentrations of Cobalt in CAG are (0.333,0.333) which are very similar and also found very close or undistinguishable from ideal CIE coordinates i.e. (0.333, 0.333).

Similarly, the values of CRI for all the doping concentrations of Cobalt seem same 95 and CCT is also distinguished by very negligible difference for all samples. Apart from its Color Purity (CP) is the very important chromaticity property of phosphor/garnet for white light and by calculating CP for all the doping concentrations, observed that all the values are very close but at 0.10 concentrations of cobalt CP (0.13%) is most favorable and demonstrating the vivid white light emission.

Table 5.4. CIE, CP, CCT, and CRI of cobalt-doped CAG at excitation 294 nm.

Conc.	CIE	CP (%)	CCT	CRI
0	(0.331,0.333)	0.5%	5576	96
0.05	(0.333, 0.333)	0.17	5469	95
0.10	(0.332, 0.333)	0.19	5452	95
0.15	(0.333, 0.333)	0.15	5465	95
0.20	(0.333, 0.332)	0.19	5453	95

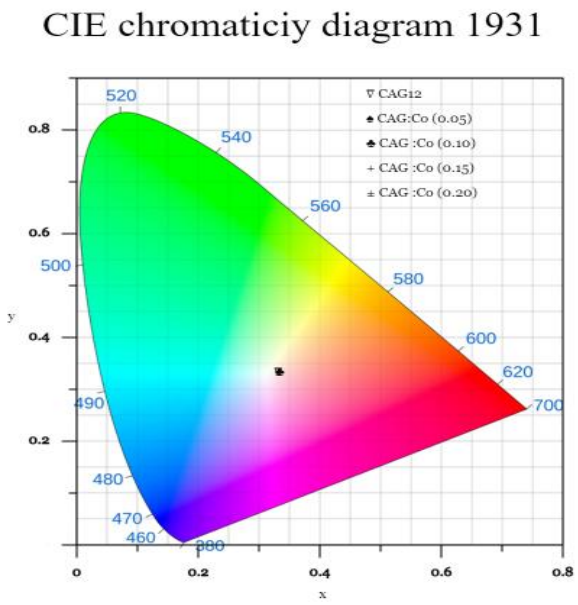

Fig 5.18 CIE chromaticity diagram for CAG: Co at 294 nm excitation.

5.3. Cerium Aluminum Garnet doped with Chromium

The investigation into Cerium Aluminum Garnet (CAG) stands as a significant exploration into the nuanced relationship between sintering temperatures, structural and optical properties, and the potential for white light generation. Successful synthesis of the CAG phase is achieved at 1200°C, leading to the formation of a pure garnet phase exhibiting emissions in the visible region. This observation suggests the potential for white light generation, laying the foundation for further enhancements. However, recognizing the need

for further refinement and enhancement, the study pivots towards the strategic introduction of dopants, specifically transition metals and rare earth ions. The primary goal is to stabilize the crystal structure and generate effective red phosphors. In this context, the study places particular focus on the incorporation of Chromium (Cr3+) into CAG phosphors to intensify the red component emission. The rationale behind selecting Chromium as the dopant lies in its unique electronic configuration and significant transitions in the far-red region. Specifically, the doped Cr3+ ions are expected to exert influence over the energy levels and transition lines within the CAG lattice. This, in turn, is anticipated to facilitate a highly efficient energy transfer mechanism between Chromium and Cerium ions (Cr3+ and Ce3+, respectively). The far-red region transitions of Chromium make it an ideal candidate to enhance the red component emission, a key aspect in the pursuit of white light generation.

This comprehensive investigation employs techniques such as X-ray Diffraction (XRD), Fourier Transform Infrared Spectroscopy (FTIR), Scanning Electron Microscopy (SEM), and fluorescence measurements to thoroughly characterize and quantify the impact of Chromium (Cr3+) doping on CAG phosphors, shedding light on the intricate details of the structural and optical modifications induced by this deliberate dopant introduction.

5.3.1 X-ray Diffraction

The XRD pattern of $Ce_3Al_5O_{12}$ has been compared with XRD pattern of chromium doped CAG sintered at $1200^{O}C$ at different doping concentrations of Cr and the XRD pattern depicted in figure 5.19. Sintering at high temperature improves the crystallinity and sharp peaks obtained in pattern. From the obtained XRD pattern we can clearly see that the pure phase of garnet remains same (JCPDS:) as doping of Cr^{3+} changes. Thus, the garnet phase remains unchanged because there is no impurity peak of extra peak found in XRD pattern even after doping of Cr^{3+} in CAG indicating that doping of Cr^{3+} is effective to stabilize the garnet structure. The crystalline size of material is estimated by calculating through the Scherrer formula shown in equation 3.2 and found crystalline maintained between 45-51 nm. The calculated results depicts in table 5.5.

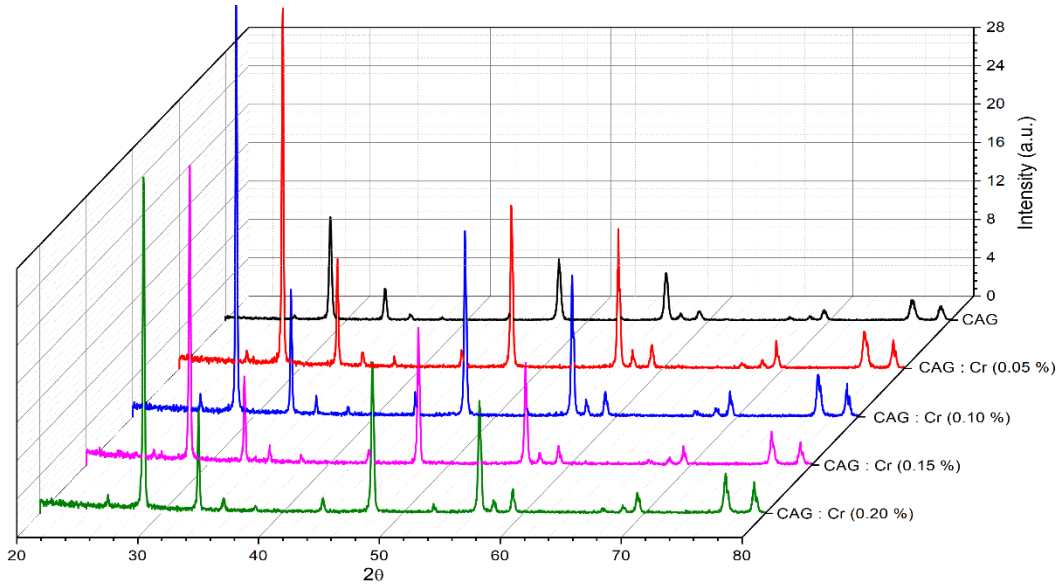

Fig 5.19. XRD pattern of CAG: Cr powders sintered at 1200°C.

The difference of ionic radius (△) among dopant (Cr^{3+}) and host (Ce^{3+}) ions was considered to recognize the substitution of Ce^{3+} by Cr^{3+} ions via the equation 5.8. [27]

Here, R_H symbolize the host cation has ionic radius i.e. Ce $^{3+}$ = 115 pm and Al^{3+}=53.5 pm, R_D denotes the actual radius of the dopant (Cr $^{3+}$ = 61.5 pm) and the coordination number denotes with CN of corresponding ions. The adequate percentage variance of ionic radius between ions is up to 30%, though, in the current study, Ce^{3+}/Cr^{3+} values is considered to be 73% and for Al^{3+}/Cr^{3+} value is 14.9%, hence signifying the effective substitution of Al^{3+} with Cr^{3+} ions within the host lattice.

Table 5.5 Crystallite size (D), d-spacing, lattice constant (a), and peak shift of CAG: Cr at 1200^{0}C.

Doping Conc.	2Θ (degree)	Crystalline Size, D(nm)	d-spacing	Lattice Constant	Lattice Volume	Peak Shift	lattice strain ($\varepsilon\times10^{-6}$)	Dislocation density (10^{-4})
0	28.66	33.8	3.115	8.8003	681.5	0	4.3	8.7
0.05	28.55	45.0	3.123	8.8353	689.7	0.107	3.2	4.9
0.10	28.55	46.8	3.123	8.8355	689.8	0.108	3.1	4.5
0.15	28.53	51.0	3.125	8.8390	690.5	0.120	2.8	3.8
0.20	28.53	46.0	3.126	8.8395	690.7	0.121	3.0	4.7

5.3.2 Fourier Transform Infrared Spectroscopy:

The FTIR spectra carried out to analyses the chemical bonding of CAG: Cr^{3+} garnet. Figure 5.20 depicts the spectrum of synthesized garnet (CAG: Cr) in the range of 400-4000 cm^{-1}. In the spectra range 400 to 800 cm−1, the metal–oxygen (Al–O, Ce–O, and Cr–O) vibrations in the garnet structure are detected. The characteristics band at 435 cm^{-1}appears due to Cr-O [28] and the absorption band around 850 $cm^{-1}$and 561 cm^{-1} were allocated due to Ce-O vibrations. [29,30] The occurrence of absorption peaks at 502 cm^{-1} and 635 cm^{-1} indicates the Al-O bond starching.[31]

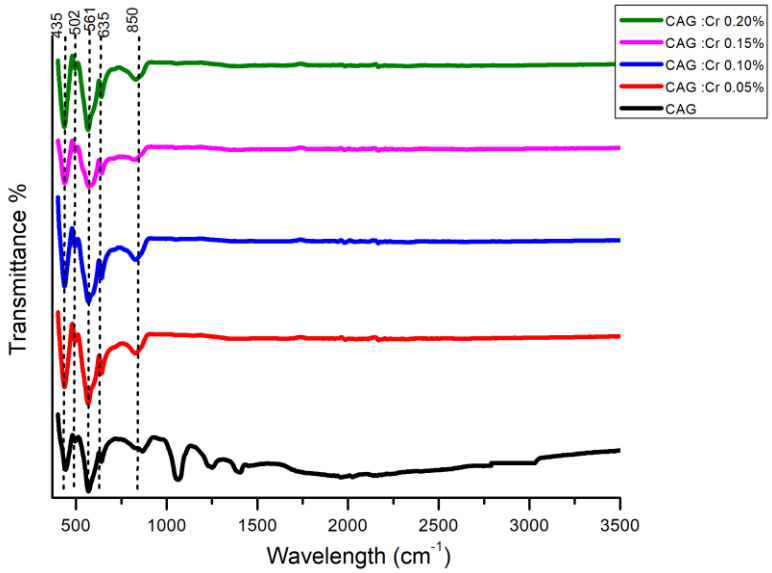

Fig 5.20. FT-IR analysis of CAG: Cr synthesized by different Chromium concentrations $R = 0.05$, 0.10, 0.15, and 0.20.

5.3.4 UV-Vis Spectroscopy:

Fig 5.21(a) depicts the UV-Vis spectra of CAG: Cr with different doping concentrations. The spectra show the broad absorption band between 200-400 nm and these spectra arise due to the transition of Ce^{3+} because of its partially filled 4f orbital. Fig 5.21(b) shows the optical band gap, which is calculated by use of equation 5.2. [32]

It was found that the band gap of the material decreases with the increase in doping concentration. The Optical band gap is calculated by plotting graph αhν(y-axis) and Eg (x-axis). The optical band gap was observed to rise with increase in the doping concentration.

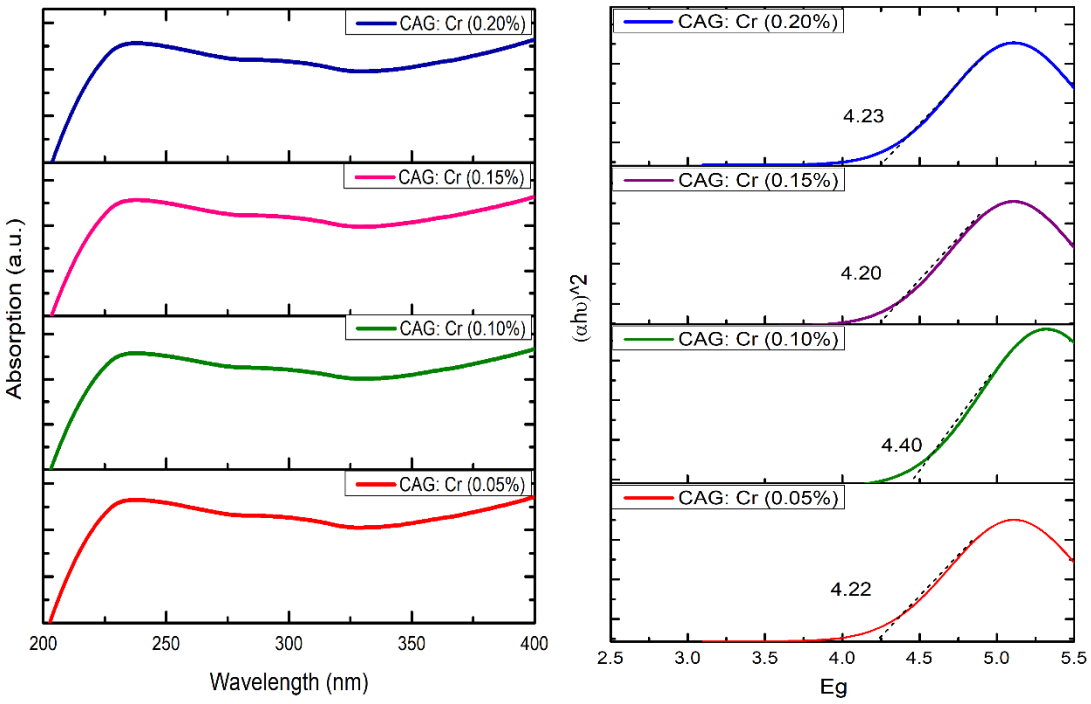

Fig 5.21. (a) UV- Vis absorption spectra for CAG: Cr and (b) optical band gap with different doping concentrations of Cr^{3+}.

5.3.5 Fluorescence spectroscopy

The Cerium Aluminum Garnet doped with chromium (CAG: Cr) illustrates the exciting fluorescent properties of other garnets such as YAG and GAG suitable for white light sources. GAG show excellent fluorescence properties and emission in visible region that favors the emission suitability for white light. The cerium aluminum garnet doped with chromium also shows the spectra in the visible region 400-750 nm. The spectra illustrate the multiple peaks in the visible region.

The typical fluorescence spectra for the CAG: Cr at various doping concentrations of Cr3+ sintered at 1200°C, illustrated in Figure 5.22, show the multiple emission lines in the region

400-800 nm assigned due to characteristics transitions of Cr^{3+} and Ce^{3+}. The most intense peak found near 532 nm caused by the energy transfer from Ce^{3+} to Cr^{3+} and overlapping of transition $5d^1$-$4f^1$ ($^2F_{5/2}$) transitions of Ce^{3+} ion to the $^4A_2 \rightarrow {}^4T_2$ transition of Cr^{3+}. A peak around 608nm is also due to the same transition of Cr^{3+}. The peak at 700 nm was assigned because of the transition $^4T_2 \rightarrow {}^4A_2$of Cr^{3+}. [33-34]

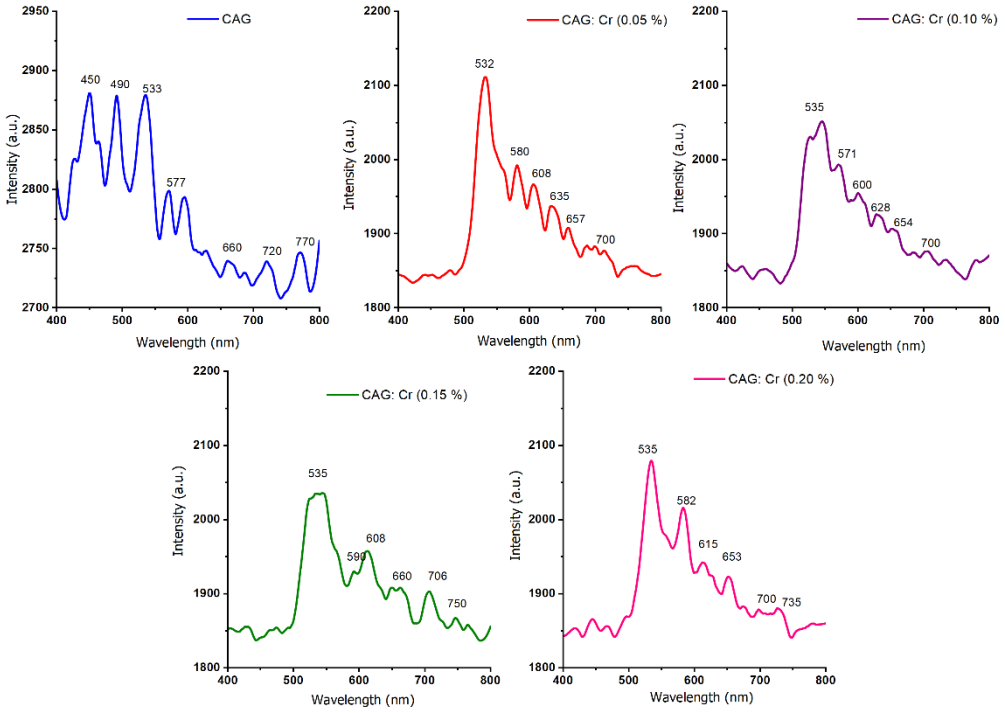

Fig 5.22. Typical fluorescence spectra at excitation 294 nm for chromium-doped CAG at different doping concentrations.

Figure 5.24 depicts the integrated intensity of chromium-doped CAG at different concentrations and it shows integrated intensity in the visible range i.e., 400-700 nm and Infrared range i.e. 700-800 nm. The results concluded that the doping of chromium at 0.05 mol% in CAG has the highest integrated intensity in the visible region among all the doping concentrations of chromium. Although all the integrated intensities at different doping concentrations are very near to each other. Thus, can conclude that 0.05 doping concentration of chromium in CAG gives the best florescent properties.

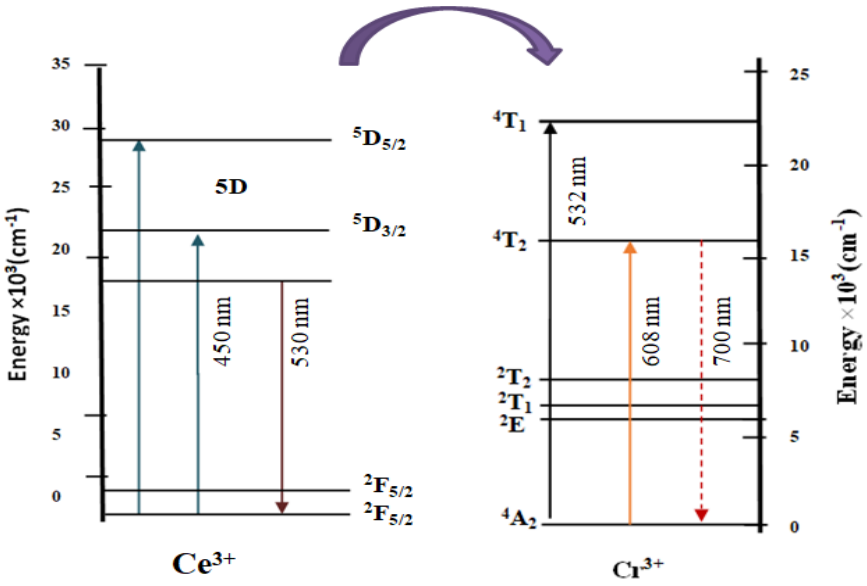

Fig 5.23. Representation of energy transfer process via transition energy level diagrams of Ce3+ and Cr3+.

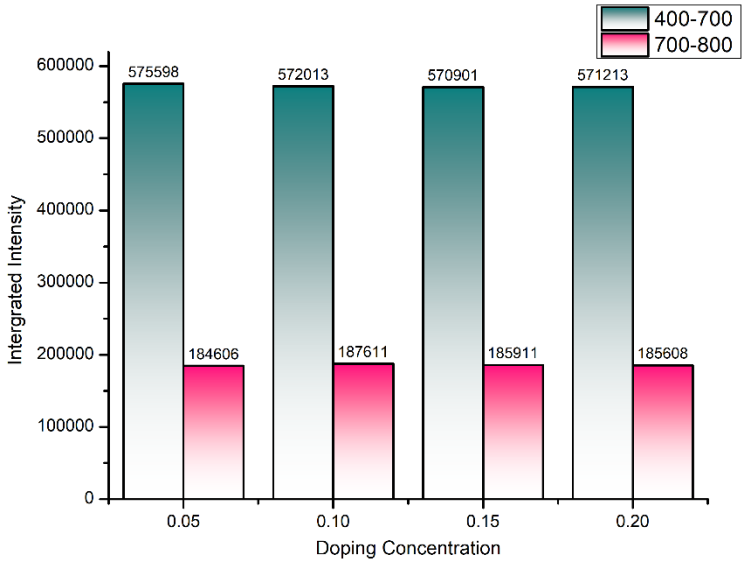

Fig 5.24. Bar graph representing the integrated intensity of CAG: Cr with variation in doping concentration of Cr^{3+}.

Figure 5.25 displays the CIE chromaticity coordinates and color temperature of the chromium-doped CAG sintered at 1200°C. The various doping content of chromium shows CIE coordinates very close to the ideal coordinates (0.333, 0.333) for an ideal white color on the chromaticity diagram. Even the values of CRI, CCT, and color purity are almost perfect for ideal value of white light. The color purity is an important chromaticity parameter, which calculated by using formula given in equation 1.4. The CCT considered by equation 1.3.

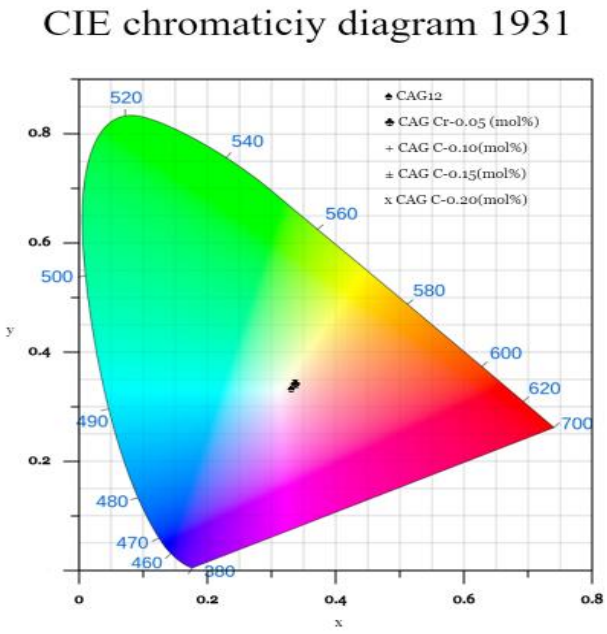

Fig 5.25. Typical chromaticity diagram for CAG: Cr with different doping concentrations sintered at 1200°C.

Table 5.6 CIE coordinates, CCT, color purity, and CRI values of chromium-doped CAG

Conc.	CIE	CP (%)	CCT	CRI
0	(0.331,0.333)	0.5	5576	96
0.05	(0.335, 0.340)	1.9	5331	96
0.10	(0.336, 0.342)	2.2	5334	97
0.15	(0.336, 0.341)	1.9	5359	97
0.20	(0.338, 0.345)	1.9	5330	96

5.4. Structural and optical properties of Cerium Aluminum Garnet co-doped with Cobalt and Chromium

Advancing the understanding of Cerium Aluminum Garnet's (CAG) optical and structural properties remains a central focus of ongoing research, with a keen eye on its potential applications in solid-state lighting. Previous investigations into CAG have extensively explored the impact of single doping with cobalt and chromium, revealing positive enhancements in the material's properties and positioning it as a promising candidate for solid-state light sources. Building on these findings, the study delves into the realm of co-doping with Cr^{3+} and Co^{3+}, anticipating energy transfer dynamics within the host lattice and between the two dopants. Leveraging the distinctive transition lines of Cr^{3+} and Co^{3+}, the research anticipates a synergistic emission, promising favorable outcomes for achieving white light emission. Extending the scope of inquiry, the present study shifts its focus to comprehensively understand the influence of Cr^{3+} and Co^{3+} co-doping on the structural and luminescent properties of CAG. The overarching objective is to refine emission characteristics, color rendering, and overall efficiency. The anticipated outcomes carry significant implications for a broad spectrum of applications, encompassing display devices, white light-emitting diodes (WLEDs), and solid-state light sources. This study employs a multifaceted approach, utilizing XRD, FTIR, FE-SEM, and Fluorescence measurements for thorough characterization of CAG and aim to contribute valuable insights, shaping the tailored properties of CAG for advanced applications in optoelectronics.

5.4.1 X-Ray Diffraction (XRD)

The X-ray diffraction (XRD) analysis for investigating the phase composition of the prepared CAG: Cr, Cr material was conducted at room temperature using Cu-Kα radiation with nickel filtration in the 20-80° range. The XRD pattern obtained for CAG: Co, Cr is depicted in the provided Figure 5.26. Based on visual inspection, it is evident that the CAG: Co, Cr phase maintains the pure CAG phase sintered at 1200°C. Even after variations in the concentration of Co^{3+}/Cr^{3+}, the garnet structure of CAG remains unaltered, indicating

that the co-doping of Co/Cr does not significantly change the host structure of CAG. The primary peak at (220) was selected for further analysis, and its characteristics were used to calculate the crystalline size, lattice constant, d-spacing, and dislocation density for CAG: Co, Cr. Changes in these parameters, such as crystalline size, lattice strain, defects, and unit cell expansion, may be attributed to the replacement of Al^{3+} or Co^{3+} following the doping of Cr^{3+} and Co^{3+} in CAG. The crystalline size was determined using Scherrer's formula, indicating an increase from approximately 33 nm for pure host CAG to 46 nm and 48 nm for CAG: Co (0.10), Cr (0), and CAG: Co (0), Cr (0.05), respectively. CAG: Co (0.10), Cr (0.05) exhibited a crystalline size of around 38 nm.

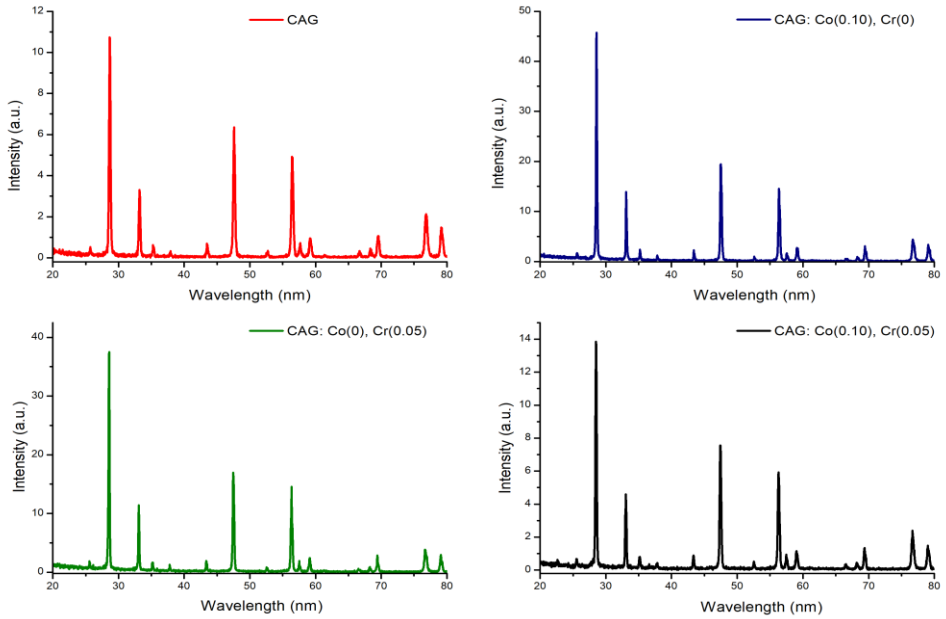

Fig 5.26. Typical XRD pattern for CAG: Co, Cr sintered at 1200°C with variation in doping concentrations.

Bragg's law (equation 3.1) was employed to calculate the d-spacing, revealing variations associated with the doping. The observed changes in crystalline size and d-spacing indicate that dopants have entered the crystal lattice. Additionally, the dislocation density for the prepared sample, determined using a specific formula applicable to the cubic phase structure of GAG: Cr/Co, was also discussed. This comprehensive XRD analysis sheds

light on the structural modifications induced by Co/Cr co-doping in CAG, providing valuable insights into the material's crystalline characteristics.

5.4.2 Fluorescence spectroscopy

The fluorescence spectra of Co^{3+}/Cr^{3+} co-doped CAG, as illustrated in Figure 5.27, were obtained by monitoring at 294 nm excitation. In the spectra of CAG: Co, Cr samples, distinct peaks appeared at 437 nm, 505 nm, 560 nm, 606 nm, and 637 nm.

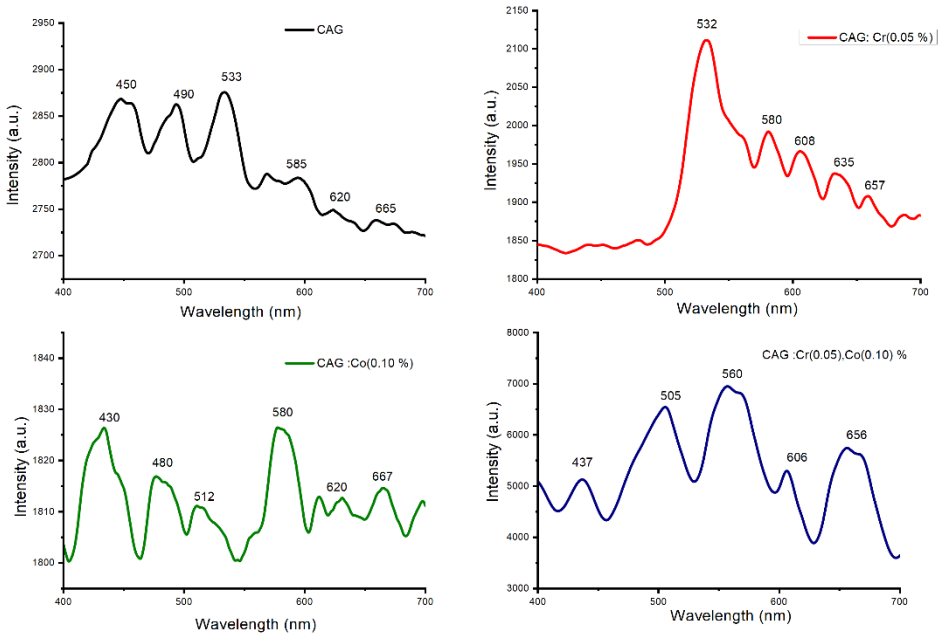

Fig 5.27. Fluorescence spectra for CAG: Co, Cr at various doping concentration under the 294 nm excitation.

When comparing the spectra of optimized concentrations of singly doped Co^{3+} and Cr^{3+} with co-doped CAG: Co^{3+}/Cr^{3+}, it became evident that energy transfer occurred from Ce to both Co and Cr. Consequently, emission peaks at 437 nm and 505 nm were attributed to the $^4f_1$ ($^2F_{7/2}$) → $^4f^0 5d^1$ and $5d^1$-$4f^1$ ($^2F_{5/2}$) transitions of Ce^{3+}. [10,11] Additionally, the peak `at 560 nm was identified as arising from the $^4A_2$ (F) → $^4T_1$ (P) transition of Co^{3+}, and another emission peak in the 637 nm region was attributed to the $^4T_1$ (4P) - $^4A_2$ (4F) transition of Co^{3+}. [25, 26] The intense peak at 506 nm was explained by the $^4A_2$→$^4T_2$

transition of Cr^{3+}. The presence of multiple peaks in the visible region strongly suggests the emission of white light from the material.

The calculated values of CIE, CRI, and color purity from the fluorescence spectra further support the likelihood of white light emission. These optical parameters closely align with the values associated with ideal white light, affirming the potential for the material to exhibit high-quality white light emission.

Table 5.7 CIE coordinates, CCT, color purity, and CRI values of cobalt and chromium co-doped CAG

Sample Code	CIE coordinates	CCT	Color Purity	CRI
CAG	(0.331,0.330)	5576	0.5	96
CAG: Co (0.10)	(0.332,0.333)	5452	0.2	95
CAG: Cr(0.05)	(0.335,0.340)	5331	1.9	94
GAG: Cr(0.05) Co(0.10)	(0.331,0.361)	5590	0.9	91

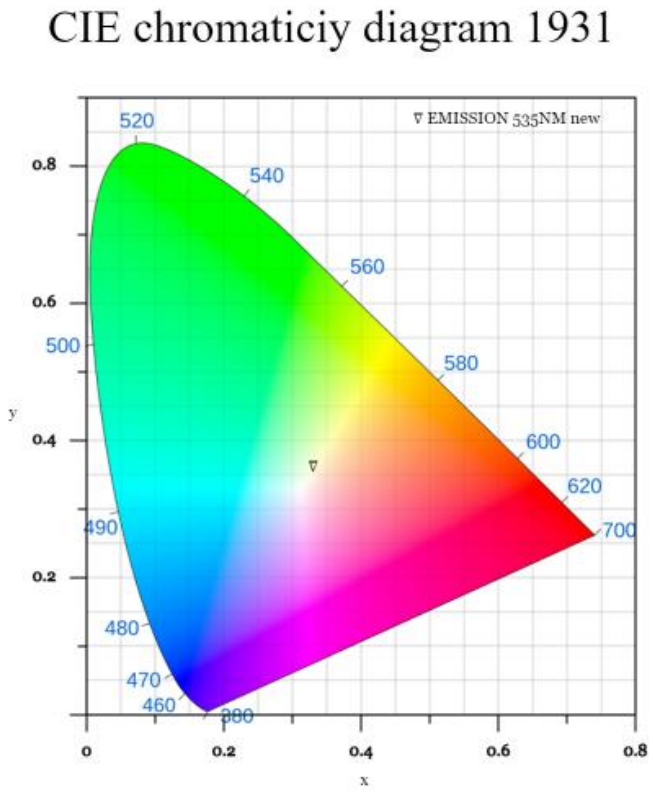

Fig 5.28. Chromaticity diagram showing CIE coordinate of CAG: Cr, Co under the 294 nm excita

References

1. X. He, X. Liu, R. Li, B. Yang, K. Yu, M. Zeng, and R. Yu, "Effects of local structure of Ce3+ ions on luminescent properties of Y3Al5O12: Ce nanoparticles," Sci. Rep., vol. 6, no. 1, pp. 1-11, 2016.
2. A. Bala and S. Rani, "UV excited emission spectra of gadolinium aluminum garnet," *J. Opt., pp. 1-7, 2022.
3. S. Rani, J. Kaur, and B. Lal, "Structural and optical properties of Eu-doped terbium aluminum garnet," AIP Conf. Proc., vol. 2220, no. 1, p. 020066, May 2020.
4. X. Zhang, X. Sun, H. Liu, C. Xia, C. Wu, Y. Li, Y. Li, C. Li, and F. Zeng, "The effect of Ce concentration on the structural and optical properties of YGG: Ce phosphor," Mater. Chem. Phys., vol. 278, p. 125619, 2022.
5. V. Tucureanu, A. Matei, I. Mihalache, M. Danila, M. Popescu, and B. Bita, "Synthesis and characterization of YAG: Ce, Gd and YAG: Ce, Gd/PMMA nanocomposites for optoelectronic applications," J. Mater. Sci., vol. 50, pp. 1883-1890, 2015.
6. H. L. Muttashar, N. B. Ali, M. A. M. Ariffin, and M. W. Hussin, "Microstructures and physical properties of waste garnets as a promising construction material," Case Stud. Constr. Mater., vol. 8, pp. 87-96, 2018.
7. S. Rani, B. Lal, S. Saxena, and S. Shukla, "Optical properties of TAG co-doped with Ce and Eu," Bull. Mater. Sci., vol. 42, no. 4, p. 144, 2019.
8. J. A. Gadsden, "Infrared spectra of minerals and related inorganic compounds," vol. 40, no. 313, pp. 277, 1976.
9. G. Ju, Y. Hu, L. Chen, Y. Jin, Z. Yang, and T. Wang, "Photoluminescence properties of Ce3+ and Tb3+-activated Ba2Mg(PO4)2," Opt. Mater. Exp., vol. 5, no. 1, pp. 1-10, 2015.
10. J. Ueda, S. Tanabe, and T. Nakanishi, "Analysis of Ce3+ luminescence quenching in solid solutions between Y3Al5O12 and Y3Ga5O12 by temperature dependence of photoconductivity measurement," J. Appl. Phys., vol. 110, no. 5, 2011.

11. G. Blasse and A. Bril, "A new phosphor for flying-spot cathode-ray tubes for color television: yellow-emitting Y3Al5O12-Ce3+," Appl. Phys. Letter., vol. 11, no. 2, pp. 53-55, 1967.
12. W. S. Silveira, A. J. S. Silva, P. A. M. do Nascimento, I. da Silva Carvalho, and M. V. D. S. Rezende, "Improving the luminescence properties of YAG: Ce3+ phosphors by co-doping Sr2+ ions," Optik, vol. 231, p. 166363, 2021.
13. B. P. Kafle, Chemical Analysis and Material Characterization by Spectrophotometry. Elsevier, 2019.
14. J. R. Lakowicz, Principles of Fluorescence Spectroscopy. Springer US, 2006.
15. A. Bala and S. Rani, "Down conversation visible emission spectra of Cr3+ doped gadolinium aluminum garnet," Opt. Quantum Electron., vol. 55, no. 10, p. 866, 2023.
16. A. Verma, D. P. Bisen, N. Brahme, I. P. Sahu, and A. K. Singh, "Yttrium aluminum garnet-based novel and advanced phosphor synthesized by combustion route activated by Dy, Eu, and Tb rare earth metals," J. Mater. Sci.: Mater. Electron., vol. 34, no. 7, p. 644, 2023.
17. C. S. McCamy, "Correlated color temperature as an explicit function of chromaticity coordinates," Color Res. Appl., vol. 17, pp. 142-144, 1992.
18. A. Bala and S. Rani, "Down conversions excitation dependent luminescent properties of Terbium Aluminum Garnet," J. Phys.: Conference Series*, vol. 2267, no. 1, p. 012113, IOP Publishing, May 2022.
19. V. S. Vinila and J. Isac, "Synthesis and structural studies of superconducting perovskite GdBa2Ca3Cu4O10.5+ δ nanosystems," Design, Fabrication, and Characterization of Multifunctional Nanomaterials, Elsevier, 2022, pp. 319-341.
20. B. Kisan, R. K. Bhuyan, and R. K. Mohapatra, "Nanocrystalline NiO powder: Synthesis, characterization and emerging applications," in Nano-Biosorbents for Decontamination of Water, Air, and Soil Pollution, 2022, pp. 529-550.
21. K. Sankarasubramanian, B. Devakumar, G. Annadurai, L. Sun, Y. J. Zeng, and X. Huang, "Novel SrLaAlO4: Mn4+ deep-red emitting phosphors with excellent

responsiveness to phytochrome P FR for plant cultivation LEDs: synthesis, photoluminescence properties, and thermal stability," RSC Adv., vol. 8, no. 53, pp. 30223-30229, 2018.

22. H. L. Muttashar, N. B. Ali, M. A. M. Ariffin, and M. W. Hussin, "Microstructures and physical properties of waste garnets as a promising construction material," Case Stud. Const. Mater., vol. 8, pp. 87-96, 2018.
23. A. Dwivedi, K. Mishra, and S. B. Rai, "Multi-modal luminescence properties of RE3+ (Tm3+, Yb3+) and Bi3+ activated GdNbO4 phosphors—upconversion, downshifting and quantum cutting for spectral conversion," J. Phys. D: Appl. Phys., vol. 48, no. 43, p. 435103, 2015.
24. L. Chen et al., "Charge deformation and orbital hybridization: intrinsic mechanisms on tunable chromaticity of Y3Al5O12: Ce3+ luminescence by doping Gd3+ for warm white LEDs," Sci. Rep., vol. 5, no. 1, p. 11514, 2015.
25. I. Krol, I. Sergun, O. Barinova, and K. Zh, "Effect of cobalt doping on the optical properties of glasses in the ZnO-B2O3 system," Sci. Euro., no. 68-2, pp. 8-13, 2021.
26. H. G. Abd-Elbaky, M. Rasly, R. G. Deghadi, G. G. Mohamed, and M. M. Rashad, "Strong-base free synthesis enhancing the structural, magnetic and optical properties of Mn/Co and Zn/Co substituted cobalt ferrites," J. Mater. Res. Technol., vol. 20, pp. 905-915, 2022.
27. M. M. Upadhyay, K. Shwetabh, and K. Kumar, "Comparative studies of upconversion luminescence and optical temperature sensing in Tm3+/Yb3+ codoped LaVO4 and GdVO4 phosphors," RSC Adv., vol. 13, no. 30, pp. 20674-20683, 2023.
28. T. Ivanova, K. Gesheva, A. Cziraki, A. Szekeres, and E. Vlaikova, "Structural Transformations and Their Relation to the Optoelectronic Properties of Chromium Oxide Thin Films," J. Phys.: Conference Series, vol. 113, no. 1, p. 012030, May 2008, IOP Publishing.
29. A. A. Ansari and A. Kaushik, "Synthesis and optical properties of nanostructured Ce(OH)4," J. Semicond., vol. 31, no. 3, p. 033001, 2010.

30. G. Jayakumar, A. A. Irudayaraj, and A. D. Raj, "Investigation on the synthesis and photocatalytic activity of activated carbon–cerium oxide (AC–CeO2) nanocomposite," Appl. Phys. A, vol. 125, no. 11, p. 742, 2019.
31. A. Dwivedi, K. Mishra, and S. B. Rai, "Multi-modal luminescence properties of RE3+ (Tm3+, Yb3+) and Bi3+ activated GdNbO4 phosphors—upconversion, downshifting and quantum cutting for spectral conversion," J. Phys. D: Appl. Phys., vol. 48, no. 43, p. 435103, 2015.
32. L. Wang, X. Zhang, Z. Hao, Y. Luo, X. J. Wang, and J. Zhang, "Enriching red emission of Y3Al5O12: Ce3+ by codoping Pr3+ and Cr3+ for improving color rendering of white LEDs," Opt. Exp., vol. 18, no. 24, pp. 25177–25182, 2010.
33. P. I. Paulose, G. Jose, V. Thomas, N. V. Unnikrishnan, and M. K. R. Warrier, "Sensitized fluorescence of Ce3+/Mn2+ system in phosphate glass," *J. Phys. Chem. Solids., vol. 64, no. 5, pp. 841–846, 2003.
34. R. Ma, C. Ma, J. Zhang, J. Long, Z. Wen, X. Yuan, and Y. Cao, "Energy transfer properties and enhanced color rendering index of chromaticity tunable green-yellow-red-emitting Y3Al5O12: Ce3+, Cr3+ phosphors for white light-emitting diodes," Opt. Mater. Exp., vol. 7, no. 2, pp. 454-467, 2017.

Chapter 6

Summary and Future Scope

Transition metal doped Gadolinium Aluminum Garnet (GAG) and Cerium Aluminum Garnet (CAG) were successfully synthesized for solid-state light sources by the sol-gel method. GAG and CAG doping specifically employ incorporating transition metals cobalt and chromium. The cobalt and chromium were chosen as dopants due to their well-known transition lines for visible emission. The optimum temperatures for synthesizing precursor ceramic material were determined to be 1100ºC for GAG and 1200ºC for CAG. The structural and optical properties were investigated. X-ray diffraction (XRD) analyses confirmed a pure-phase and single-phase cubic structure for both CAG and GAG. Further, found no alteration in crystalline structure was observed after the introduction of chromium and cobalt dopants. As an indication of the sol-gel method spherical shape and nano-sized particles were confirmed by SEM and agglomeration for the material was also confirmed by SEM. The EDS results revealed the effective stoichiometric composition of elements in both garnets.

Interestingly, the Dopants exhibited a discernible influence on the strain and porosity within the crystal lattice. To delve deeper into the materials' characteristics, extensive analyses of their optical properties were conducted using Fourier-transform infrared spectroscopy (FTIR), ultraviolet (UV) spectroscopy, and fluorescence spectroscopy. The FTIR results support the XRD findings and identify the functional groups present in the material.

In the case of GAG, the observed emission spectrum under the UV-excitation and spectrum shows the transition lines of Gd^{3+} i.e. $^{8}S_{7/2}$ - $^{6}P_{J}$, $^{6}I_{J}$ - $^{8}S_{7/2}$, $^{6}P_{J}$ - $^{6}G_{7/2.}$ The emission spectra show the CIE coordinates of (0.332,0.334), color purity of 0.2%, and CRI of 96. To enhance the optical efficiency of the GAG doping of Cobalt (Co) and Chromium (Cr) was undertaken. The introduction of cobalt doping in GAG did not bring about a discernible change in the optical parameters such as CIE, CRI, and color purity, even the integrated

intensity also increased with a minor difference from the host. But from emission spectra, the transition lines of cobalt are seen and the energy transfer between the host and dopant is shown in Figure 4.28. The major peaks 463 nm and 601 nm were observed due to cobalt ^{4} T_1 (F) to $^4T_1$ (P) and $^4T_1$ to $^4A_2$ transition as discussed in section 4.3.6. Thus, cobalt did not make a major change or effect on the optical behavior of GAG. On comparing cobalt doping in GAG, the best results were optimized on the 0.2 concentration of GAG: Co.

Furthermore, chromium doping in GAG had a notable impact on the behavior of the garnet. While the GAG: Cr material is excited with the UV the emission is found in the visible region and the emission spectra include several peaks due to Gd^{3+} and Cr^{3+} transition lines. How energy gets transferred between Gd^{3+} and Cr^{3+} is illustrated in Figure 4.15 clearly and transition lines are also shown. The integrated intensity increased with doping and the CIE, CRI, and color purity values shifted the light to the greenish-blue side of the chromaticity diagram. Thus, chromium did not enhance the GAG behavior for white light. Moreover, co-doping of cobalt and chromium in GAG, utilizing their optimized concentrations (Co at 0.2 and Cr at 1.0), yielded more promising results. The values of CIE coordinates, CRI, and color purity were enhanced, approaching closer to the ideal values for good white light. This suggests that the combined presence of cobalt and chromium had a synergistic effect, positively influencing the optical properties of GAG and moving it closer to the desired characteristics for white light emission. The obtained results for co-doping were excellently favorable for the ideal white light as it has CIE is (0.333,0.333), CRI is 95 and color purity is 0.2%.

On the other side, in the case of another host CAG while the material gets excited with the UV light the material exhibits a broad emission spectrum characterized by multiple peaks in the visible region. The sharp and clear peaks due to transition lines of Ce^{3+} were found in spectra at 455 nm [$4f^1$ ($^2F_{7/2}$) $\rightarrow$ $4f^0 5d^1$] and 530 nm [and $5d^1$-$4f^1$ ($^2F_{5/2}$)]. The cerium transition lines show the yellow color emission and with UV excitation complete emission spectra give the near white light emission which is verified with calorimetry (CIE, CCT, CP, CRI) results. The CIE (0.331, 0.332), CRI of 95, and color purity of 0.5% for CAG

indicate its optical properties. The chromium and cobalt transition metals were doped in CAG to enhance the optical properties and investigate the effect of doping on the CAG. Surprisingly, the results indicated that the incorporation of Co and Cr did not significantly alter the behaviors of the CAG host material. the fluorescence emission spectra in both cases show the multiple peaks in the visible region and the transition lines of cobalt near 512 nm [$^4T_2$ (F) → $^2T_1$ (G)] and 580 nm [$^4T_1$ (P) → $^4T_2$ (F)] observed and due to Ce^{3+} and Co^{3+} transition lines the spectra emission of multiple color and overall emission spectra found quite advantageous for the production of white light in CAG: Co case. Similarly in the case of CAG: Cr the clear transition lines of Cr^{3+} and Ce^{3+} are found as explained in section 5.3.5 and energy transfer between Ce^{3+} and Cr^{3+} is shown in figure 5.23. However, a detailed analysis comparing different doping concentrations revealed that optimal improvements occurred at concentrations of 0.10 for CAG: Co and 0.05 for CAG: Cr. Thus, on the comparison of doping concentrations in both dopants 0.10 for CAG: Co and 0.05 for CAG: Cr were optimized as the best doping concentrations for co-doping. Thus, these concentrations are considered for co-doping. The co-doping of Co and Cr demonstrated visible enhancements in CAG properties notably reflected in the increased integrated area of the spectrum with the introduction of dopant. Moreover, the CIE, CRI, and color purity values approached those ideal for white light. In essence, the co-doping strategy at the specified concentrations proved to be the most effective in achieving desirable optical characteristics for CAG, showcasing promising outcomes for potential applications.

Cr^{3+} and Co^{3+} doped GAG & CAG as a Solid- State White Light Emission Excited by 310 nm on UV chip

The synthesized material comprising CAG and GAG exhibits promising optical characteristics and colorimetry parameters conducive to emitting white light. To evaluate its performance, we subjected the material to examination using a UV chip emitting light at 310nm. Remarkably, the material displayed white emission upon exposure to this UV light source. The accompanying figure 6.1 illustrates a visual comparison between the UV chip with and without the synthesized material. This outcome suggests that the synthesized material effectively converts the UV light emitted by the chip into white light, showcasing its potential utility in various applications requiring white light emission. These applications could range from advanced lighting technologies to optoelectronic devices where the generation of white light is essential.

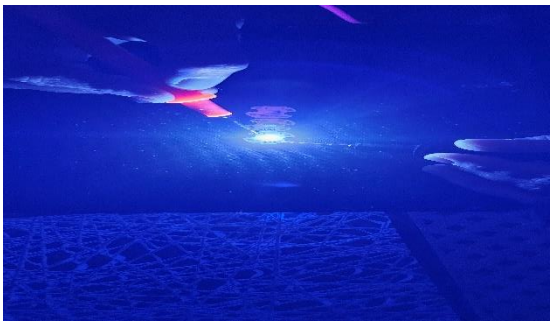

(a)

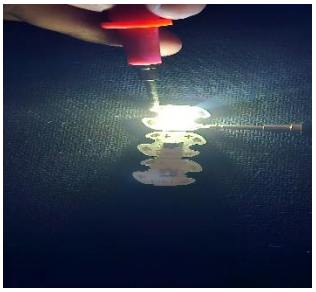

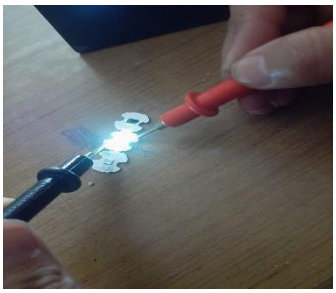

(b) **(c)** **(d)**

Fig 6.1. (a)UV Chip light 310 nm without material, (b) UV Chip light with CAG Coating, (c) UV Chip light with CAG: Cr Coating, and (d) UV Chip light with GAG: Co Coating.

Annxure-1

List of papers published

List of publications in the journal

1. Bala, A. and Rani, S., 2023. UV excited emission spectra of gadolinium aluminum garnet. *Journal of Optics*, *52*(2), pp.868-874.

J Opt
https://doi.org/10.1007/s12596-022-01052-2

COVER ARTICLE

UV excited emission spectra of gadolinium aluminium garnet

Anu Bala[1] · Suman Rani[1]

Received: 17 May 2022 / Accepted: 7 December 2022

Abstract Gadolinium aluminum garnets (GAG) in recently times are examined for their application in enhancing the efficiency of photonic devices. A sequence of samples for gadolinium aluminum garnet ($Gd_3Al_5O_{12}$) was synthesized effectively using the sol–gel method. The prepared sample was sintered at various temperatures, but at 1100 °C pure phase developed was identified by X-ray diffraction, and luminescence properties were studied by several characterizations such as Fourier transform infrared spectroscopy (FTIR), UV–Vis spectroscopy, and fluorescence spectroscopy. XRD gave the confirmation of the phase formation of GAG, and analyses of FTIR were also coordinated with XRD results. Emission spectra corresponding to $^6I_{7/2}$, $^6D_{9/2}$, and $^6G_{7/2}$ energy transition from state $^6S_{7/2}$ were determined for three UV excitations, i.e., 256 nm, 290 nm, and 391 nm, and show mixed color components on the chromaticity diagram.

Keywords Garnets · Gadolinium · Energy transition · $Gd_3Al_5O_{12}$ · UV excitation

Introduction

As per economical demand, energy is a basic need for the evolution of the contemporary world and humanity has always been looking for material that can give a more efficient source of energy. Newly developed garnets have become a vigorous area for researchers to enhance solid-state light sources as they have excellent properties and superior color rendering properties. These are highly challenging for light-emitting diodes (LEDs), display panels, field emission displays (FEDs), luminescent solar concentrators (LSC), and more. Primarily in the case of the garnets formula, host material plays a significant job in the enhancement of luminescence properties [,]; for the synthetic garnets, the general formula is $A_3B_2C_3O_{12}$ with cubic symmetry of space group Ia3d where A in the site is dodecahedral, B is octahedral, and C is tetrahedral. But in the case of commonly used ternary synthetic garnets, a general chemical formula $A_3B_5O_{12}$ is used because it considers B = C. Nowadays, rare-earth aluminate garnets ($RE_3Al_5O_{12}$) have generated great interest from researchers since they have distinctive photoluminescence (PL) properties and have excellent thermal, and photochemistry stability and efficiency. In $RE_3Al_5O_{12}$, rare earth (RE) = A and Al = B [–]. There are some well-known rare-earth garnets are yttrium aluminum garnet ($Y_3Al_5O_{12}$), terbium aluminum garnet ($Tb_3Al_5O_{12}$), lutetium aluminum garnet ($Lu_3Al_5O_{12}$), gadolinium aluminum garnet ($Gd_3Al_5O_{12}$) listed in Table , etc.

Along with REAG, yttrium aluminum garnet (YAG) is a commonly used garnet, and in YAG the Y^{3+} can be effortlessly replace by other rare-earth ions like Ce^{3+}, Tb^{3+}, Eu^{3+}, and more. Among these ions, the Tb^{3+} in YAG reveals a green emission through a narrow band, and that is why it has found excellent applications in cathode tubes and display devices [–]. However, in Garnet's formula placement of Gd^{3+} at sites A and B leads to the formation of stable garnet $Gd_3Al_5O_{12}$ (GAG). At the room, temperature GAG has cubic space-grouped I a3-d [ ]. Doped GAG can transfer charge easily as gadolinium has less electro-negativity. GAG can attain stability around 1300 K, and above this temperature, it may be decomposed into $GdAlO_3$ and Al_2O_3. The study aims

✉ Suman Rani
suman.rani@lpu.co.in

[1] Department of Physics, School of Chemical Engineering and Physical Sciences, Lovely Professional University, Phagwara, Punjab 144411, India

Published online: 30 December 2022

2. Bala, A. and Rani, S., 2023. Down conversation visible emission spectra of Cr3+ doped gadolinium aluminum garnet. *Optical and Quantum Electronics*, *55*(10), p.866.

Optical and Quantum Electronics (2023) 55:866
https://doi.org/10.1007/s11082-023-05105-z

Down conversation visible emission spectra of Cr^{3+} doped gadolinium aluminium garnet

Anu Bala[1] · **Suman Rani**[1]

Received: 30 April 2023 / Accepted: 17 June 2023 / Published online: 23 July 2023

Abstract
The preparation of gadolinium aluminium garnet (GAG) doped with Cr^{3+} ions (Cr: GAG) was carried out using the sol–gel technique, followed by sintering at 1100 °C. X-ray diffraction characterization was performed to investigate the effects of Cr^{3+} doping on the GAG phase. The results revealed that Cr^{3+} doping induced strain in GAG, leading to a phase effect and an increase in crystallite size. Field emission scanning electron microscopy was utilized to observe the particle size, morphology, and a comparison of crystallite size with particle size. Fourier transform infrared spectroscopy was used to confirm the interaction between metal and oxygen in the lattice and assess the material's composition. UV spectroscopy and fluorescence spectra were employed to comprehensively study the optical characteristics of Cr: GAG. Chromaticity coordinates, correlated color temperature, and color rendering index were explored at 282 nm excitation. Decay curve analysis revealed that the material's lifetime increased with an increase in the Cr^{3+} doping concentration in GAG. Fluorescence spectra exhibited multiple peaks, indicating multicolor emission and suggesting the potential for creating efficient white light sources using Cr: GAG. Overall, these findings highlight the potential of Cr^{3+} doping in GAG for tuning the optical properties and creating novel light-emitting energy- efficient materials with promising applications.

Keywords Sol–gel process · Crystal structure · Garnets · Absorption · Fluorescence · Energy efficiency

1 Introduction

Garnets proved as great candidates for their promising chemical stability, and luminescent and thermal properties when doped with transition metal ions or rare earth ions (Birkel et al. 2012). The general formula of garnets is $[A]_3[B]_5O_{12}$ have cubic face-cantered lattice crystal structure with complex positioning of different cations in the unit cell due to which behaves exclusively in their luminescence properties and these properties changes or

✉ Suman Rani
suman.rani@lpu.co.in

[1] Department of Physics, School of Chemical Engineering and Physical Sciences, Lovely Professional University, Phagwara, Punjab 144411, India

3. Bala, A., Rani, S., Sharma, A., Lokhande, P.E. and Kumar, D., 2023. Effect of Cobalt doping on luminescence properties of gadolinium aluminum garnet. *Journal of Materials Science: Materials in Electronics*, *34*(36), p.2321.

J Mater Sci: Mater Electron (2023) 34:2321

Effect of Cobalt doping on luminescence properties of gadolinium aluminum garnet

Anu Bala[1], Suman Rani[1,*], Ajit Sharma[4], P. E. Lokhande[2,3], and Deepak Kumar[4]

[1] Department of Physics, School of Chemical Engineering & Physical Sciences, Lovely Professional University, Punjab 144411, India
[2] Advanced Physics Laboratory, Department of Physics, SavitribaiPhule Pune University, Pune, India
[3] Department of Mechanical, Manufacturing and Biomedical Engineering, Trinity College Dublin, Dublin, Ireland
[4] Department of Chemistry, School of Chemical Engineering and Physical Sciences, Lovely Professional University, Phagwara, India

Received: 30 March 2023
Accepted: 8 November 2023
Published online: 15 December 2023

ABSTRACT

The luminescent properties of GAG: Co ($Gd_3Al_5O_{12}$:Co) arises from the absorption of light in the visible and near-infrared regions by the Co ions. When excited by light, the Co ions can transfer their energy to other ions in the material, which can emit light of a different color. The color of the emitted light depends on the specific energy levels of the ions involved in the luminescent process. In GAG: Co, the emitted light is typically in the blue-green region of the spectrum. A series of singly doped gadolinium aluminum garnet with cobalt (GAG: Co) of different concentrations were synthesized by the sol–gel method after sintering at a temperature 1100 ℃. The X-ray Diffraction (XRD) and Scanning Electron Microscopy (SEM) show the precipitation of GAG: Co with a size around 25–40 nm and phase formation was acknowledged by X-ray Diffraction. Fourier infrared transformation spectroscopy (FTIR) analysis gives the system evaluation and composition of a material. Energy Dispersive X-ray (EDX) analysis confirms the incorporation of Cobalt ions in GAG. The luminescence properties of the material were investigated by FTIR, UV–Vis spectroscopy, and Fluorescence spectroscopy. Analyses of FTIR were also supportive of XRD results. Emission spectra were determined for excitations 270 nm and 282 nm and lifetime was found to decrease with an increase in doping concentration. The material shows mixed color components on the chromaticity diagram which makes it a supportive material for application in white light sources.

1 Introduction

In the current era of research, the Rare-Earth Aluminate Garnets (REAG) with a general formula $Re_3Al_5O_{12}$ is a category of best-known cubic oxides and these are the most active inorganic materials that are used in the application of display devices and white light sources. They are well-known for their good efficiency, thermal stability, and photochemical stability [1–9].For its optical characteristics and applications, Yttrium aluminum garnet (YAG), Terbium aluminum garnet (TAG), and Lutetium aluminum garnet (LuAG) has been the subject of much investigation. Gadolinium Aluminum Garnet (GAG)

List of publications in proceedings

1. Bala, A. and Rani, S., 2022. Garnet: Structural and Optical Properties. In *Advances in Functional and Smart Materials: Select Proceedings of ICFMMP 2021* (pp. 365-371). Singapore: Springer Nature Singapore.

Garnet: Structural and Optical Properties

Anu Bala and Suman Rani

Abstract Garnets are seems like good material for solid-state light because of their excellent chemical and physical stability and favorable luminescence properties. These materials emit multicolors (red, blue, and green). They have been recommended optical properties as they have large emission range and have excellent thermal conductivity, high mechanical strength, high-temperature resistance, and radiation resistance. Research had been done for the improvement of luminescence properties with doping at sites A and B in $[A]_3[B]_2[C]_3[O]_{12}$ (Garnet). Garnets included rare-earth series have great luminescence properties and were also very defendable for the amazing down-conversion properties.

Keywords Garnet · Rare earth · Optical · Luminescence

1 Introduction

Garnets have general formula $[A]_3[B]_2[C]_3[O]_{12}$, where A site is occupied by dodecahedral coordination and B site by octahedral coordination and C site by tetrahedron coordinate. Garnet has cubic lattice structure where space A can be occupied by alkali metal, alkali earth metal, and rare-earth metals. They belong to body-centered cubic Ia3d space group. Garnets are seems like good material for solid-state light because of their excellent chemical and physical stability and favorable luminescence properties. These materials emit multicolors (red, blue, and green). Most common garnets like Terbium aluminum garnet (TAG), Yttrium aluminum garnets (YAG), gadolinium gallium garnet (GGG), Europium Gallium Garnet (EGG), etc. have been

A. Bala · S. Rani (✉)
Department of Physics, School of Chemical Engineering and Physical Sciences, Lovely Professional University, Phagwara, Punjab 144411, India
e-mail: Suman.rani@lpu.co.in

C. Prakash et al. (eds.), *Advances in Functional and Smart Materials*, Lecture Notes in Mechanical Engineering, https://doi.org/10.1007/978-981-19-4147-4_37

2. Bala, A. and Rani, S., 2022, May. Down conversions excitation dependent luminescent properties of Terbium Aluminum Garnet. In *Journal of Physics: Conference Series* (Vol. 2267, No. 1, p. 012113). IOP Publishing.

Down conversions excitation dependent luminescent properties of Terbium Aluminum Garnet

Anu Bala and Suman Rani*
Department of Physics, School of Physical Sciences and Chemical Engineering, Lovely Professional University, Punjab – 144411,India
*suman.rani@lpu.co.in

Abstract TAG (terbium aluminum garnet, $(Tb_3Al_5O_{12})$ is being investigated recently for their applications in the realization of photonic devices because of its broad transmission ranging from 350 to 1500nm. An emission property of any material depends upon electronic transition levels, temperature, excitation wavelength etc. A lot of research had been reported on temperature dependent emission properties of TAG .In this study an attempt had been made to explore the excitation dependent emission properties of TAG.TAG was prepared by sol gel technique followed by sintering at 1100°C .Structural phase was analysis from the XRD spectra .XRD studies confirmed the formation of nano material and has cubic structure. The emission properties were studied by exciting the TAG by UV light and blue light i.e. 280nm, 300nm, 380 nm, 400nm, 480 and 484nm .Spectra power distribution curve was obtained from emission data excited by with UV radiation and blue light. From emission spectra, Colour co-ordinates (CIE), colour correlated temperature (CCT) and colour purity were calculated for TAG at different excitation .Emission properties indicates that TAG is potential nanophosphor for optical devices.
Key words: CIE coordinates, CCT, colour purity, TAG, UV light, excitation wavelength

1. Introduction

In down conversion (DC), high-energy visible photons are absorbed and re-emit two or more photons of lower energy at higher wavelengths. DC luminescence has number of host lattices but highly extensively include single or multi-cation oxides, oxysulfide, phosphates, vanadates, borates and tungstates. In crystal growing technology, garnets attract great interest of researchers for its luminescence properties because it has unique optical, magnetic and electric properties. Hence, this develops its vast area of applications in various fields. The general formula of garnets is $[A]_3[B]_5O_{12}$. They have cubic face centred lattice crystal structure with complex positioning of different cations in unit cell. Due to this garnet behaves uniquely in their luminescence properties and these properties changes with the replacement of different sites as A, B with unlike elements like rear earths [1,2]. The garnets have distinct chemical composition, photoluminescence emission and their corresponding implementations. Most widely used yttrium aluminium garnet ($Y_3Al_5O_{12}$, YAG), doped with rear earth materials to produce white light but YAG is a good candidate for producing luminescence transforming LEDs which are tremendous for warm white LED applications as there is absence of red component in it. So, terbium aluminium garnets (TAG) rises as best alternative for YAG in luminescence as it able to absorb radiation in huge range i.e. from UV to blue whereas it emits radiations of broad spectrum 350nm to 1500nm i.e UV, visible and infrared. Moreover, TAG also shows the red colour range of spectrum which is advantageous to overcome with high temperature problem in LEDs. [3]

List of conferences

1. International Conference on Recent Advances in Fundamental and Applied Sciences (RAFAS 2021) June 25- June 26, 2021, Online mode Lovely Professional University, Phagwara.

Certificate No. 225316

LOVELY PROFESSIONAL UNIVERSITY
Transforming Education Transforming India

RAFAS

Certificate of Participation

This is to certify that **Ms. Anu Bala**

of **Lovely Professional University Phagwara Punjab**

has given poster presentation on **Down conversions excitation dependent luminescent properties of Terbium Aluminum Garnet**

in the International Conference on "Recent Advances in Fundamental and Applied Sciences" (RAFAS 2021) held on June 25-26, 2021, organized by School of Chemical Engineering and Physical Sciences, Lovely Faculty of Technology and Sciences, Lovely Professional University, Punjab.

Date of Issue : 15-07-2021
Place of Issue: Phagwara (India)

Prepared by
(Administrative Officer-Records)

Organizing Secretary
(RAFAS 2021)

Convener
(RAFAS 2021

2. Conference on Optics Photonics and Quantum Optics COPaQ 2022 November 10-13, 2022 Indian Institute of Technology Roorkee, India.

Certificate of Participation

ANU BALA

Presented a paper

Wet chemical route to synthesis of Ce3Al5O12 Garnet structure at high temperature

in

XLV symposium of Optical Society of India

Conference on Optics, Photonics and Quantum Optics

COPaQ 2022

November 10-13, 2022

Indian Institute of Technology Roorkee, India

Vipul Rastogi

Ajay Wasan

Conference Chairs

3. 2nd International Conference on Advanced Functional Materials & Devices AFMD-2023 IQAC & department of Physics, ARSD College (University of Delhi).

ATMA RAM SANATAN DHARMA COLLEGE

(University of Delhi)

Accredited Grade 'A' By NAAC
All India 7th Rank in NIRF (MHRD)

Certificate No: AFMD-2023/P/005

2nd International Conference on

"Advanced Functional Materials & Devices" (AFMD-2023)

Organized by

IQAC & Department of Physics, ARSD College

This is to certify that Prof./Dr./Mr./Ms. ANU BALA from Lovely professional university jalandhar has participated in 2nd International Conference on "Advanced Functional Materials and Devices" (AFMD-2023) organised by IQAC & Department of Physics, ARSD College, University of Delhi during 13-15th March 2023 via online mode.

(DR. SHANKAR SUBRAMANIAN)
CONVENER

(DR. VINITA TULI)
CONFERENCE CHAIR

(PROF. GYANTOSH KUMAR JHA)
PRINCIPAL

4. International Conference On Energy Materials & Rechargeable Batteries (ICEMRB-2023) December 19-22, 2023 Manav Rachna University, Faridabad.

INTERNATIONAL CONFERENCE ON ENERGY MATERIALS AND RECHARGEABLE BATTERIES (ICEMRB)-2023
(DECEMBER 19-22, 2023)

CERTIFICATE OF PRESENTATION

Reference Number: RP23057

This is to certify that Prof. Dr/Mr/Ms. Anu Bala from Department of Physics, LPU has presented (oral/poster) his/her research work entitled "Optical and Electrical properties of Chromium doped Gadolinium Aluminium Garnet" at International Conference on Energy Materials and Rechargeable Batteries organized by the Department of Sciences (Physics) & University Instrumentation Center (UIC), Manav Rachna University (MRU), Faridabad, Haryana, India.

We wish him/her a great success.

Dr. Virendra Pal Singh, Convener - ICEMRB2023
Prof. (Dr.) Meena Kapahi, Dean-School of Sciences
Prof. (Dr.) Goldie Gabrani, ED & Dean Research, MRU
Prof. (Dr.) L. K. Bhat, Vice Chancellor, MRU

Annexure- 2

Vita